Advances in Carbon Nitride-Based Materials and Their Electrocatalytic Applications

Farzaneh Besharat, Fatemeh Ahmadpoor, Zahra Nezafat, Mahmoud Nasrollahzadeh,* Nilesh R. Manwar, Paolo Fornasiero, and Manoj B. Gawande*

ABSTRACT: As a group of large-surface-area nonmetal materials, polymeric carbon nitride (C_xN_y) and its hybrid structures are nowadays of ever-increasing interest for use in energy devices involved in energy conversion and storage, offering low expenses and facile production processes. With the growing requirement for clean and renewable energy generation and storage systems, progress in the replacement of expensive noble-metal catalysts with C_xN_y-based materials as efficient electrocatalysts has expanded considerably, and the demand for these materials has increased. The modified C_xN_y architectures are beneficial to electrocatalytic applications, improving their moderate electrical conductivities and capacity loss. The present review strives to highlight the recent advances in the research on the aforementioned identities of C_xN_y-derived materials and their structurally modified polymorphs. This review also discusses the use of C_xN_y-based materials in fuel cells, metal−air batteries, water splitting cells, and supercapacitor applications. Herein, we deal with electrocatalytic oxidation and reduction reactions such as hydrogen evolution, oxygen evolution, oxygen reduction, CO_2 reduction, nitrogen reduction, etc. Each device has been studied for a clearer understanding of the patent applications, and the relevant experiments are reviewed separately. Additionally, the role of C_xN_y-derived materials in some general redox reactions capable of being exploited in any of the relevant devices is included.

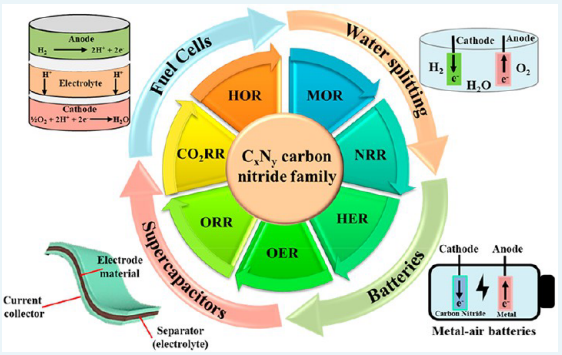

KEYWORDS: *carbon nitride, electrocatalysis, fuel cell, water splitting, supercapacitor, metal−air batteries*

1. INTRODUCTION

With increasing environmental concerns and energy demands, the exploration of clean and renewable energy systems to reduce fossil fuel consumption has turned into a worldwide research priority. In this regard, renewable energy conversions with carbon dioxide (CO_2) and water can effectively generate hydrocarbon fuels and hydrogen (H_2), respectively, through electrocatalytic processes[1,2] or produce mixtures (e.g., syngas) to be directly utilized in other reactions.[3−5] Today, the great general interest in energy related-systems (e.g., fuel cells, batteries, sensors, and supercapacitors)[6,7] is mostly related to the need to develop sustainable technologies that are feasible and based on inexpensive and renewable resources and energy cycles.[8] For example, in metal−air batteries there is a huge demand for low-cost, abundant, and efficient bifunctional catalysts.[8]

Electrocatalysis has attracted specific interest for academic purposes and great interest for technical industrial-scale uses. However, an underexplored gap exists between fundamental concepts and application-oriented progress for the commercialization of such technologies due to the inconsistencies between research parameters and industrial ones.[9,10] High-performance redox electrocatalysis favors the prospect of processing fuels using renewable energy materials. It is noted that appropriate metals and alloys are supposed to be efficient electrocatalysts. However, the fabrication of low-dimensional nanostructured catalysts is an important target[11] because the morphology of the applied material can influence the final efficiency in this context.[12] Namely, the fabrication of porous metal nanocatalysts is assumed to be a beneficial strategy for reaching high-surface-area candidates that fulfill the need for both desirable electrocatalytic activity and pore structures.[13] Besides, compared to porous and one-dimensional (1D) nanomaterials, two-dimensional (2D) nanomaterials can deliver a larger quantity of electrocatalytically active sites, which are much simpler to identify due to the ordered 2D molecular framework. They also demonstrate the economic advantage of substituting precious metals.[14,15]

It is important to note that these energy systems operate based on diverse key redox reactions, which include the oxygen reduction reaction (ORR), the hydrogen evolution reaction (HER), the oxygen evolution reaction (OER), the CO_2 reduction reaction (CO_2RR), the methanol oxidation reaction (MOR), and the nitrogen reduction reaction (NRR). The development of catalysts as electrode materials can speed up these reactions and improve the efficiencies of energy systems. Various metal-based catalysts containing metal-free polymeric graphitic carbon nitride (g-C_3N_4) have been employed for a variety of electrocatalytic applications.[16−18] Metal-based nanocomposites usually exhibit ideal surface areas for catalysis[19] and hydrogen storage.[20] However, they are associated with low selectivity and durability and destructive environmental effects, which hinder their application. Hence, developing abundant, inexpensive, more stable, and highly active metal-free catalysts is currently desirable.[21] In fact, one of the key limiting factors in the development of new energy devices is the availability of an adequate catalyst; in response to this, carbon-based structures are assumed to be key materials because of their large surface areas, simple processing, high stabilities, and low cost.[22] Multiple carbon-based electrocatalysts can be pointed out, including porous carbon nanoparticles,[23] graphene, and carbon nanospheres, fibers, sponges, ribbons, shells, and sheets, nanocages, as well as different carbon hybrids, including carbon−C_3N_4, carbon−carbon, monometal- and bimetal-modified carbon, and carbon with metal sulfides, carbides, nitrides, oxides, and phosphides.[24] Doping carbon-based materials with heteroatoms such as nitrogen (N), boron (B), selenium (Se), sulfur (S), and phosphorus (P) leads to high stability, appropriate catalytic activity, and cost reduction in energy storage and conversion devices such as supercapacitors, fuel cells, H_2 storage, and batteries.[25−28] In 1920, the concept of heteroatom doping in carbon materials was first introduced. Currently, more than ten nonmetallic elements have been doped into carbon materials. The size and type of the heteroatom strongly influence the catalytic performance of carbon materials in energy systems.[28] Among the various heteroatom-doped carbon materials, nitrogen-doping enhances the electrochemical performance and is widely used in metal-free catalysts. In addition, the nitrogen atoms are more negative than the carbon atoms, leading to an increase in the electron density of carbon; hence, the interaction with positive particles becomes stronger. Additionally, the nitrogen doping strategy can provide channels for ion and electrolyte diffusion.[29,30] The surface wettability and electrical conductivity of carbon materials can also be improved by nitrogen doping.[25,28] Two common approaches for nitrogen doping into carbon-based methods are (i) "in situ" doping and (ii) post-treatment doping. In the first approach, nitrogen-doped carbon is prepared with carbon and nitrogen atoms from the precursors. In the post-treatment method, some carbon atoms are replaced with nitrogen atoms in the presence of a nitrogen source.[29,31,32]

Regarded as metal-free catalysts for ORR, HER, and OER processes, materials consisting of nitrogen-doped carbon, such as N-doped carbon nanotubes and N-doped graphene, have attracted considerable interest due to their excellent electrocatalytic activities. However, the research has indicated that 1D and 2D materials often carry trace amounts of impurities, which nevertheless considerably influence the eventual electrocatalytic functionality in terms of promoting or inhibiting different reaction catalysis.[24,33] Different N-configurations can be formed by doping the carbon backbone with a nitrogen atom, among which pyridinic and quaternary N are assumed to be the main active sites for the above-mentioned reactions. Carbon-based single-atom catalysts (SACs) are also members of the important carbon-based catalysts category, exhibiting extraordinary features like ordered porosity, adjustable morphologies, and uncomplicated immobilization in multiple metals.[34] Regarding the improved features of their nitrogen-modified forms, the conversion of CO_2 into methanol as chemical fuel using single-atom carbon nitride−ruthenium photocatalysts to eventually yield a large amount of methanol has been reported.[35]

Aside from all the considerable features of C_xN_y structures, ongoing limitations such as a relatively insufficient nitrogen content (2−5 atom %), an unstable carbon structure, and weak functionality under extreme electrochemical conditions necessitate continued research and development in this area.[7] Structures containing carbon and nitrogen are increasingly grabbing attention due to their potential to construct materials with outstanding electrical and chemical properties. Such assemblies, including organic frameworks and 2D inorganic materials, have dedicated a diverse range of functionalities to the design field of electrochemical materials.[36] For instance, polymeric carbon−nitrogen-based catalysts are among the systems that can be obtained through strategies such as noble-metal cocatalysts (Pt, Au, Ag, etc.), non-noble metals (Ni, Fe, Cu, etc.), and nitrogen doping, in brief.[16] Among polymeric C_xN_y structures, the g-C_3N_4 composition is very well-known for its thermal and chemical stability and has a significant catalyzing capability toward a wide range of chemical reactions.[37] This structure covers various materials applicable to different electrocatalytic reactions, from porous solid materials such as covalent triazine-based frameworks (CTFs) to porous nitrogen-doped carbon catalysts (NdCs).[38] Since nitrogen is one element after carbon in the periodic table, replacing one C with N means the total number of electrons can be tuned one electron at a time with no significant lattice mismatch. Besides, via N-doping, the n-type electronic regulation of the carbon structure promotes the semiconducting applications of C−N materials.[39]

Graphitic carbon nitride (g-C_3N_4) is highly recognized as a stable allotrope, and it is a unique 2D material in energy-related applications. The 2D framework with nitrogen heteroatoms substituted in graphite is generated through the sp^2 hybridization of nitrogen and carbon atoms. Based on previous research, tri-*s*-triazine is regarded as the basic unit of the g-C_3N_4 network. In contrast to conductive graphite, g-C_3N_4 has exhibited wide-band semiconductor properties. Various fabrication methods have been applied in the synthesis of g-C_3N_4 structures to achieve the challenging goal of totally condensed samples, and the obtained g-C_3N_4 structures usually have degrees of defects and eventually exhibit condensation.[22] Such distortions are created specifically at temperatures above the melem thermal stability limit and may induce excessive n-to-π^* transition pathways, which is mostly applicable in electrocatalytic applications.[40]

Recent reviews were focused on photocatalytic studies of C_xN_y structures as a result of their visible light response[41−47] or specific catalytic reactions,[15] and less critical attention has been paid to emerging electrochemical applications. In this context, herein we identified some relevant reviews. The study of efficient and cost-effective doped g-C_3N_4 architectures in photocatalytic wastewater treatment and gas purification is one

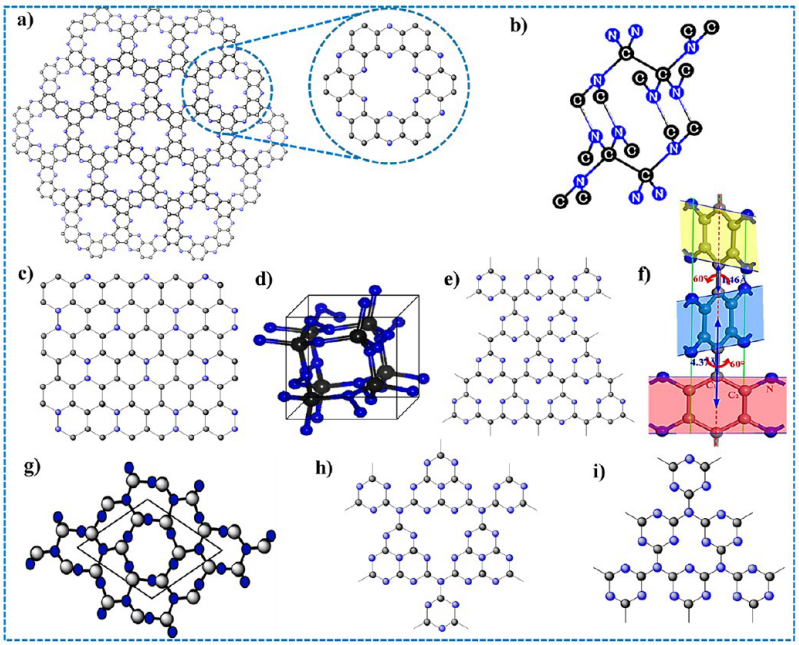

Figure 1. Schematic representation of multiple possible C_xN_y structures, including (a) C_2N, (b) CN, (c) C_3N, (d) CN_2, (e) g-C_3N_4, and (f) spiral-C_3N, and different g-C_3N_4 structures, including (g) β-g-C_3N_4, (h) heptazine g-C_3N_4, and (i) triazine g-C_3N_4. Nitrogen atoms are depicted in blue. Panel a was reproduced with permission from ref 49. Copyright 2015, Springer Nature. Panel b was reproduced with permission from ref 48. Copyright 2016, American Chemical Society. Panel c was reproduced with permission from ref 51. Copyright 2012, Wiley-VCH. Panel d was reproduced with permission from ref 50. Copyright 2015, Springer Nature. Panel e was reproduced with permission from ref 59. Copyright 2018, American Chemical Society. Panel f was reproduced with permission from ref 54. Copyright 2020, American Chemical Society. Panel g was reproduced with permission from ref 60. Copyright 2014, Hindawi.

of the aforementioned works. It summarizes the multiple C_3N_4 doping strategies, including metal and nonmetal doping, heterojunctions, and codoping, for improving the photocatalytic activies of such materials in terms of the charge separation and charge carrier lifetime by tuning their crystal and electronic structures.[41] Besides, the review of the recent progress in the use of defective C_xN_y structures as photocatalysts toward different oxidation and reduction processes, nitrogen fixation, organic synthesis, and pollutant removal is another example in this setting that exclusively evaluates the vacancy-defect-modified C_xN_y photocatalysts.[42] One of the other worthy review investigations on g-C_3N_4 was concerned with the improvement of their photocatalytic (solar-driven) water splitting roles, with a focus on the surface strategies. The study highlighted the three stages of surface regulation, surface functionalization, and surface assembly and discussed the challenges involved with artificial photosynthesis.[43] Further, design and synthesis-directed studies have been carried out that focused on the advances in the construction of g-C_3N_4-based materials. Melamine self-assembly-born C_xN_y structures addressed as ordered materials are reviewed with respect to the self-assembly mechanisms, synthesis methods, and the material features, and the review presents insights into the design and fabrication of enhanced-performance ordered g-C_3N_4 for energy and environmental fields.[44] In reference to the studies over a specific type of reaction, the review on photocatalysts and electrocatalysts based on polymeric carbon nitride can be named, which describes various design methods of vacancy induction and doping toward NRR and discerns the mechanisms of electrocatalytic and photocatalytic NH_3 evolution with the aid of theoretical simulations.[45] Ironically, techniques such as structural and crystallographic tailoring, interface regulation, and defect engineering are reviewed to a large extent for heterogeneous NRR catalysts production.[46] There are also extensive reviews on general attempts to construct and apply 2D graphitic photocatalysts. Considering the crucial role of 2D−2D interfaces in such photocatalytic systems on the development of charge separation and the final photocatalytic efficiency, the synthesis, characterization methods, and stability of 2D-*g*-C_3N_4 structures were also covered, particularly focusing on water splitting applications.[47]

Thus, an overview of the relevant literature indicates that reviews covering the correlations among the structure, properties, and performance of C_xN_y materials with an exclusive attention to their electrocatalytic features should be prepared. Moreover, it was realized that a comprehensive and detailed description of the function of C_xN_y materials in the most referenced energy storage and conversion devices in a categorized manner is still missing, which can shed some light on the general realms of the preparation, modification, characterization and applications at the same time.

In the present account, we intend to provide a compressive overview of the electrocatalytic performance of C_xN_y-based materials in different applications. This Review mainly displays the advancements attained so far in C_xN_y-based electrocatalysts and gives multiple perspectives of the existing challenges experienced in the preparation of catalysts and their efficiencies. In the beginning of this study, the recently updated details of C_xN_y structures, synthesis methods, properties, possible modification routes, and general electrochemical mechanisms are reviewed. In the subsequent sections, the main focus is on the separate applications of C_xN_y materials in energy devices, including fuel cells, metal−air batteries, water splitting systems, and supercapacitors. In the following,

the performances of some synthesized C_xN_y architectures in various catalytic redox reactions, such as ORR, HER, OER, CO_2RR, NRR, etc., have been reviewed as well.

2. C_xN_y-BASED STRUCTURES

So far, various types of carbon nitrides (C_xN_y) structures with specific stoichiometries have been theoretically predicted or experimentally synthesized, as presented in Figure 1a–f. These structures can be categorized as 1:1 stoichiometry 3D CN,[48] layered C_2N,[49] 2D and 3D CN_2 structures,[50] layered C_3N,[51] C_4N_3,[52,53] spiral C_3N, and different C_3N_4 structures that will be explained in the following sections.[54] Imidazole-based ionic liquids have been assumed to be appropriate precursors for the synthesis of a number of C_xN_y structures, such as C_4N_3 for which EMIm (1-ethyl-3-methylimidazolium) and BMIm (1-butyl-3-methylimidazolium) were applied.[52] Similarly, 1,2-diaminobenzene was considered to be a possible precursor for the fabrication of spiral-C_3N.[54] However, in an elemental synthesis approach that applied high pressure and temperature, no organic precursors were used for C_xN_y synthesis.[48]

Regarding theoretical investigations, multiple structural phases have been proposed for C_3N_4-based materials (Figure 1g–i), including α-C_3N_4, β-C_3N_4, cubic C_3N_4, pseudocubic C_3N_4, and graphitic compounds (g-C_3N_4) such as g-h-triazine, g-h-heptazine, and g-o-triazine.[55,56] Among them, it is recognized that g-C_3N_4 is the most stable allotrope under ambient conditions, where the 2D π-conjugated layers with *s*-triazine or tri-*s*-triazine (s-heptazine) rings are linked via tertiary amines. The tri-*s*-triazine lattice has larger carbon vacancies and is more stable energetically than the other isomer at ambient temperature. The tri-*s*-triazine units consist of a nitrogen species with a lone pair of electrons, which has a significant role in the electronic structure of g-C_3N_4. This lone pair of electrons creates the band structure by forming a lone-pair valence band and, along with the π-bonding electron states, stabilizes the lone-pair state.[57] Similar to graphite, g-C_3N_4 has a planar structure with atoms located in a honeycomb configuration, with covalent forces within the layers and van der Waals interactions between the layers supporting the semiconducting properties.[56,58]

g-C_3N_4 exhibits unique physicochemical properties and has a yellow powder appearance with polymeric condensed tri-*s*-triazine (C_6N_7) units in each layer. According to thermal characterizations, the C–N heterocycles existent in the g-C_3N_4 framework led to a stable structure up to almost 600 °C in an air atmosphere. Besides, its chemical stability does not allow g-C_3N_4 to be dissolved in organic, basic, or acidic solvents. g-C_3N_4 is a metal-free semiconductor with a low band gap of 2.7 eV. g-C_3N_4-based materials have more advantages, such as high surface areas, chemical stability, and good selectivity. In addition, g-C_3N_4 is the most stable phase of C_xN_y materials in ambient conditions. Different synthetic approaches can prepare different morphologies of g-C_3N_4. Bulk g-C_3N_4, one of the forms of g-C_3N_4, has a 3D structure like graphite. Bulk g-C_3N_4 can be synthesized from the pyrolysis of urea, melamine, and dicyandiamide. This basic form has shown poor electronic features such as a high contact resistance and slow reaction kinetics, owing to the stacking of the layers. In the bulk form, however, poor properties such as the high contact resistance, large band gap, small surface area result in an inefficient final performance in terms of conductivity, catalysis, etc.[61] However, some methods for improving the features of g-C_3N_4 include exfoliating bulk g-C_3N_4 into nanosheets, nanotubes, and quantum dots; doping g-C_3N_4 with other elements; and composing g-C_3N_4 with another material. The exfoliation of g-C_3N_4 into 2D nanosheets can be performed due to the strong covalent bonds between the carbon and nitrogen atoms and the weak van der Waals forces of attraction between the layers of bulk g-C_3N_4. Thermal exfoliation, chemical exfoliation, and liquid exfoliation are three common approaches for producing g-C_3N_4 nanosheets with high surface areas. Moreover, the exfoliation process can reduce the g-C_3N_4 band gap.[62−64] In chemical exfoliation, reagents such as concentrated sulfuric, nitric, and hydrochloric acids have been applied, and the exfoliation degree is dependent on reagent's concentration. However, this approach is not ecofriendly and has some disadvantages, such as a low yield, poor controllability, long and tedious processes. In thermal exfoliation, the weak van der Waals forces of the attraction between the layers of g-C_3N_4 are broken by heat. A reaction between oxygen and the hydrogen attached to the tri-*s*-triazine occurs during the heating process, forming gas that causes the formation of pores in the bulk g-C_3N_4. However, the thermal exfoliation route provides the material with a low crystallinity and a relatively low surface area. During the liquid exfoliation process, the bulk g-C_3N_4 is sonicated in a suitable solution.[62] Increasing the exfoliation degree increases the number of nitrogen vacancies by reducing the N species of the triazine rings (C—N═C), providing a large surface area and high catalytic activity.[65,66] Therefore, the exfoliation of g-C_3N_4 can provide a porous structure and a large surface area.

C_xN_y materials can adopt distinct structures of bulk or nanostructures. C_xN_y nanostructures are produced with multiple morphologies, from zero-dimensional (0D) to three-dimensional (3D) structures such as nanospheres, quantum dots, nanorods, nanotubes, and nanosheets. Among these morphologies, 1D and 2D nanostructures have become major research focuses due to their high surface area and C/N aspect ratio and significant ionic and electronic charge transportation properties along the longitudinal axes.[67] For instance, due to their unrivalled photocatalytic activities, g-C_3N_4 tubes have been found to be appropriate candidates for both photosynthetic water splitting and CO_2 reduction.[68] Multiple g-C_3N_4 hybrid structures have been introduced to this point. Among these compounds, binary nanocomposites, g-C_3N_4–carbon nanomaterial composites, g-C_3N_4–metal sulfide nanocomposites, and nanocomposites with conductive polymers were recently categorized.[56]

It is possible to control the structure of g-C_3N_4 through a number of preparation paths, including the different precursor ratio, the condensation temperature, the porosity, and doping.[69] CN 3D nanoarchitectures are normally obtained from 0D–2D building blocks and are of great interest due to their large interconnected surface area and accompanying simple molecule-transfer capability; however, for fabrication purposes, 3D porous structures of g-C_3N_4 are almost challenging. In addition, the sp^2 graphitic network endows a unique structure with a significant surface area to the 2D CN materials, turning them into exceptional architectures; for example, a clear increase in the density of states at the conduction band has been theoretically exhibited by g-C_3N_4 ultrathin nanosheets compared to their bulk rivals. Meanwhile, 1D g-C_3N_4 nanostructures such as nanofibers, nanotubes, and nanorods also exhibit significant electronic and electrochemical properties as a result of their light-harvesting and mass transfer capabilities and large surface area.[69] Furthermore, in contrast

to other hazardous nonenvironmentally friendly semiconductor quantum dots, 0D g-C_3N_4 nanostructures, which commonly possess a few thousand atoms, have attracted attention due to their excellent quantum confinement effects, which lead to nontoxicity on the one hand and both fluorescence and water solubility on the other.[69,70] Various morphologies of g-C_3N_4 are represented in Figure 2.

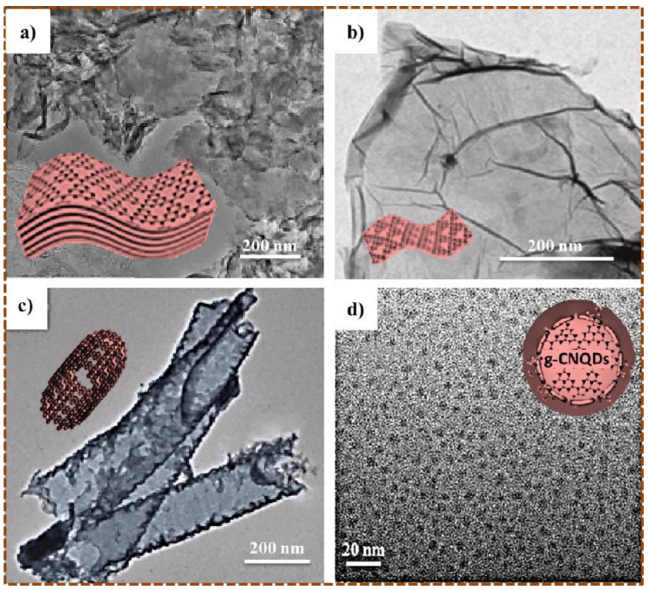

Figure 2. Multiple morphologies of g-C_3N_4, including (a) 3D (bulk) g-C_3N_4/graphene nanocomposites (SEM image), (b) 2D g-C_3N_4 nanosheets (TEM image), (c) 1D g-C_3N_4 nanotubes (TEM image), and (d) 0D g-CN quantum dots (TEM image). Panel a was reproduced with permission from ref 71. Copyright 2016, American Chemical Society. Panel b was reproduced with permission from ref 72. Copyright 2014, Wiley-VCH. Panel c was reproduced with permission from ref 53. Copyright 2016, American Chemical Society. Panel d was reproduced with permission from ref 73. Copyright 2014, American Chemical Society.

By exploring the processing techniques of g-C_3N_4 to produce more qualified C_xN_y structures, their thin films, hierarchical structures such as hydrogels, and hybrid compounds such as g-C_3N_4 or carbon nanotubes and graphene hybrids could be accounted for.[74]

3. SYNTHESIS METHODS OF C_XN_Y

In general, g-C_3N_4-based structures can be produced by replacing C atoms with N atoms through chemical and physical routes, which fall in the diverse categories listed in Figure 3. As the main preparation route of the chemical methods, thermal condensation is focused with the aid of organic oxygen-free and nitrogen-rich precursors.[75] Accordingly, compounds free of a direct C−C bond,[55] such as melamine, urea, thiourea, cyanimide, dicyanamide, etc., have been typically adopted as the chief nitrogen-rich precursor materials with respect to whether *s*-triazine (C_3N_3) or tri-*s*-triazine (C_6N_7) units would be formed as the C_3N_4 initial blocks based on the reaction path employed.[76,77] Predominantly, the precursor molecules tend to condense to melamine via nucleophilic addition or polycondensation, and the g-C_3N_4 structure forms through the subsequent polymerization of the achieved basic units along with a temperature increase.[78] Normally, the synthesis processes take place either in the air or inert atmosphere, which does not alter the bulk structure. However, it may affect the surface properties of the obtained product. It has also been realized that the basic environment may help the condensation reactions proceed at lower temperatures.[75] Additionally, the chemical acidic etching of g-C_3N_4 results in the formation of a nanoperforated structure.[79] The KOH-aided strategy was also examined for the sufficient construction of in-plane holes and $\pi-\pi$ electronic conjugated links. The physical synthesis method is another preparation approach that includes methods such as sputtering, which can be used to deposit vertically arranged crystalline g-C_3N_4 arrays on nickel or silicon substrates.[80]

The two famous nanostructure preparation strategies include bottom-up and top-down approaches that are typically used for the synthesis of C_xN_y-based materials. A number of preparation routes for the synthesis of C_xN_y-based nanocomposite electrocatalysts are specified in Figure 3. Thus far, multiple fabrication methods have been utilized to prepare C_xN_y-based nanostructures for various purposes, including physical and chemical vapor deposition, thermal condensation, microwave-assisted processes, electrodeposition, hydrothermal and solvothermal synthesis routes, sol−gel processes, thermochemical reactions such as pyrolysis and combustion, and polymerization.[35,55,81] As illustrated in Figure 4a, Fe-TCNQ (Fe-7,7,8,8-tetracyanoquinodimethane) metal−organic frameworks (MOFs) were synthesized through a hydrothermal method and then pyrolyzed to form Fe_3C/CN core−shell structures.[82] According to Figure 4b, g-C_3N_4 was produced by the thermal polycondensation of dicyandiamide followed by the design of Cu_3P with g-C_3N_4 on 3D-graphene through drop casting.[83]

A straightforward two-step method containing pyrolysis (PDA and Fe^{3+}) and acid leaching (0.2 M HCL) was employed to fabricate Fe_2N−mesoporous nitrogen−graphitic carbon spheres (Fe_2N/MNGCS) as ORR electrocatalysts with a high efficiency. Ultrafine Fe_2N nanocrystals were synthesized and introduced into the mesoporous N_2-doped graphitic carbon spheres as depicted in Figure 4c, where Fe^{3+} assisted the graphitization of PDA and promoted its mesoporous structure.[84] CN nanosheets were fabricated by thermal condensation using urea, and their surfaces were then hydrothermally decorated with Pt−Au architectures[85] as shown in Figure 4d. Using urea as the precursor, g-C_3N_4 was prepared via rapid combustion. Pd nanoparticles were then deposited on the g-C_3N_4 support through a photoassisted method to achieve Pd-*g*-C_3N_4 nanocomposites[86] (Figure 4f). The thermal condensation of melamine and thiourea was applied to obtain S-doped g-C_3N_4. Together with the S-*g*-C_3N_4, Ni and Fe precursors were dispersed in a deep eutectic solvent (DES) solution, and the mixture was then treated hydrothermally to attain NiFe-LDH (layered double hydroxide)/S-GCN hybrids[87] (Figure 4g). The prepared CN materials mainly possess a bulk structure with a low surface area, and a few active sites are weakly dispersed. Thus, they have not been very successful in certain catalysis and biological applications.[81] In order to vanquish such restrictions, the synthesis of porous structures and nanomaterials based on g-C_3N_4 has become popular due to the amplified surface area, which could promote the physicochemical properties and, as a result, the final applications.[55,78] To create new controllable C_xN_y structures with ordered porosity and diverse morphologies, templating and nontemplating approaches have been employed to design hollow and porous phases of CN. As in

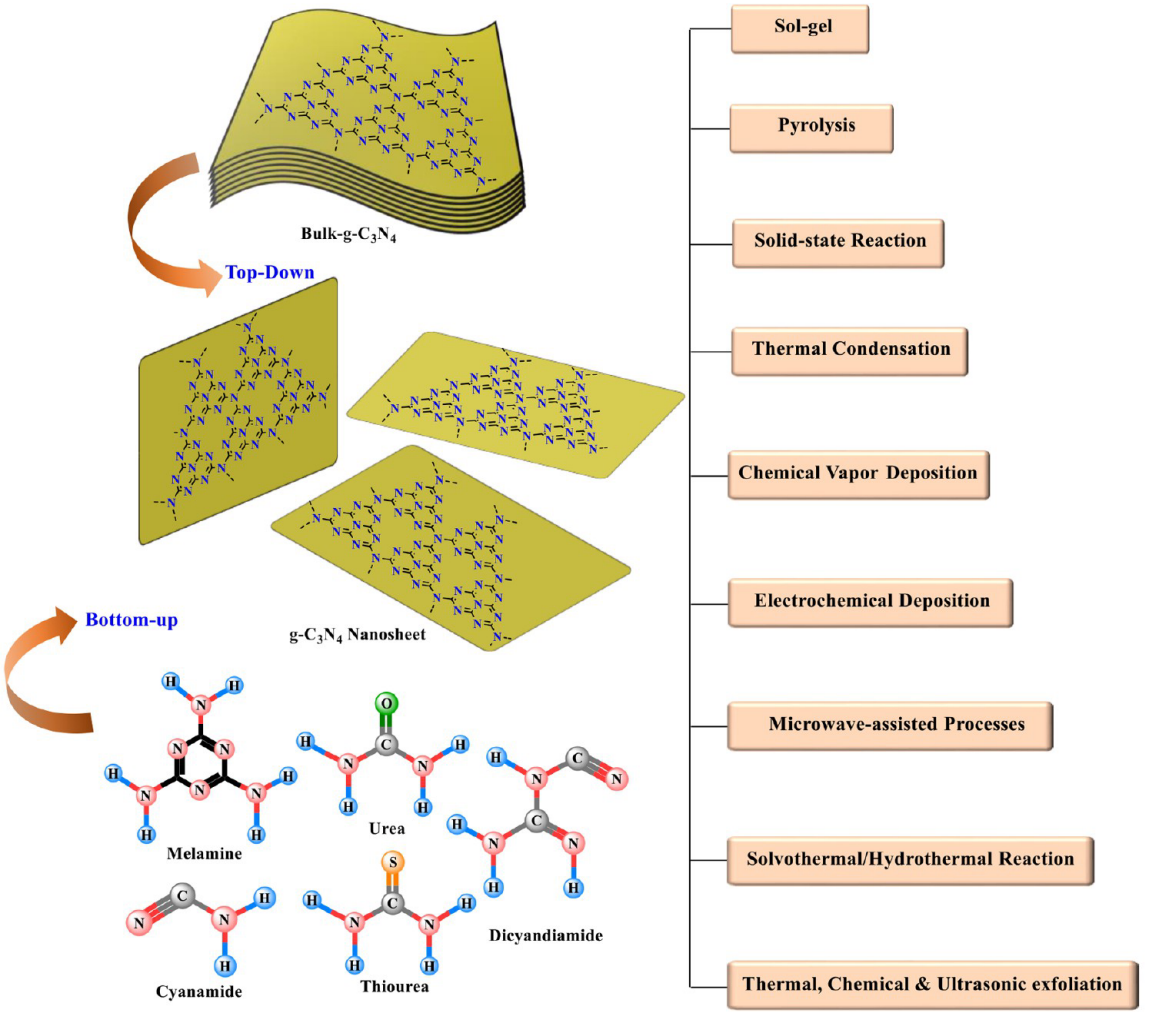

Figure 3. Various methods for the fabrication of graphitic carbon nitride-based composites.

Figure 4e, porous polydopamine nanospheres were prepared using a colloidal amphiphile-templating approach (CAM@PDA), and Fe_3C@mCN nanohybrids were then produced by loading Fe^{3+} into the polymer nanosphere framework.[88] C_xN_y structures also include nanoarchitectures with multiple dimensions, including nanoparticles, nanodots, nanosheets, nanofibers, nanorods, and nanocomposites.[78,81] Regarding nontemplating practices, a top-down template-free approach was employed to synthesize a porous carbon nitride (PCN) structure in order to prepare a CoS_x@PCN/rGO composite as an electrocatalyst. The PCN material was produced using the O_2 atmosphere pyrolysis of Co^{2+}/melamine networks, which was followed by the incorporation of graphene and CoS_x nanoparticles. Through the addition of graphene oxide (GO) to the as-synthesized PCN and a thermal process in the sulfur atmosphere to complete the sulfurization step, the CoS_x@PCN/rGO catalyst was developed.[89]

Templating methods are recognized as two categories of hard and soft templating techniques (Figure 4e). On the one hand, hard templating methods, also called nanocasting, are based on the use of hard structure-directing agents and pyrolysis reactions together with precursors. Some of such templates include silica nanoparticle colloids and their mesoporous structures and anodized alumina. This process is usually followed by an etching step using HF, NH_4HF_2, or other different strong alkaline solutions, which finally results in the desired nanomaterials.[90] However, most of the synthesis procedures and various steps involving foreign materials may cause impurities in the products, which subsequently impact the electrocatalysis performance.[33] On the other hand, soft-template fabrication employs soft structure-directing agents such as ionic liquids and amphiphilic block polymers to synthesize PCN, which cause less harm to the environment. In addition, a self-templating or template-free method of supramolecular self-assembly is a potential bottom-up technique that gives rise to sufficiently stable noncovalently bonded structures.[78] Although the application of suitable hard or soft templates within the synthesis process brings about benefits like a tunable size and larger surface area, it requires the use of toxic, expensive, and nongreen etchants to eliminate the templates afterward.[81] Correspondingly, it was realized that templating could improve the surface area of phosphorus and fluorine codoped CN nanocatalysts while simplifying the codoping process itself, which decreased the optical band gap and led to the enhanced photocatalytic reduction of CO_2 to methanol.[91] Besides, the interference of mainly F-containing agents is avoided through the use of non-templating methods, which is preferable for the design of g-C_3N_4 nanostructures.[81]

Thermal, chemical, and ultrasonic exfoliation[55] of bulk g-C_3N_4 into uniformly dispersed novel nanostructures, such as

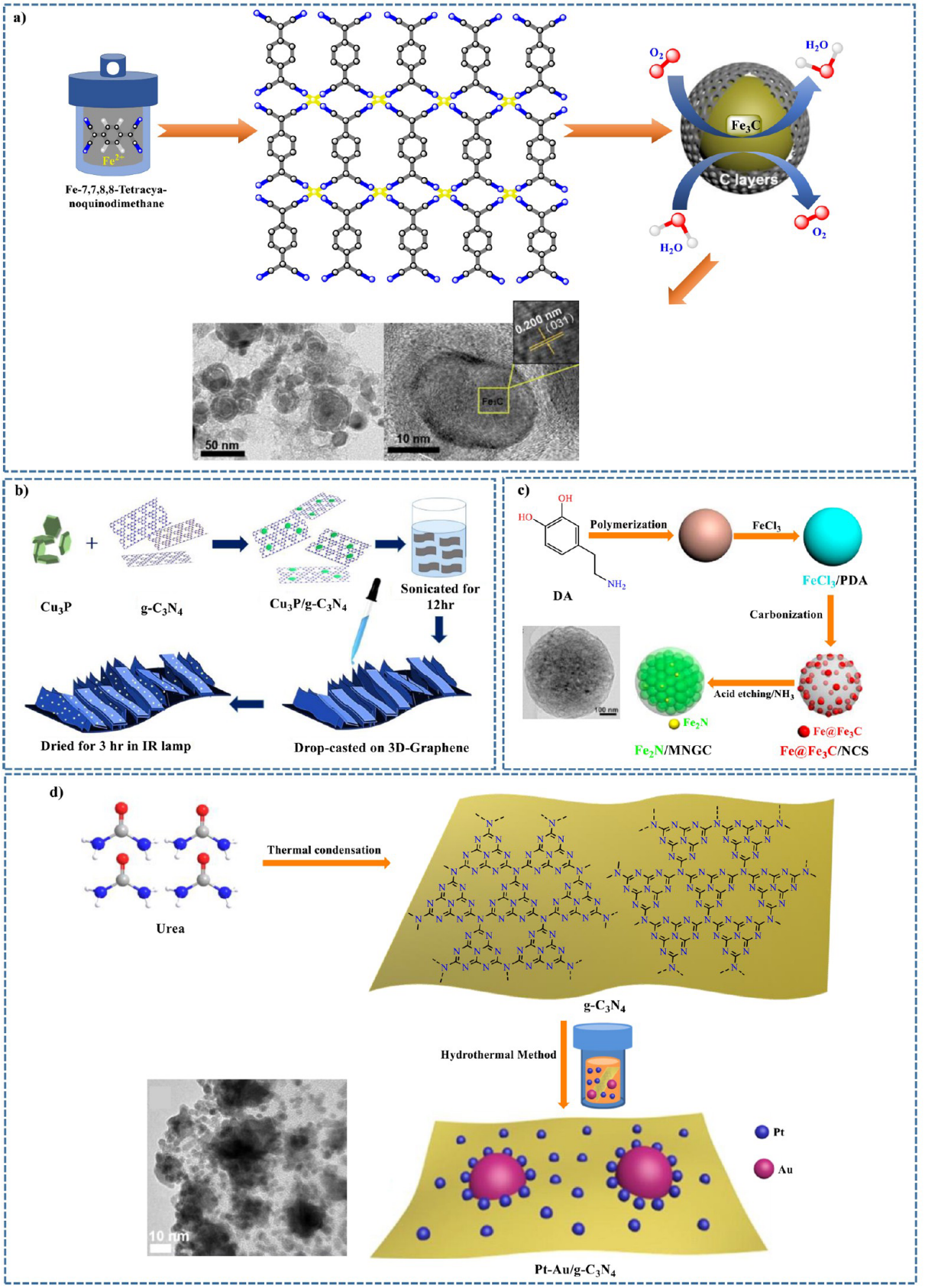

Figure 4. continued

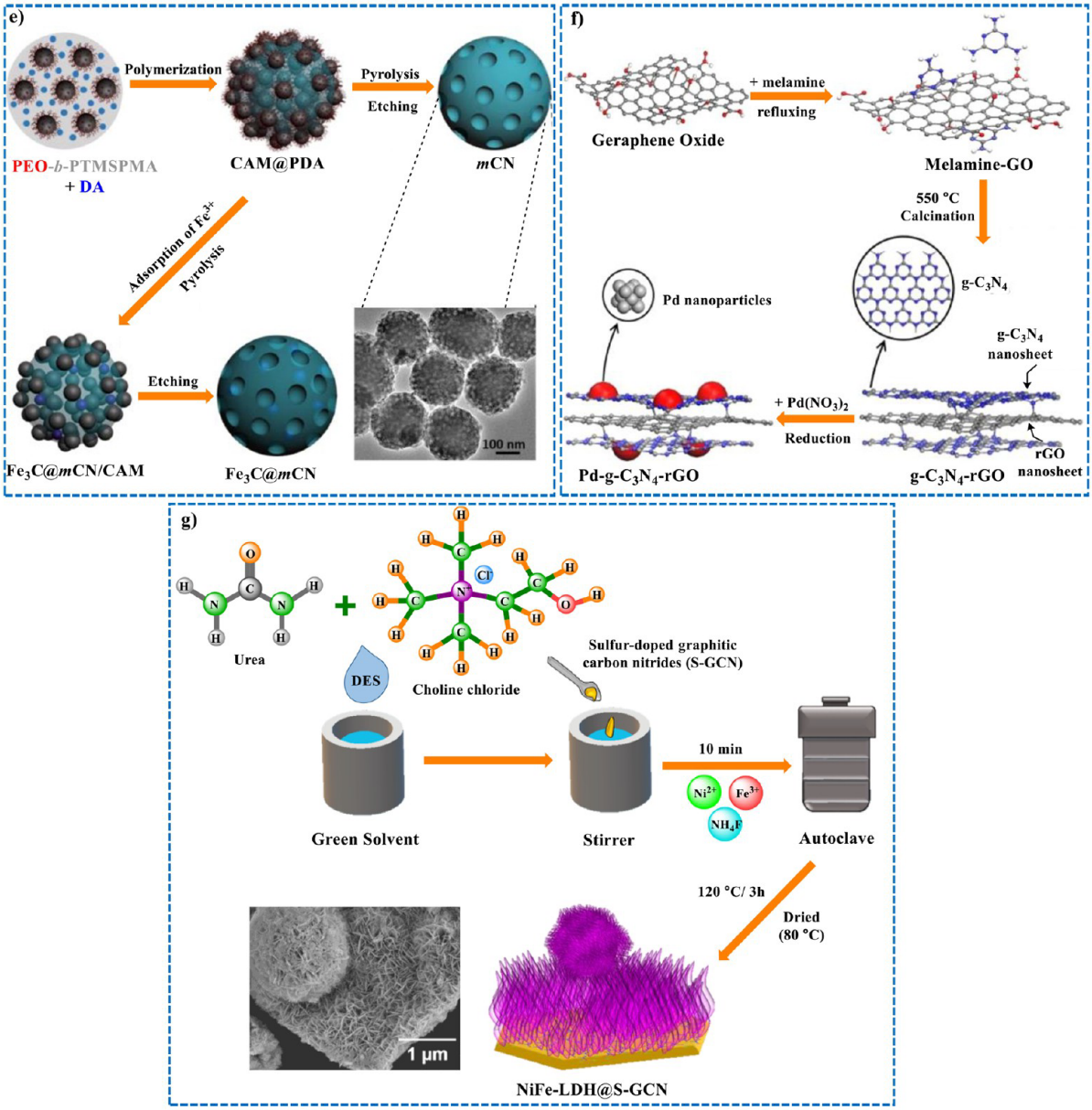

Figure 4. Representation of different synthesis routes of g-C_3N_4-based composites. (a) Hydrothermally assisted iron carbide encapsulation by porous carbon nitride ($Fe_3C@CN_x$). Reproduced with permission from ref 82. Copyright 2018, Elsevier. (b) Synthesis of hexagonal Cu_3P via thermal polycondensation, followed by the decoration of 3D graphene with a g-C_3N_4/Cu_3P composite by drop-casting. Reproduced with permission from ref 83. Copyright 2020, Wiley-VCH. (c) Mesoporous Fe_2N/MNGCS electrocatalysts fabricated through pyrolysis. Reproduced with permission from ref 84. Copyright 2016, Elsevier. (d) Diagram of the Pt−Au/CN hydrothermal synthesis process. Reproduced with permission from ref 85. Copyright 2020, Elsevier. (e) Colloidal amphiphilic CAM-template-assisted fabrication of Fe_3C@mCN electrocatalysts. Reproduced with permission ref 88. Copyright 2016, Royal Society of Chemistry. (f) Preparation of Pd-g-C_3N_4-rGO electrocatalyst composites through quick combustion. Reproduced with permission from ref 92. Copyright 2014, Royal Society of Chemistry. (g) Deep eutectic solvent (DES)-assisted hydrothermal preparation of NiFe-LDH/SGCN. Reproduced with permission from ref 87. Copyright 2020, American Chemical Society.

nanosheets, and post-thermal oxidation treatments fall under top-down methods, which are commonly performed by external forces. In return, using bottom-up routes, the anisotropic assembly of specific organic molecules occurs in growth media such as templates or favorable structure-directing agents.[78] A nanocomposite containing g-C_3N_4 and reduced graphene oxide (rGO) was produced using an in situ chemical process via the covalent coupling of the components. Additionally, palladium (Pd) nanoparticles (3.83 nm) were loaded via a soft chemistry process to complete the electrocatalytic hybrid structure, as shown in Figure 4f. Concerning instances of the bottom-up approach, a solvothermal method was utilized for the synthesis of a g-C_3N_4@RGO composite through a reflux process. Through the formation of hydrogen bonds between the amine groups in melamine and the oxygen groups in GO, together with the affinity for H_2O molecules, g-C_3N_4 was adsorbed and grown on the GO surface without a pyrolysis step. High contents of N (6−18 at. %) were achieved in addition to a 3D network structure. Moreover, Pt nanoparticles of 2−4 nm in diameter

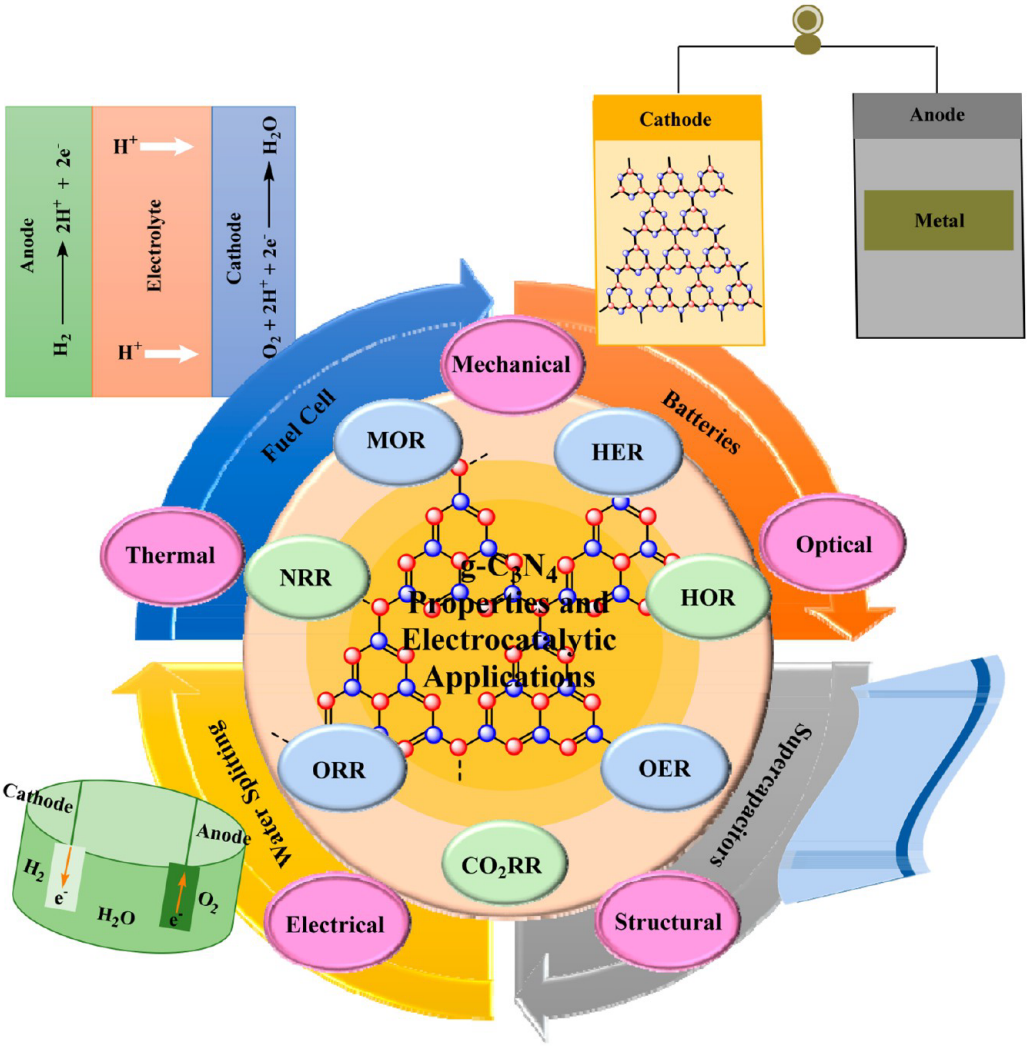

Figure 5. General properties of g-C_3N_4 structures suitable for use in various electrocatalytic applications.

were uniformly dispersed on the as-synthesized g-C_3N_4@RGO through a polyol procedure.[93] In order to produce a g-C_3N_4 nanocomposite with enhanced ORR electrocatalytic performance, the electrospinning technique was employed to produce dense and multilayered nanofibers of poly(vinyl) alcohol (PVA). Carbon nitride (CN_x) nanoparticles were homogeneously dispersed in the nanofibers to induce catalytic activity in the CN_x/PVA nanostructure.[94]

4. VARIOUS PROPERTIES OF C_xN_y-BASED MATERIALS

As mentioned earlier, C_xN_y is known for its various allotropes with different names and qualities, among which g-C_3N_4 has the most stable structure under ambient conditions.[95] In the following, the general and fundamental properties of g-C_3N_4, as shown in Figure 5, are briefly reviewed.

g-C_3N_4 is an easy to synthesize, low-cost, and nontoxic indirect semiconductor with a medium band gap suitable for sustainable chemistry. Regarding its electrical properties, a band gap equal to 2.7 eV was determined for g-C_3N_4, and the positions of the conductive and valence bands were respectively characterized at −1.1 and 1.6 eV (vs. NHE); these values are ideal for conduction pertaining to oxidation−reduction reactions. The features mentioned suggest that g-C_3N_4 is a multifunctional photocatalyst applicable under visible light irradiation, particularly for water splitting. Besides, such an attractive electronic structure introduces this metal-free catalyst as a promising option for use in electrochemical cells and energy conversion systems in general. The theoretical application of perpendicular electric fields up to 10 V nm^{-1} to a heptazine monolayer was evaluated; no change in its electrical properties was indicated, and there was no detectable buckling in its structure.[96] While g-C_3N_4 is known as a semiconductor, it exhibits a reconstructed structure with half-metallic characteristics. Density functional theory (DFT) calculations for g-C_3N_4 indicate its high electron mobility and reasonable electrical conductivity, facilitating electron release and injection mechanisms, namely for CO_2 capture.[97]

On the basis of optical characterizations of g-C_3N_4, its absorption pattern is attributed to organic semiconductors (at around 420 nm). Typically, under ambient temperature, g-C_3N_4 presents photoluminescence over a wide range from 430 to 550 nm with a maximum at 470 nm, exhibiting blue photoluminescence.[98] Additionally, a desirable two-photon absorbance performance was proven for g-C_3N_4, whose concomitant absorbance of two near-infrared photons was followed by bright fluorescence emission with a visible-light wavelength.[99]

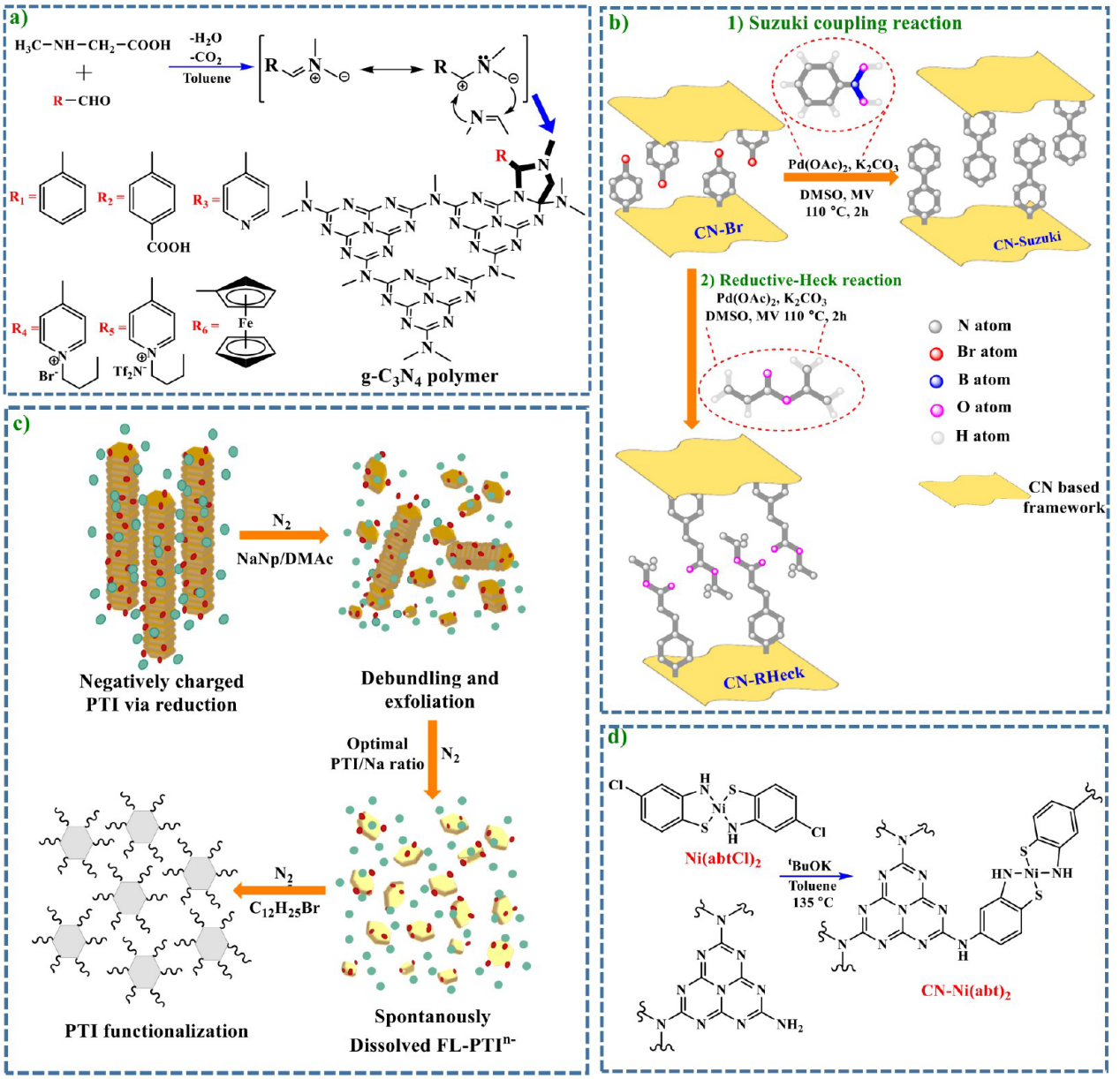

Figure 6. Schematic illustration of different g-C_3N_4 surface modification methods. (a) Cycloaddition: 1,3-dipolar cycloaddition reaction of azomethine ylides with pure g-C_3N_4. Reproduced with permission from ref 111. Copyright 2014, Royal Society of Chemistry. (b) Cross-coupling reaction: post-covalent functionalization of CN-Ph-Br through Suzuki and reductive Heck reactions. Reproduced with permission from ref 112. Copyright 2018, Wiley-VCH. (c) Reduction: polytriazineimide surface charging and exfoliation. Reproduced with permission from ref 113. Copyright 2018, Wiley-VCH. (d) Miscellaneous surface functionalization: covalent addition of molecular catalysts on g-C_3N_4. Reproduced with permission from ref 114. Copyright 2020, Royal Society of Chemistry.

Due to its low weight and metal-free structure, g-C_3N_4 presents a high mechanical power similar to those of other carbon nanomaterials.[100] Based on molecular dynamics simulations, g-C_3N_4 is a significantly flexible and strong 2D material appropriate for the mechanical reinforcement of polymers, thus expanding their commercial applications. Besides, in the *s*-triazine-based form, the thermal conductivity level along the armchair direction was reported to be almost 12% higher than that along the zigzag direction.[101] A number of polymers were blended with g-C_3N_4 to fix their thermomechanical, tribological, and surface drawbacks, including polyimide, polyurethane, epoxy, wood plastic, etc. However, effort is still required to achieve the enhanced structural stability and surface area of g-C_3N_4 as a reinforcing nanofiller.[100] Moreover, DFT calculations demonstrated that while the Poisson's ratio of a heptazine monolayer was half that of a graphene structure, its in-plane stiffness was comparable with graphene; based on calculations of their elastic and yielding points, heptazine is able to resist longer tensions in the plastic zone.[96]

Concerning C_xN_y materials, their general structural and chemical properties include low friction coefficients, low densities, super hardness, wear resistance, considerable chemical inertness, and biocompatibility.[102,103] The ring-like structure of tri-*s*-triazine provides it with a high chemical stability in both acidic and alkaline media.[104] Additionally, both triazine and heptazine exhibited lower toxicities than graphene oxide, and triazine was found to be more cytotoxic to

lung carcinoma epithelial cells when the two C_xN_y structures were compared; however, both had dose-dependent toxicological effects.[105]

Thermal characterizations have almost explained the high temperature for the full decomposition of C_xN_y (about 750 °C, at which no remnant is deposited), which offers strong thermal stability for high-temperature operations and also for the preparation of refined carbon nanostructures. However, fabrication procedures may have a corresponding effect on this temperature. Moreover, remarkable chemical stability was measured for g-C_3N_4 structures, for instance, in response to acid corrosion and alkaline solutions.[55,98] Stable aqueous dispersions of g-C_3N_4 are also ascribed to its negative surface charge depriving the solutions of aggregation.[98,106] Although the addition of nanoparticles, such as Au, for catalytic modification may require an intermediate to regulate the stability, biopolymers are economical and available compounds applied for dye removal, heavy metal ion removal, and other environmental and industrial applications that are ideal candidates for this purpose.[107] Appropriately, the modification of Au nanoparticle−CN hybrids for the HER was performed using chitosan, which efficiently decreased the aggregation of Au nanoparticles and increased both the stability and the catalytic activity of the C_xN_y structures.[108]

5. MODIFICATION AND FUNCTIONALIZATION METHODS FOR C_XN_Y-BASED MATERIALS

In order to improve the catalytic properties of catalysts, including C_xN_y-based materials, a common strategy is associated with certain modifications of the C_xN_y structures. It includes metal or nonmetal ion doping,[62] heterojunction creation,[109] the generation of carbon defects, the addition of plasmonic compounds, the incorporation of defects, and vacancy formation, as explained individually in the following paragraphs.[110] These methods of functionalizing the g-C_3N_4 surface create anchoring sites for adjusting the electronic and chemical properties. The covalent and noncovalent strategies include oxidation or reduction, cycloadditions, couplings, and noncovalent interactions.[74] In Figure 6, a comprehensive schematic of various g-C_3N_4 surface functionalization paths is illustrated.

Metal/nonmetal ion doping is one of the effective approaches to enhance the catalytic behavior of carbon nitride structures, as their pure forms suffer from a limited light absorption range. By entrapping the electrons, doping elements more effectively reduce the band gap and increase the charge separation efficiency. g-C_3N_4 can be doped with metal ions, including iron, zinc, cobalt, and bismuth, and nonmetal ions.[115] For instance, Ni-doped g-C_3N_4 exhibited a high peak current density in the electrochemical oxidation of ethanol, suggesting a correlation between the increased photocatalytic and electrochemical activities of the metal-doped C_xN_y materials and their structural modification while preserving the original morphology. The incorporation of nonmetal elements (N, P, S, etc.) into g-C_3N_4 produces more visible-light-sensitive photocatalysts, as the nonmetal element adjusts the physicochemical characteristics in terms of the particle size, surface, and thus the optoelectrical properties. Such manipulation induces a delay in the electron−hole recombination and leads to an extension of the visible-light absorption. Among nonmetals, O, N, C, S, and P are the major elements that are chemically doped to optimize the catalytic application of g-C_3N_4 nanocomposites.[116] Despite all the beneficial effects of doping, the dopants may not act positively on the electrocatalysis functions of some nanomaterials. Therefore, a wider review of the impact of dopants, and impurities in particular, on carbon-based electrocatalysts should be considered based on the recent research, as explained below.

Carbon nanomaterials such as carbon nanotubes (CNTs) and graphene, transition-metal dichalcogenides (TMDs), and black phosphorus are materials with different electrocatalytically active impurities that originate from the precursors and parent materials or remain after growth, exfoliation, and washing steps. The main impurities in carbon nanotubes, graphene, and black phosphorus are metallic, although the valence oxides and sulfides and phase impurities in TMDs are considered to leave the key effects in addition to the metallic impurities.[33] In this respect, it has been realized that certain doping levels of these materials are required for their catalytic activity to appear when either TMD or graphene are employed for the OER and the CO_2RR. Meanwhile, in the cases of applying graphene toward the ORR and TMDs toward the HER, successful performances were achieved even without dopants.[117] In graphene, nonmetal dopants like N have been shown to elevate the electrocatalytic activity, while in the case of TMDs transition-metal doping has increased the functionality and compatibility.[117] In a study on the functionality of graphene nanoribbons (GNRs) toward the HER, the presence of impurities was examined by ICP-MS (inductively coupled plasma mass spectrometry) and XPS, and the effects of impurities on the final electrocatalytic activity were studied through linear sweep voltammetry. According to the results, XPS did not successfully detect the parts per million levels of such metallic impurities, while ICP-MS confirmed their presence. Moreover, HER results revealed that W-based metallic impurities were the possible active sites in the graphene nanoribbons, and the obtained electrocatalytic activity was higher than those of the reference GC and edge-plane pyrolytic graphite (EPPG) electrodes.[118] To compare real metal-free graphene and the graphene obtained from standard synthesis methods, ultrapure graphene was prepared, and the impurities were monitored and controlled with the aid of the ICP-OES system and neutron activation analysis. Based on the results, the metallic impurities were eliminated by the reactive thermal treatment of graphene, which resulted in a slightly lower heterogeneous electron-transfer rate and yet an almost nonexistent electrocatalytic activity. Accordingly, it was claimed that the metallic impurities in graphene electrocatalysts have the largest influence on the ORR reactions and that metal-free graphene is not catalytically active in this sense.[119] To explore the effects of electrolyte- and solution-born impurities on the electrocatalytic activity, $HClO_4$ electrolytes were used to examine Cl^- anion and NO_3^- impurities (from 10^{-7} to 10^{-6} M). The inevitable effects toward the ORR were demonstrated such that the impurities influenced the available sites for O_2, and the intermediate adsorption and deactivation rate was considerably enhanced when Cl^- was incorporated as the supporting electrolyte at the aforementioned concentrations. Furthermore, the electrocatalytic effect of Cu_{upd}−Pt on CO oxidation reactions was reported to be significantly different in alkaline solutions and acidic environments.[120] Similarly, the effects of Fe impurities on Ni-based catalysts were studied, revealing that the intrinsic performance of such catalysts drops remarkably with the removal of these impurities from the electrolyte, resulting in OER activities much lower than even those of Co oxides. A

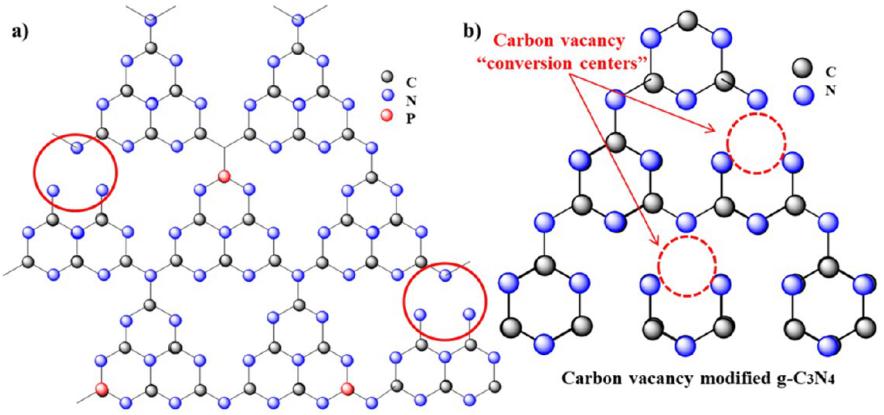

Figure 7. (a) Surface carbon defects and phosphorus doping in g-C_3N_4. Reproduced with permission from ref 132. Copyright 2017, Elsevier. (b) g-C_3N_4 modified with carbon vacancies (V_C-C_3N_4). Reproduced with permission from ref 133. Copyright 2019, American Chemical Society.

very scarce amount of Fe could decrease the OER overpotential to a large extent, while a considerable positive shift could simultaneously be observed in the reduction and oxidation potentials related to the existing Ni species.[121]

Although element doping is considered an efficient method for developing the performance of the g-C_3N_4 material, it involves some challenges that require accurate solutions and arrangements. Among these challenges, alterations in the g-C_3N_4 microstructure, including the loss of the graphitic structure and its effect on the in-plane ordering of the tri-*s*-triazine units, could be named. This implies that precise and comprehensive characterization results are needed to confirm the chemical states of the heteroatoms that exist in the doped g-C_3N_4 structure, and each of these techniques encounters shortcomings and challenges. As XPS is widely used for this purpose due to the simple determination of the bond types of the heteroatoms based on the peak positions, it should be noted that external factors may affect these XPS characteristic peaks. For instance, new XPS peaks regarding the in-planar distance computation of the nitride pores appear as a result of the replacement of C atoms in the corners by P atoms in P-doped g-C_3N_4 structures.[122]

Besides, other challenges still remain in doping strategies. Accordingly, the effective modulation of the HOMO and the LUMO with the orientation is required for high oxidation and reduction potentials. However, a profound understanding of doping-assisted origin of visible-light absorption, the nature of the newly born chemical states, and dopant locations is missing, the doping-induced photocatalytic enhancement mechanisms are not totally clear, and also it is vital to clarify the site and role of the metal ion and the heteroatom.[41]

The creation of a heterojunction (HJ) is another assisting contrivance to solve the g-C_3N_4 structure restrictions. The various types of HJs include Schottky, type II, and Z-scheme heterojunctions. Accordingly, the transfer of charges at the interface formed between the two structures would be prolonged such that charge transfer activities would not hamper the reaction process. Due to their separate active sites for reduction and oxidation and improved light-harvesting abilities, g-C_3N_4 with Z-scheme heterojunctions are among the most effective catalysts, exhibiting more straightforward charge transfer than type II heterojunctions.[123] Correspondingly, through the creation of an effective heterojunction consisting of TiO_2 and g-C_3N_4, improved visible light absorption and declined charge recombination were reported in Cu−Ni-based nanostructure-modified TiO_2/g-C_3N_4 nanorods as PEC catalysts.[124] In this regard, a hydrothermal synthesis process was used to obtain nanocomposites with nanodimension hierarchical heterostructures. Cu, Ni, and bimetallic Cu−Ni nanoparticles were homogeneously incorporated into g-C_3N_4, which exhibited enhanced methanol oxidation reaction (MOR) activity when exposed to visible-light illumination.[125]

Despite the numerous successful examples of heterojunctions, especially in terms of their superior photocatalytic activity over that of isolated C_xN_y, there are still limitations involved in the deep realization of charge carrier dynamics and consequently the design of rational optimal junctions. To monitor the charge carrier dynamics in heterojunctions, time-resolved photoluminescence techniques and absorption spectroscopy methods have normally been used. However, finding correlations between the lifetime and the activity has not resulted in a clear trend because of the inconsistent monitoring of the reactive charges, which shadows the anticipated links between interfacial charge separation and shorter or longer charge lifetimes such that clear consistency is often not found while the charge lifetime is observed, even when similar materials are used in the junction. Thus, to provide a model for understanding the charge dynamics and activity links, more accurate spectral assignments are required.[126] Further, the composition of the components in a heterojunction is a very determinative factor, and high-performance heterojunctions are usually achieved by the overwhelming trial and error method.[127]

Moreover, through the introduction of carbonaceous materials into g-C_3N_4 matrices, new compensated properties are created rather than each individual component, particularly regarding the photocatalytic activity. The combination of systems with π-conjugation contributes to the stabilization of the created hybrids with extended optical wavelength absorption with respect to solar spectra. This is attributed to the lowered band gap position along with the improved electron channelization and charge separation.[128]

In spite of the prodigious developments in the incorporation of carbonaceous materials into C_xN_y (photo)catalysts, critical limitations still need to be resolved. In surface modifications, the interface contacts may not become so intimate, giving rise to weak bond strengths and electron transport. Thus, enhanced compatibility between the carbon additive and the catalyst is required. Moreover, carbon nanomaterials, such as carbon dots, nanotubes, etc., in their powdered forms are quite

challenging to recycle after the process is over, leading to possible secondary pollution. This is why 3D solid (photo)-catalysts are favored while 3D carbonaceous ones are currently limited in number. However, adequate stability should be ensured via the direct assembly of the composites. Besides, for a better mechanistic understanding of carbon-aided catalysis of these materials, a comparable testing standard, such as the whole type of junction established, should be considered in addition to the existing fundamentals.[129]

The incorporation of plasmonic metals, such as Pt, Au, Ag, etc., is employed to produce g-C_3N_4-based composites with enhanced characteristic activities. In this way, the metal experiences electronic excitation through the absorption of electromagnetic radiation, which supplies an adequate amount of energy both for crossing the junction barrier and charge migration.[110,130]

Although the application of plasmonic metals for the catalytic improvement of C_xN_y materials is an efficient modification process, unfortunately these sorts of strategies are probably limited to lab-scale research because of their high cost. Typically, the chosen materials for modification should be cost-effective, abundant, and also nontoxic to fulfill the economic and environmental aspects of the process. Besides, the molecular orbitals and the charge transfer dynamics in noble-metal deposition and other modification strategies require deep investigations to uncover the basics of the (photo)catalytic improvement.[127]

Defects in the g-C_3N_4 structure, as depicted in Figure 7, are conventionally generated via thermal and chemical treatments in addition to other methods such as ultrasound and microwave-assisted measures.[131] The covalent approaches usually cause defects by damaging the sp^2 domains, dramatically affecting the electrical features. Nevertheless, by carefully tuning the defect density, the created defects can strongly aid the catalysis and composite applications.

One of the routes to modify the electronic band of g-C_3N_4 is the modification of its structure through induced C or N vacancies. This also increases the rates of charge separation and hole−electron movement. The relevant strategies for creating defective g-C_3N_4 with nitrogen or carbon vacancies mainly include post-heat processing under a H_2 or Ar atmosphere or with accompanying reductants, polymerization under special conditions and atmospheres, rapid thermal treatment, and copolymerization.[116] Because they provide extra energy levels and active sites, vacancies in g-C_3N_4 appear to be a practical path, especially for the fabrication of highly effective catalysts and other energy-related and environmental devices.[134]

The low-resolution characterizations do not allow us to correlate the features, structure, and activity of the catalyst or the defect degree. Besides, the vacancies may occur in different parts of the catalysts, including the body and the surface, requiring advanced techniques to quantify the amount of vacancy defects in the material. Thus, it is challenging to manage the type, location, and structure parameters of the defects simultaneously. As vacancies in CN catalysts are considered useful for light absorption yet inappropriate for redox activity, finding a threshold for decreasing the disadvantages and increasing advantages via optimized design seems quite necessary. Moreover, tuning the stability of the defect is difficult in terms of practical trials, as the influencing factors and the method of adjusting the format of the vacancies are still unclear. This adds to the ambiguous understanding of the structural evolution of defects during the catalytic process.[135]

Metal oxide doping and the formation of type-II and Z-scheme heterojunctions sound more common among the modification processes for enhancing the catalytic efficiency of g-C_3N_4.[130] However, the highest efficiency may be obtained through the integration of multiple modification strategies or codoping methods, benefiting from the synergistic results on the one hand and covering the drawbacks of each separate method on the other.[127]

6. C_XN_Y-BASED ELECTROCATALYTIC APPLICATIONS

6.1. General Mechanisms. Precise knowledge of the electron transfer during adsorption and catalysis processes should be acquired through exact calculations and sensitive characterization of active sites and transformation mechanisms.[136] Two-electron pathways are proposed for the ORR in an aqueous medium, namely (1) the reduction from O_2 to H_2O through four electrons and (2) the reduction of O_2 to H_2O_2 (hydrogen peroxide) by two electrons.[137] These pathways are explained in the following equations.

For an acidic solution,

$$O_2 + 4H^+ + 4e^- \rightarrow 2H_2O \quad (1)$$

$$O_2 + 2H^+ + 2e^- \rightarrow H_2O_2 \quad (2)$$

$$H_2O_2 + 2H^+ + 2e^- \rightarrow 2H_2O \quad (3)$$

For an alkaline solution,

$$O_2 + 2H_2O + 4e^- \rightarrow 4OH^- \quad (4)$$

$$O_2 + H_2O + 2e^- \rightarrow HO_2 - + OH^- \quad (5)$$

$$HO_2 - + H_2O + 2e^- \rightarrow 3OH^- \quad (6)$$

Since unfinished oxygen reduction occurs via the two-electron pathways, resulting in a lower energy conversion efficiency and the formation of intermediates and free radicals (as explained below), the four-electron pathway is favored for achieving high-efficiency fuel cell devices.[138]

In an acidic solution,

$$O_2 + 2H^+ + 2e^- \rightarrow H_2O_2 \quad (7)$$

$$H_2O_2 + 2H^+ + 2e^- \rightarrow 2H_2O \quad (8)$$

In an alkaline solution,

$$O_2 + H_2O + 2e^- \rightarrow OOH^- + OH^- \quad (9)$$

$$OOH^- + H_2O + 2e^- \rightarrow 3OH^- \quad (10)$$

When carbon electrodes are applied as the cathode, two successive reactions with the two-electron pathways dominate, producing H_2O_2 intermediates. The ORR mechanism is normally managed by parameters such as the electrode material, the current density, and the pH level. Accordingly, on glassy carbon and pyrolytic graphite electrodes, the ORR proceeds through the two-electron pathway, leading to H_2O_2 formation; however, H_2O_2 is later reduced to H_2O by the oxidized forms of the electrodes. Besides, ORR involves three rate-controlling steps as follows: (1) O_2 adsorption at the electrode surface active site, (2) bond dissociation of O_2, and (3) electron transfer. Generally, as used in alkaline electrolytes, carbon materials exhibit electrocatalytic efficiency toward the ORR. Graphite and other carbon-based electrodes usually

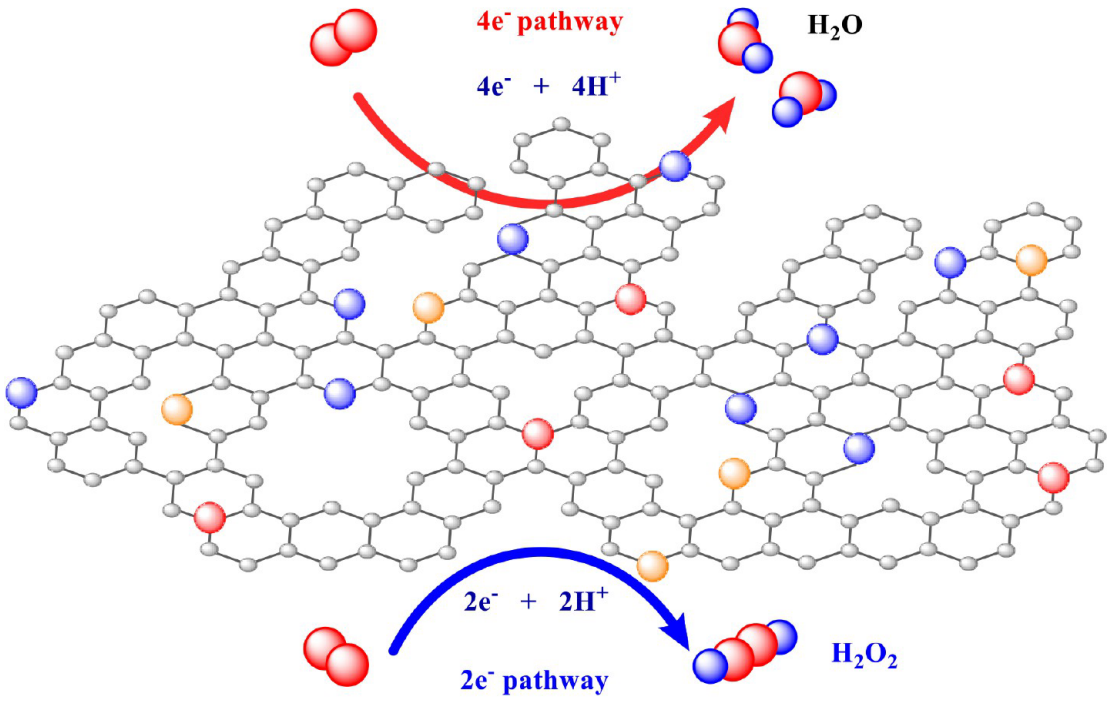

Figure 8. A schematic representation of the two ORR pathways on carbon electrocatalysts doped with a heteroatom. The four-electron pathway represents the full reduction of oxygen to water, while the two-electron pathway involves the partial reduction of oxygen to H_2O_2 for either direct use or a subsequent reduction to water. Reproduced with permission from ref 139. Copyright 2021, Royal Society of Chemistry.

encounter the ORR through a mechanism that depends on HO_2^- formation-assisted reduction.[137] The two-electron transfer pathways in the ORR are depicted in Figure 8.

Hydrogen evolution is the half-cell reaction at the cathode side in acidic electrolyzers, which can be defined as [$2H^+ + 2e^- \rightarrow H_2$]. In return, the anodic half-cell reaction is hydrogen oxidation in the fuel cell mode in the form of [$H_2 \rightarrow 2H^+ + 2e^-$], as explained in the following equations[140]

	at the fuel electrode (Anode)	at the oxygen electrode (Cathode)	
Electrolysis	$2H^+ + 2e^- \rightarrow H_2$	$H_2O \rightarrow \frac{1}{2}O_2 + 2H^+ + 2e^-$	(11)
Fuel cell	$H_2 \rightarrow 2H^+ + 2e^-$	$\frac{1}{2}O_2 + 2H^+ + 2e^- \rightarrow H_2O$	(12)

The overall reaction rate is mainly calculated based on the free energy of the hydrogen adsorption step. This step (Volmer) would be the limiting step when hydrogen and the surface are linked together very weakly, whereas the desorption phase (Heyrovsky and Tafel) would be the rate-limiting step for very strong linkages.[141]

The HER and the hydrogen oxidation reaction (HOR) are associated with the electrochemical generation of gaseous H_2 and the operation of the fuel cell anode, respectively. Both reactions are sensitive to the nature and structure of the electrode, and their rates depend on the hydrogen isotopes.[142] A heavier isotope forms a stronger bond, and the resulting molecules are less likely to dissociate. The increase in energy needed to break the bond results in a slower reaction rate and the observed isotope effect. The HER is explained as two reaction mechanisms of Volmer–Heyrovsky and Volmer–Tafel reactions. In the former type, hydrogen is generated through two initial stages (a and b), while in the latter type hydrogen is generated by the three subsequent initial stages.[143]

(a) Volmer reaction (hydrogen intermediate adsorbed):

$$H^+ + e^- + (\text{active site})^* \rightarrow H^* \quad (13)$$

(b) Heyrovsky and Tafel reaction (hydrogen desorption):

$$H^* + e^- + H^+ \rightarrow H_{2(g)} \quad (14)$$

(c) Volmer reaction (hydrogen intermediate desorbed):

$$H^+ + e^- + (\text{active site})^* \rightarrow H^* \quad (15)$$

(d) Volmer reaction (hydrogen intermediate adsorbed):

$$H^{*+}H^+ + e^- \rightarrow 2H^* \quad (16)$$

(e) Heyrovsky and Tafel reaction (hydrogen desorption):

$$2H^* \rightarrow H_{2(g)} \quad (17)$$

When hydrogen evolution takes place, hydrogen fuel can be produced as water or protons are reduced at the electrode's surface,[137] the kinetics of which relate to parameters such as the adsorption isotherms of the intermediate, the rates of the steps, the solution's nature, and the surface.[142] Compared to the HER, the HOR has been evaluated less deeply due to diffusion limitation effects interfering with the delivery of H_2 to the surface.[142] Considering aqueous solutions, the consecutive reaction steps of the HER in acidic and alkaline media can be observed as follows:[137−144]

Acidic medium	Alkaline medium	
$H^+_{(aq)} + e^- \rightarrow H_{(ad)}$	$H_2O + e^- \rightarrow H_{(ad)} + OH^-$	(18)
$H_{(ad)} + H_{(ad)} \rightarrow H_{2(ad)}$	$H_{(ad)} + H_{(ad)} \rightarrow H_{2(ad)}$	(19)
$H^+_{(aq)} + H_{(ad)} + e^- \rightarrow H_{2(ad)}$	$H_2O + H_{(ad)} + e^- \rightarrow H_{2(ad)} + OH^-$	(20)

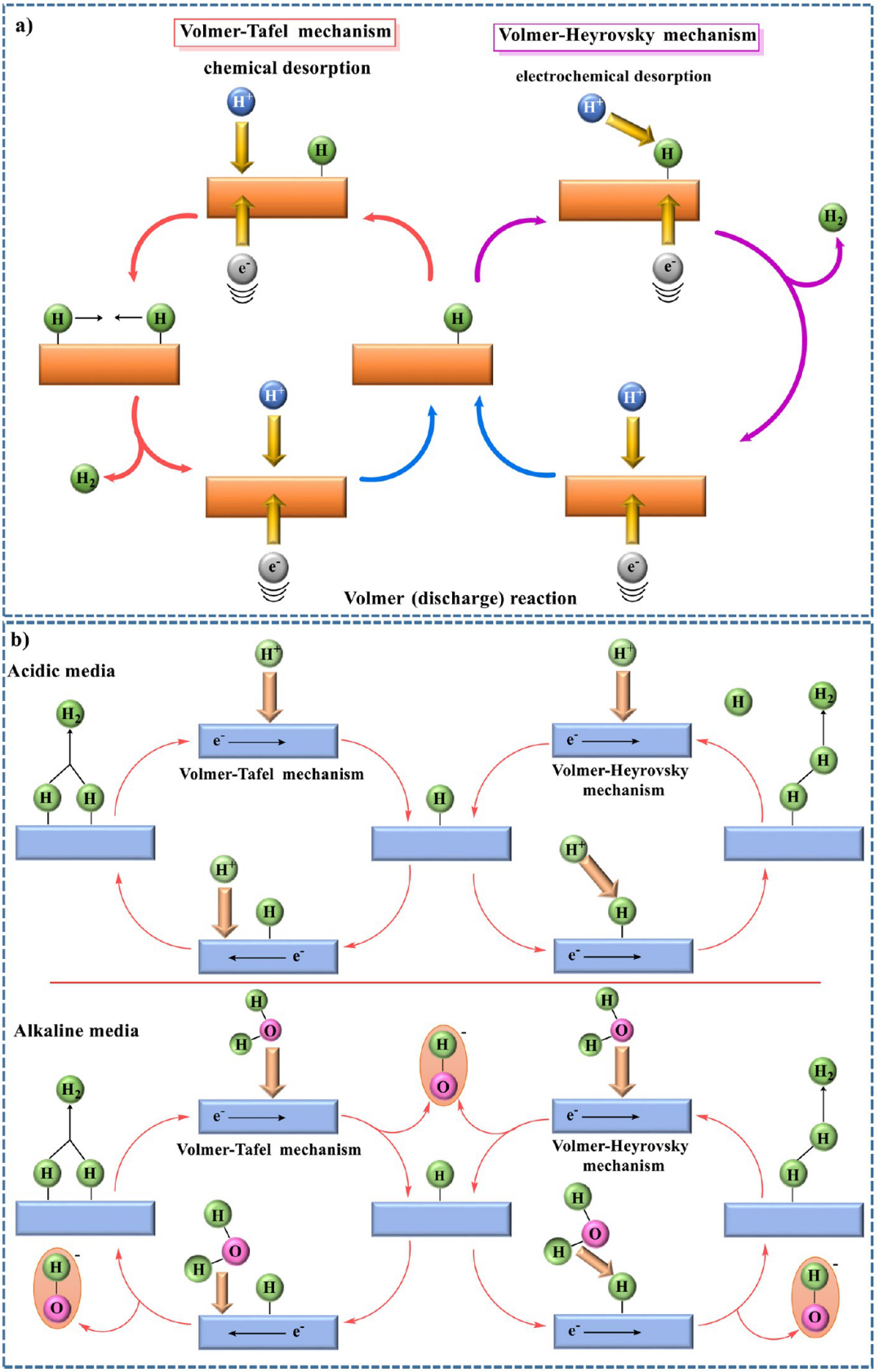

Figure 9. (a) An illustration of HER steps. The Volmer reaction (blue arrows) involves electron transfer toward the electrode coupled with proton adsorption on the electrode active site, which produces absorbed hydrogen. (b) The HER mechanism in acidic and alkaline environments. Reproduced with permission from ref 145. Copyright 2021, MDPI.

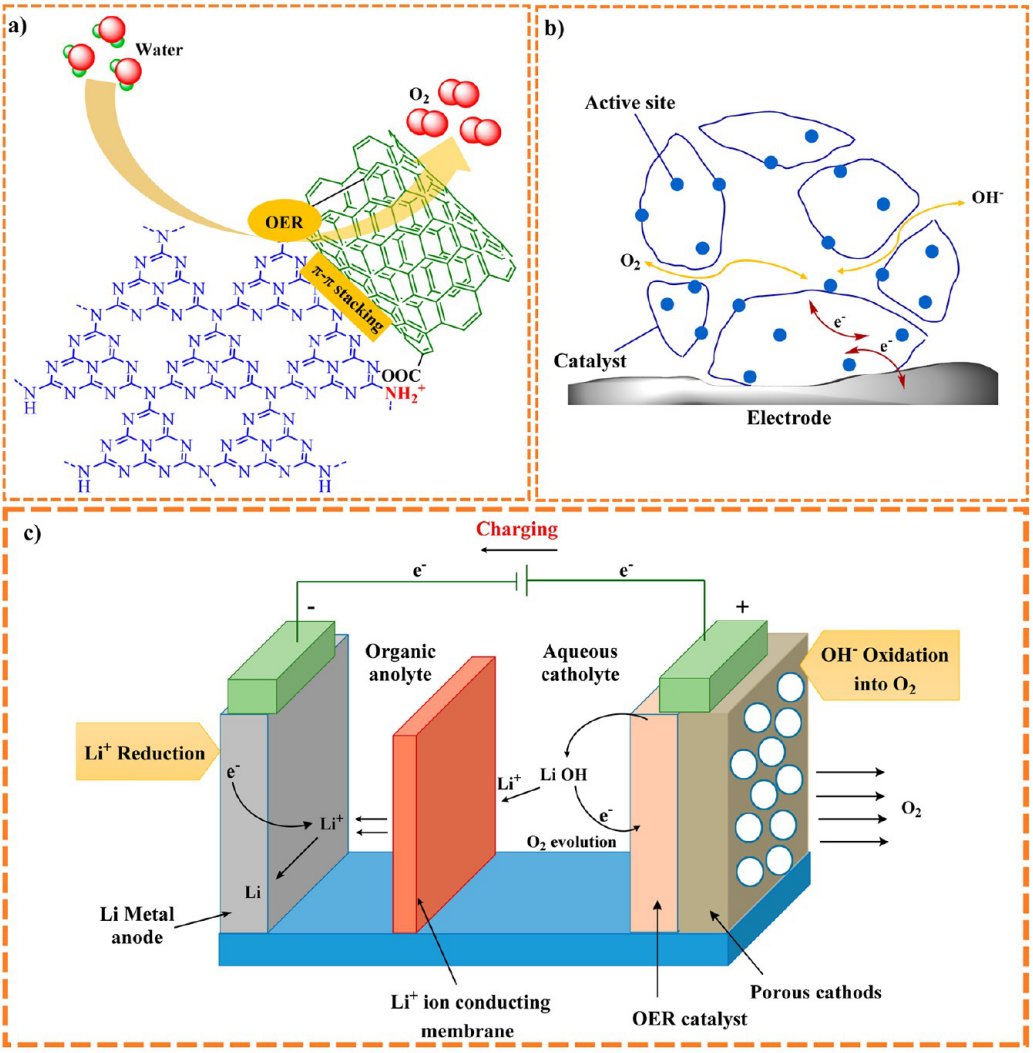

Figure 10. (a) Representation of the OER mechanism of porous 3D g-C_3N_4 nanosheet−CNT composites. Reproduced with permission from ref 149. Copyright 2014, Wiley-VCH. (b) Required structural characteristics of ORR and OER bifunctional electrocatalysts. Reproduced with permission from ref 150. Copyright 2018, Wiley-VCH. (c) Schematic illustration of the function of the OER electrocatalyst during charging in a Li−air battery system. Reproduced with permission from ref 151. Copyright 2020, IOP Publishing.

where aq and ad denote the aqueous and adsorbed states, respectively

At different potentials, the rate-controlling HER step would change as well; accordingly, the rate limiting step at low potentials is the hydrogen adsorption step, while that at high potentials is the desorption reaction.[137] According to Sabatier principle, if an electrocatalyst can promote a strong bond with the adsorbed H, thus simplifying the proton and electron transfer while guaranteeing easy bond breakage and the formation of gaseous H_2, it is considered an efficient electrocatalyst toward the HER.[145] The hydrogen evolution process in acidic and alkaline media is depicted in Figure 9.

In the case of the oxygen evolution reaction, as well as the overpotential needed to obtain a certain current density, lower Tafel slopes are more desirable. Considering the OER mechanism, the following reactions can be represented:[146]

Acidic solution:

$$2H_2O \rightarrow O_2 + 4H^+ + 4e^- \quad (21)$$

Alkaline solution:

$$4OH^- \rightarrow O_2 + 2H_2O + 4e^- \quad (22)$$

In an alkaline medium, a series of reaction steps are involved.[147]

$$(\text{single active site})^* + OH^- \rightleftharpoons {}^*OH + e^- \quad (23)$$

$$^*OH + OH^- \rightleftharpoons {}^*O + H_2O + e^- \quad (24)$$

$$^*O + OH^- \rightleftharpoons {}^*OOH + e^- \quad (25)$$

$$^*OOH + OH^- \rightleftharpoons {}^*OO^- + H_2O \quad (26)$$

$$^*OO^- \rightleftharpoons (\text{single active site})^* + O_2 + e^- \quad (27)$$

Figure 10 illustrates the OER mechanism and depicts the porous electrocatalysts, whose increased surface areas and thus numerous surface oxygen vacancies enhance the OER efficiency. The OER involves four-exciton transfer, which leads to slow electrochemical kinetics and makes it a limiting reaction in the generation of molecular oxygen in water

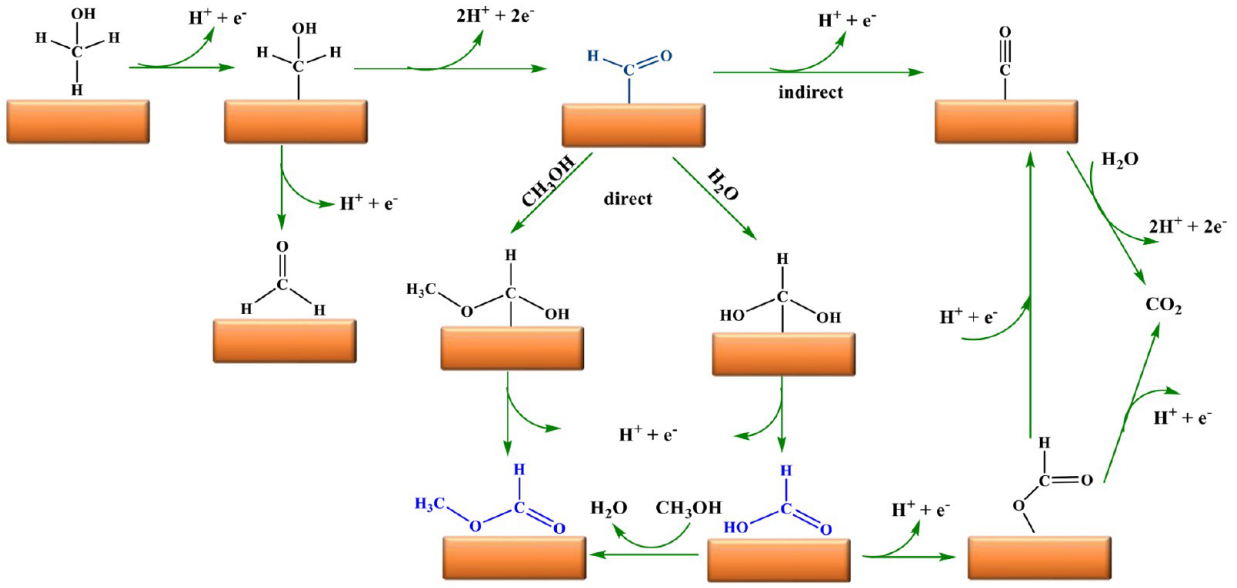

Figure 11. Schematic presentation of the methanol oxidation mechanism via direct and indirect routes. Reproduced with permission from ref 157. Copyright 2019, American Chemical Society.

splitting processes. Some of the intermediates mainly observed in the OER include O*, HOO*, and HO*.[148−151]

The reaction that occurs at the anode of direct methanol fuel cells (DMFCs) is the MOR, a six-electron route of oxidizing the solution of methanol and water that is different in acidic and alkaline media.[152]

$$CH_3OH + H_2O \rightarrow 6CO_2 + 6H^+ + 6e^- \quad (28)$$

The MOR mechanism is a series of steps consisting of methanol adsorption, the dehydrogenation of carbon-containing intermediates, and CO_2 formation. Through electrochemical methanol oxidation, various products can be formed in the same conditions. Therefore, reactions can occur in the following different routes (as shown in Figure 11):

(a) Step-by-step dehydrogenation to CO_{ad} and then oxidation to CO_2.
(b) Direct reaction process to CO_2.
(c) Partial oxidation to formic acid or formaldehyde.

In acidic media, the desired procedure for the MOR is the direct oxidation of methanol to CO_2 on the surface of the electrode, transferring six electrons and six protons. However, CO_{ad} cannot be disregarded in the actual reactions, leading to a decrease in the electrocatalytic efficiency due to the reduction of number of active sites. The mechanism for the electro-oxidation of methanol under acidic conditions can be represented by[153,154]

$$CH_3OH \rightarrow CO_{ad} + 4H^+ + 4e^- \quad (29)$$

$$H_2O \rightarrow OH_{ad} + H^+ + e^- \quad (30)$$

$$CO_{ad} + OH_{ad} \rightarrow CO_2 + H^+ + e^- \quad (31)$$

$$CH_3OH + 8OH^- \rightarrow CO_3^{2-} + 6H_2O + 6e^- \quad (32)$$

In the alkaline media, the oxidative reaction of CO_{ad} removal can occur via two mechanisms. Free OH^- directly takes part in the reaction according to eq 34, which is well-known as the Eley−Rideal (E-R) mechanism, and consecutively eliminates CO_{ad} from the electrocatalyst's surface.[155] On the other hand, CO_{ad} can react with OH_{ad} in eq 35, which is called the Langmuir−Hinshelwood (L-H) mechanism, to generate OH_{ad} on the sites of electrocatalyst.[156]

$$CH_3OH \rightarrow CO_{ad} + 4H^+ + 4e^- \quad (33)$$

$$CO_{ad} + 2OH^- \rightarrow CO_2 + H_2O + 2e^- \quad (34)$$

$$CO_{ad} + 2OH_{ad} \rightarrow CO_2 + H_2O \quad (35)$$

These two distinct reaction mechanisms give various electrocatalyst design pathways. In the E-R mechanism, the electrocatalytic activity is impacted by the strength of the CO_{ad} bond, while in the L-H mechanism a bifunctional electrocatalyst with two adsorbed CO and OH sites takes priority.

6.2. Operation Basics. In fuel cell systems, H_2 is often generated by the electrolysis of water as the input fuel. In a typical system, the components consist of anode and cathode electrodes, an electrolyte to transport the electrons from the anode to the cathode and a catalyst. A continuous flow of H_2 fuel is delivered to the anode, while the oxidizing agent (oxygen or air) is passed through the cathode so that the redox reactions occur. Hydrogen molecules are oxidized (HOR) at the anode side and converted into electrons and protons. The protons, H^+, travel through the electrolyte toward the cathode, while oxygen molecules produce O^{2-} as reduction takes place at the cathode (ORR). At the same time, the electrons generated at the anode move to the cathode through an external circuit to neutralize the system charge. Thus, a direct current is generated from the process, and water and heat are produced as reaction products.[158] In the direct reaction of methanol electro-oxidation at the fuel cell anode, methanol reacts with H_2O, producing electrons, protons, and CO_2 (MOR). However, several intermediates may form in indirect paths that undergo reactions without producing electron−proton pairs. CO is an intermediate that limits the methanol oxidation rate, as it is more stable and blocks the active catalyst sites.[158] In metal−air batteries, the metal anode is oxidized, producing electrons toward the external circuit (discharge). At

the same time, oxygen at the cathode receives the incoming electrons, and oxygen-species form through reduction (ORR). These oxygen species pass across the electrolyte with the remaining metal ions and merge to generate metal oxides. In the case of rechargeable batteries, the process is reversed and oxygen evolution occurs at the cathode (OER). Normally, a catalyst is needed to accelerate oxygen reduction due to its low solubility in liquid electrolytes; thus, the cathode reactions mainly occur at a three-phase interface in the air electrode.[159] In water splitting systems, water is reduced to generate hydrogen gas (HER) at the cathode side, which is also where hydroxide ions form. These ions then dissociate at the anode side, releasing gaseous oxygen molecules (OER) and water.

The high overpotential of the oxidation reaction at the anode originates from the slow four-electron kinetics path, in contrast to the two-electron transfer that occurs at the cathode side during reduction.[160] As g-C_3N_4 contains of C−N bonds in its skeleton and a high number of N sites are found at certain positions in the layers, it is a stable compound during electrocatalysis. Additionally, these numerous sites potentially improve the catalytic activity. In the g-CN materials, carbon atoms are linked to nitrogen atoms with full valence states and are thus completely oxidized. Such a configuration supports a band structure that brackets the H^+/H_2 and O_2/H_2O potentials with no corrosion of the C−N bond in the backbone.[161] Based on recent research, graphitic nitrogen and pyridinic N-doping can redistribute the electron density of neighboring carbon and support its electroactivity for the adsorption and desorption of O_2 during catalysis, which promotes reactions such as ORR and OER. Thus, because of the high number of pyridinic-N active sites, g-C_3N_4 materials have attracted attention as catalysts for facilitating and accelerating the oxidation−reduction reactions, as explained above in the aforementioned energy devices.[162]

6.3. C_xN_y-Based Materials for Fuel Cell Applications. With the aim of improving the production efficiency of electrical energy, fuel cells are used extensively. These high-performance electrochemical devices are capable of directly converting chemical energy to electricity, although more effectively and with less release of greenhouse gases compared to conventional fossil fuel combustion-based systems.[84] The fuels, including H_2, would be oxidized in the anode side, releasing water or e^- or H^+ in alkaline or acidic media, respectively. That is followed by a flow of electrons toward the cathode and the reduction of O_2 to OH^- or H_2O.[24] A critical challenge that remains unsolved with respect to fuel cells is finding strongly efficient design strategies to reduce the high overpotential levels required for the oxygen reduction reaction (ORR).[86] Accordingly, the development of nonprecious, efficient, and durable catalysts to promote the ORR with remarkable activities and rates is of crucial importance in fuel cell commercialization. Carbonaceous materials have attracted high hopes as catalysts for the ORR, as doping their frameworks with heteroatoms such as nitrogen can greatly enhance the ORR efficiency through charge rearrangement and improve O_2 chemisorption through considerably weakening the O−O bonds. Therefore, among carbonaceous materials, g-C_3N_4 has received significant attention for use in electrocatalytic oxygen reduction processes.[24]

6.3.1. C_xN_y-Based Materials As Electrocatalysts. Porous graphitic carbon nitride was composited with acetylene black (ep-GCN-AB composite) to be evaluated as a cathode catalyst in a microbial fuel cell (MFC). The synthesized composite exhibited a marked oxygen reduction reaction performance, with a charge transfer resistance comparable with that of Pt/C. The maximum power densities obtained for MFCs that used ep-GCN-AB composite electrodes were much higher than those obtained using an acetylene black coated-cathode, demonstrating ep-GCN was an efficient MFC cathode catalyst with expenses 20× lower than those of Pt/C. Besides, a higher surface area and better electron conduction and separation were achieved in the presence of acetylene black. In addition, ep-GCN showed better ORR activity at a potential of −0.393 V than Pt/C.[163] A cathode membrane was fabricated by fixing a g-$C_3N_4/Fe^0(1\%)/TiO_2$ catalyst in carbon fiber cloth using a PVDF coating, followed by loading the catalytic components on granular activated carbon (GAC) to form a GAC cathode with MnO_2/TiO_2/g-C_3N_4. This was the first report of a cathode with a catalytic membrane serving simultaneously with a modified GAC electrode to enhance the electricity generation and pollutant elimination of microbial fuel cell-microbial bioreactor (MFC-MBR) systems. This electrode exhibited an ORR peak at 0.041 V, suggesting its considerable catalytic activity. This concomitant performance of the cathode membrane for cathodic catalysis and filtration along with the packed MnO_2/TiO_2/g-C_3N_4/GAC function showed higher catalytic behavior in terms of power generation and greater removal of the ammonium produced by the anodic bioconversion of pollutants compared to single-component systems, verifying its promising potential for the treatment of coking wastewater in MFCs.[164]

Platinum nanoparticles were bonded on a binary g-C_3N_4 and ZIF-67 cobalt metal−organic framework to produce a novel catalyst through an eco-friendly method. The PtNPs@g-C_3N_4-ZIF-67 was evaluated with respect to its electrocatalytic performance toward butanol oxidation using EIS (electrochemical impedance spectroscopy), LSV (linear sweep voltammetry), CV (cyclic voltammetry), and CA (chronoamperometry) analyses in alkaline electrolytes. Highly improved butanol electro-oxidation with a great surface area and current density, a low charge transfer resistance and oxidation potential, and long-term stability was exhibited by the as-prepared catalyst. All these enhanced features could be attributed to the synergistic effect between Pt nanoparticles and the g-C_3N_4-ZIF-67 support. A poisoning tolerance limit of 7 M in KOH was reported, suggesting the use of the novel catalyst as a great antipoisoning material in direct butanol fuel cells.[165]

Consequently, a novel Cu_2O-*g*-C_3N_4/Vulcan carbon (VC) composite was obtained by an additive-free hydrothermal method with different ratios of g-C_3N_4 and VC (1:1, 1:2, and 2:1) for use as an anode catalyst for urea oxidation. The electrochemical features of the as-prepared Cu_2O-*g*-C_3N_4/VC composites were analyzed for urea oxidation, which was influenced by alterations to the g-C_3N_4 to VC ratio. Using 2 M urea, a current density of 25.3 mA cm^{-2} was obtained at 6 V for the Cu_2O-*g*-C_3N_4/VC (1:2) composite, which was higher than those of both the Cu_2O-*g*-C_3N_4/VC (1:1) and Cu_2O-*g*-C_3N_4/VC (2:1) materials. Thus, the results of the Cu_2O-*g*-C_3N_4/VC (1:2) catalyst were ascribed to the surface area in the composite increasing with the larger VC content due to the different shape and morphology formed, the larger surface area, and the smaller ohmic resistance. Besides, the overall electrochemical oxidation of urea was improved for the composite compared to the individual components, and

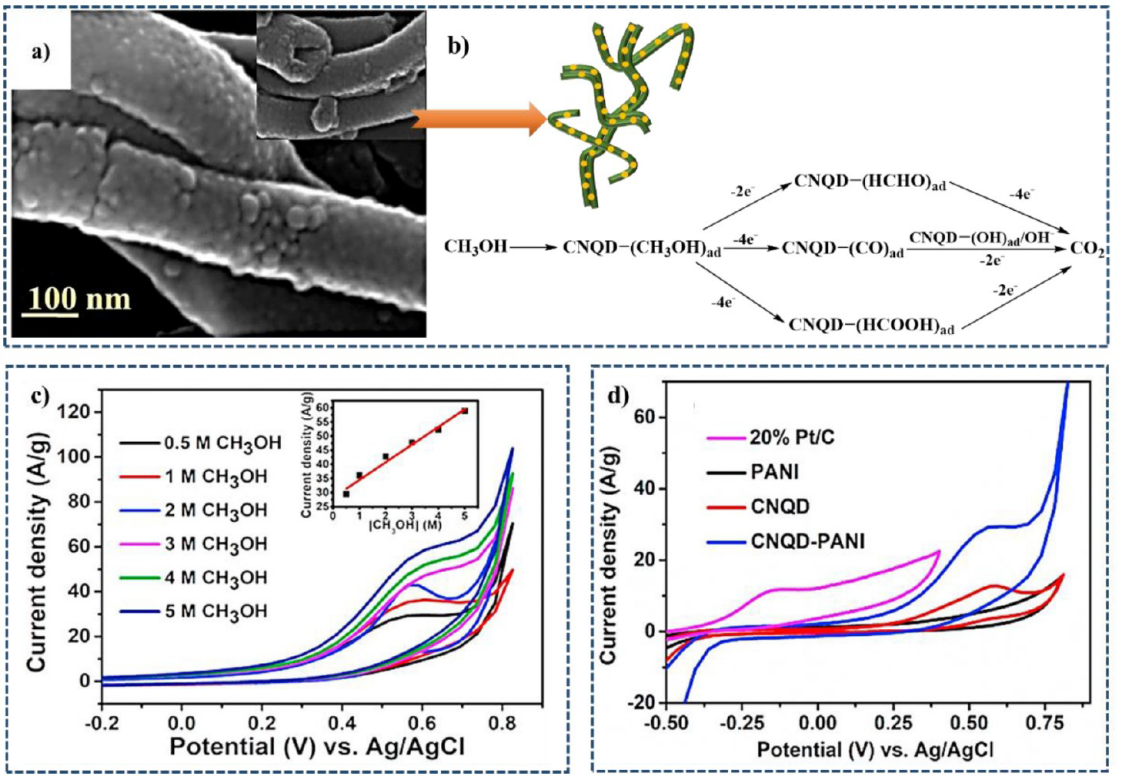

Figure 12. (a) FE-SEM image of polyaniline-supported g-C_3N_4 quantum dots (CNQD-PANI); (b) the proposed MOR mechanisms of the CNQD-PANI electrocatalyst in an alkaline medium; (c) CV curves for the MOR of CNQD-PANI at different methanol concentrations; and (d) comparison between the CV curves of Pt/C, CNQD-PANI, and their single component rivals for methanol oxidation. Reproduced with permission from ref 169. Copyright 2020, Elsevier.

chronoamperometric measurements revealed an increased stability of about 2 h with no current density degradation.[166]

A g-C_3N_4@RGO composite nanocatalyst was synthesized with a high specific capacitance ranging form 220 to 258 F g^{-1} at 10 mV s^{-1} and a very small resistance against charge transfer. The nanocatalyst displayed a large electrochemically active surface area (ECSA) of 81.5 m^2 g^{-1} together with a current density of 13.7 mA cm^{-2} for methanol electrochemical oxidation. Besides, the forward current peak to reverse current peak ratio (I_F/I_R), a parameter denoting the CO poison tolerance, was as high as 1.38 for the Pt/g-C_3N_4@rGO hybrid, and long-term stability was also exhibited. The material's outstanding electrochemical ability was reported to originate from both its specific structural features (2D g-C_3N_4 and 2D graphene), the highly exposed surface area for electrochemical activity supplied by the uniform dispersion of Pt on the hybrid, and the existence of various C−N groups with high N contents. The MOR was carried out at 50 mV s^{-1} with 10 mV s^{-1} scan rates. The forward current peak obtained for Pt/g-C_3N_4@RGO (8:1) was about 1.5−3× higher than those of the other test electrodes and also exhibited a smaller onset potential. In the chronoamperometric tests, in addition to a high final current density of 2.1 mA cm^{-2}, the lowest current decay rate was achieved by the Pt/g-C_3N_4@RGO (8:1) electrode after a full test period. In an accelerated durability test (ADT), 73% of the initial forward oxidation current peak (IF) was lost by the hybrid after 100 cycles, evidencing its reasonable stability toward methanol oxidation. The mentioned result showed that Pt/g-C_3N_4@RGO has a high electrocatalytic stability compared to Pt/RGO.[93] An effective method was applied for the large-scale production of Pt-decorated 3D architectures based on graphene and g-C_3N_4 nanosheets (Pt/G-CN) to evaluate their methanol oxidation activity as an anode electrocatalyst. Following a procedure similar to that for graphene oxide hydrogel formation, a uniform suspension of GO and g-C_3N_4 freestanding nanosheets was obtained through sonication and thermal treatment to form the final 3D hybrids. To maintain their porous structures, the products were further dried in the CO_2 medium of the critical point. The g-C_3N_4 nanosheets were prone to locate in the pores or spaces formed among the graphene oxide layers. The fabricated 3D structures offered large exposed multisized pores for quickly transfer the reactants toward the electroactive sites, and a sufficiently high level of electrical conductivity was preserved in the final catalysts due to the presence of graphene with conducting channels. The overall 3D Pt/G-CN composites were found to possess great electrocatalytic features such as extraordinary poison tolerance, high electrocatalytic activity, and long-term stability, leading them to outperform the conventional Pt-Vulcan XC-72 (Pt/C) and Pt/graphene (Pt/G) electrodes for the methanol oxidation reaction (MOR). CV was performed in a 1 M H_2SO_4 solution. Among various G-CN ratios, the highest ECSA value of 69 m^2 g^{-1} obtained for Pt/G_3-$(CN)_7$ via Coulombic charge calculation for hydrogen adsorption, showing that the Pt/G_3-$(CN)_7$ nanocatalyst with more catalytic sites and a high electrolyte diffusion rate was more electrochemically accessible. In the MOR, the poison tolerance increased with increasing content of g-C_3N_4 nanosheets from 30 to 90%. High amounts of nitrogen in the hybrids could activate more adjacent carbon atoms, speeding up OH formation through water dissociation and enhancing the oxidative elimination of

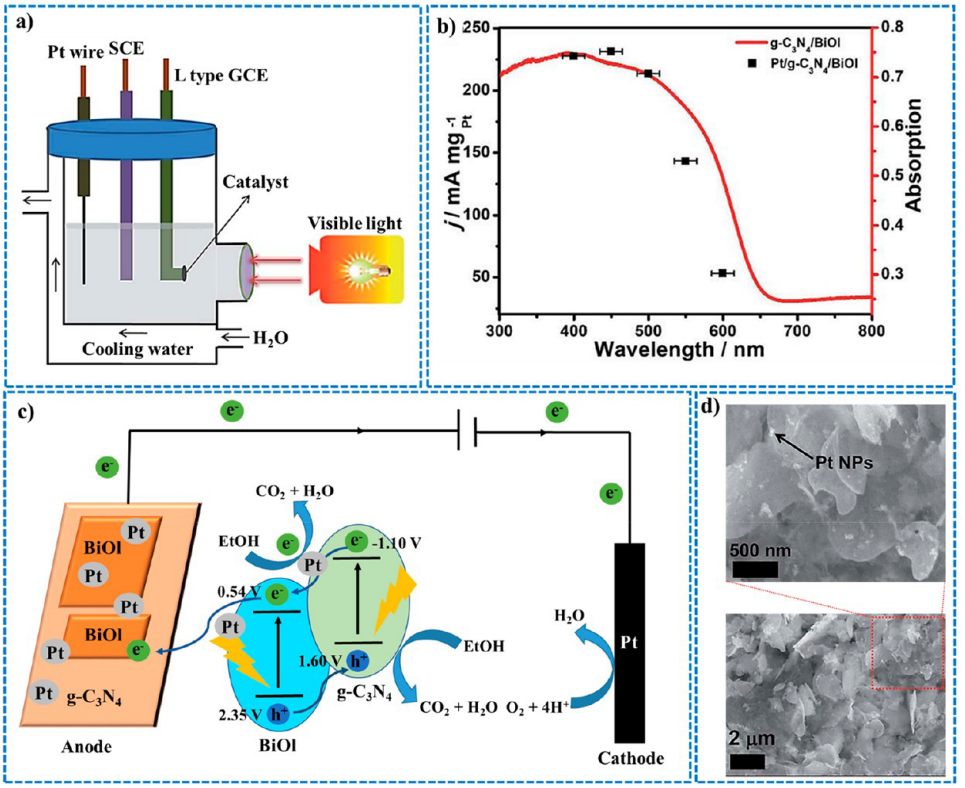

Figure 13. Representation of the ethanol oxidation reaction (EOR) by the Pt/g-C_3N_4/BiOI electrocatalyst with visible-light assistance. (a) Schematic of the photoassisted electrocatalytic reaction system. (b) Wavelength dependence of the mass activities on the EOR and g-C_3N_4/BiOI optical absorption. (c) Mechanism for the photoassisted ethanol electro-oxidation activity of the graphitic C_3N_4/BiOI carrier. (d) SEM image of Pt/g-C_3N_4−BiOI nanocomposite. Reproduced with permission from ref 171. Copyright 2019, Royal Society of Chemistry.

the poisonous carbonaceous intermediate groups. The high content of N_2 could stabilize the Pt nanoparticles by assisting the interaction of the metal with the support. Chronoamperometry tests with conditions of 0.5 V and 2000 s were carried out to measure the long-term stability of the composites. The Pt/G_3-$(CN)_7$ sample again demonstrated the highest current gained through oxidation and the slowest current decay.[167]

Regarding the ADT tests, an increase in the amount of surface oxide groups on the a-CB was observed, which changed virtually proportional to the potential cycle number. This led a-CB to become majorly oxidized. In contrast, no apparent electrochemical oxidation was seen after the a-CB@pg-CN samples were cycled (potentials up to 1.9 V) .[168] In recent work, a novel g-C_3N_4 with an engineered morphology, enhanced catalytic efficiency, high mass activity was produced as a cost-effective and favorable electrocatalyst for the methanol oxidation reaction (MOR) in fuel cells. Using bulk carbon, thermochemical etching method was applied to fabricate various morphologies of graphitic carbon nitride, including nanosheets, nanorods, and quantum dots, and the morphologies were evaluated in an alkaline medium for methanol oxidation reaction by means of cyclic voltammetry. Due to their numerous formed edges and the maximum atomic content of pyridinic N active sites in the nanoscale morphology, g-C_3N_4 quantum dots exhibited the highest methanol oxidation activity.

The zero-dimensional g-C_3N_4 quantum dots (CNQDs) were deposited on conducting polyaniline (PANI) as a support to form a metal-free anode catalyst (CNQD-PANI) in DMFCs (Figure 12). The as-prepared electrocatalyst outperformed the commercial 20 wt % Pt/C due to both its higher oxidation activity toward methanol and fantastic CO poison tolerance, which highlighted its potential as an applicable catalyst in DMFCs. Regarding the electrostatic interaction induced between the conducting polyaniline fibers and the g-C_3N_4 quantum dots, developed electrical conductivity and enhanced methanol adsorption were observed for the CNQD-PANI electrocatalyst. This electrostatic interaction was assumed to be responsible for catalyzing the oxidization of CO, which was adsorbed on the catalyst, into CO_2 in the basic solution within the MOR, leading to a boosted CO tolerance. Moreover, it also efficiently caused the CNQDs to keep the dissolution under control. Fundamentally, the electrostatic interaction between the −COO− groups and N sites of the CNQDs and PANI, respectively, distributed the carbon nitride quantum dots in the nanocomposite uniformly and limited their agglomeration, which eventually increased the catalytic activity. However, a level of instability was observed in the CNQD electrocatalytic process such that a remarkable fall in the current density from 13 A g^{-1} to 10.8 A g^{-1} was measured over 100 cycles. This instability was ascribed to the catalyst's slow dissolution in the basic medium and lower electrode electrical conductivity. Therefore, the as-synthesized metal-free nanocomposite revealed an increased current density of 28.4 A g^{-1} in the initial cycle, which decreased only 8% of the primary amount over 1000 catalysis cycles.[169]

CuAg/Cu_2O nanoparticles were synthesized on the surface of 2D carbon nitride through a galvanic exchange method for the preparation of a CO_2 reduction and methanol oxidation electrocatalyst. Bimetallic CuAg/Cu_2O nanoparticles were

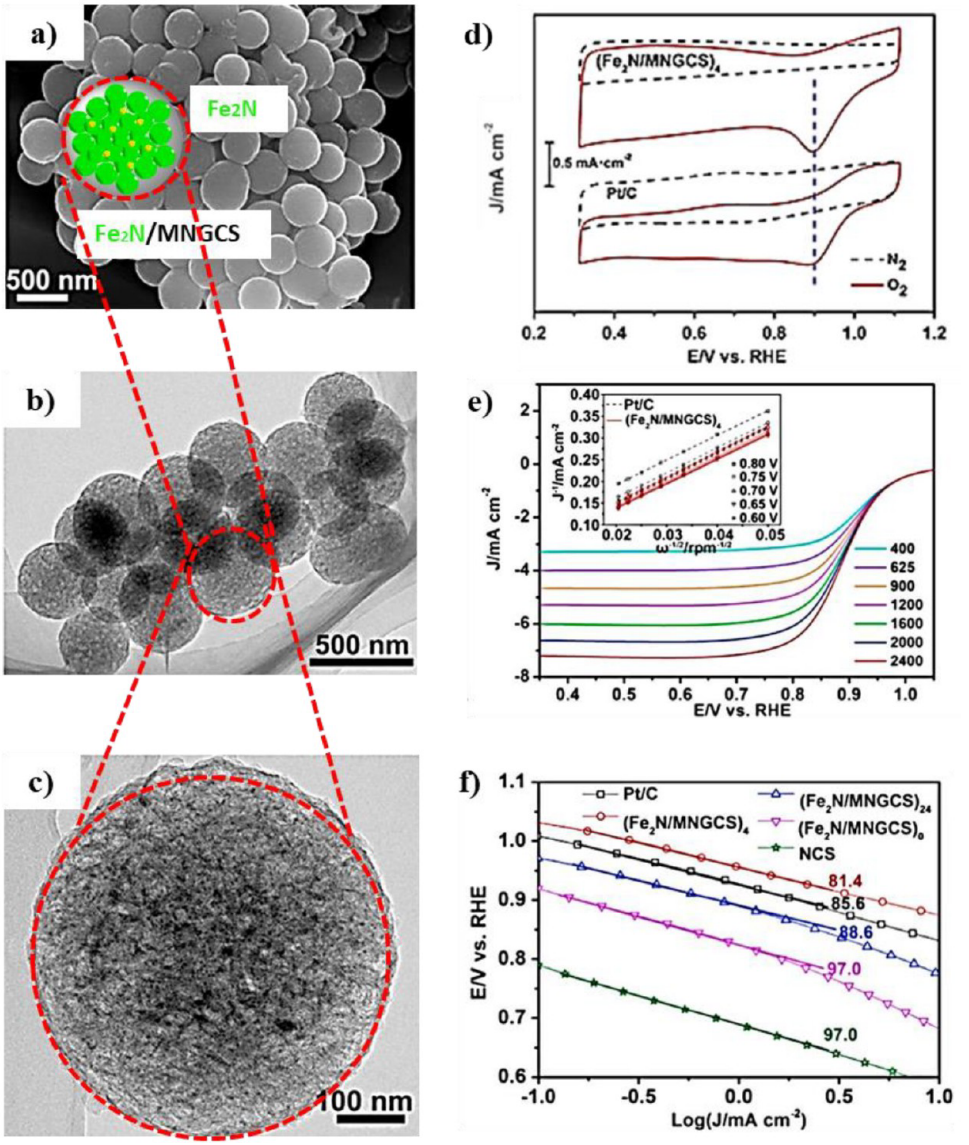

Figure 14. (a) The SEM and (b and c) TEM images of mesoporous nitrogen-doped graphitic carbon spheres $(Fe_2N/MNCNS)_4$. (d) CV curves of Pt/C and $(Fe_2N/MNGCS)_4$ at 10 mV s^{-1} in a N_2/O_2-saturated 0.1 M solution of KOH/ (e) The ORR polarization curves of $(Fe_2N/MNGCS)_4$ at 400−2400 rpm. (f) The Tafel plots of Pt/C, nitrogen-doped carbon spheres (NCS), $(Fe_2N/MNGCS)_0$, $(Fe_2N/MNGCS)_4$, and $(Fe_2N/MNGCS)_{24}$. Reproduced with permission from ref 84. Copyright 2016, Elsevier.

formed through the partial atomic exchange of copper and copper oxide by silver atoms. The synthesized carbon nitride/Cu/Cu_2O catalysts and $C-N/CuAg/Cu_2O$ were assessed electrocatalytically in methanol oxidation and carbon dioxide reduction reactions. Considering a 0.5 M methanol solution, the silver-containing electrocatalysts revealed double the current density efficiency for the oxidation of methanol compared to that of the $C-N/Cu/Cu_2O$ monometallic catalysts due to the oxygen bonds on silver being weaker than those on the copper substrate. Regarding the selective reduction of CO_2, the oxidation of formate as the product took place on a Pt rotating ring disc electrode, and $C-N/CuAg/Cu_2O$ exhibited a higher selectivity for the formation of formic acid. That was attributed to the reduced oxophilicity and decreased hydrogen evolution of the compressively strained copper. Therefore, it can be anticipated that the selectivity of carbonyl products would increase as a result of the addition of Ag to Cu.[170] Bismuth oxyiodide (BiOI) and g-C_3N_4 nanosheets were coupled to form a long-wavelength-absorption 2D−2D composite, as presented in Figure 13. The produced heterojunction with a high charge separation possessed a wide visible-light-collecting potential useful for the unification of solar energy. The g-C_3N_4/BiOI electrode was decorated with Pt nanoparticles, and its final visible-light catalytic activity indicated a 16.9× improvement compared to the conventional electrocatalytic oxidation under dark conditions, exhibiting 5.07 and 2.82× increases in comparison with Pt/g-C_3N_4 and Pt/BiOI, respectively. An ethanol oxidation mass activity of about 53.1 mA mg_{Pt}^{-1} was obtained for the as-prepared Pt/g-C_3N_4/BiOI electrocatalyst with the use of even 600 ± 15 nm red light illumination. Moreover, an improved electrocatalytic stability was also achieved under visible light. Altogether, this electrocatalyst presents an appropriate model for the construction of high-efficiency direct ethanol fuel cells.[171] Copper-doped carbon nitride (Cu-g-C_3N_4) was prepared by a facile single-step pyrolysis method as an effective cathodic

material with a considerable electrocatalytic response for the ORR in an alkaline environment. A reduction peak at 0.66 V was observed in the presence of this electrocatalyst. This modified Cu-g-C_3N_4 electrocatalyst had low expenses and demonstrated a strong methanol tolerance, long-term durability, an E-onset of 0.92 V (plus a 79.7 mV dec^{-1} Tafel slope), a four-electron transfer reduction pathway, and less than 4% H_2O_2 formation compared to Pt/C. Such a performance was attributed to the strong integration of the Cu−N_x active sites with the nitrogen−carbon matrix.[172] Under an inert atmosphere, the pyrolysis of silver hexacyanoferrate-(II) supported by polycarboxylate-functionalized graphene nanoplatelets (GNPs) was conducted to prepare silver/iron−carbon nitride as an ORR electrocatalyst for use in alkaline solutions. Compared to silver nanoparticles deposited on GNPs and iron−carbon nitride, the performance of the hybrid catalytic material revealed that oxygen reduction took place at more positive potentials (higher than 0.3 V) and that the amount of H_2O_2 formed during the reduction process was lower at such potentials in the 0.1 M KOH electrolyte medium. The observed improvement was attributed to the strong effect of silver on H_2O_2 reduction and decomposition in basic electrolytes. However, modified GNP electrocatalysts (annealed at 800 °C), including $FeCN_x$/GNP800-C, Ag/GNP800-C, and $AgFeCN_x$/GNP800-C hybrids, were reported to be less selective with respect to the four-electron oxygen reduction pathway than Pt/C, and they were found to exhibit much lower HO_2^- oxidation currents than the unmodified GNPs. Moreover, as a result of the robust metal complexes fixed to the CN shells, such CN-based nanocomposites exhibited high stabilities and maintained their electrocatalytic performance, even passing continuous acidic medium polarization.[173]

Hierarchical heterojunctions of Ni, Cu, and Cu−Ni nanostructures decorated on ultrathin 2D graphitic carbon nitride were prepared and deposited on GC (glassy carbon) anodes.[125] The methanol electro-oxidation reaction was performed to evaluate their catalytic activities in an alkaline medium. The Ni nanoparticle-embedded g-C_3N_4 electrocatalysts showed high activities, with an onset potential of 0.35 V and a charge transfer resistance of 0.12 kΩ. During a 160 min chronoamperometric experiment, the modified GC electrodes exhibited a stable current density of 12 A cm^{-2} with a 4 wt % loading of NiO. The current densities attained under alkaline conditions with the same weight percentage of Ni/CN, Cu−Ni/CN, and Cu/CN were 58.79, 5.51, and 1.71 A g^{-1}, respectively, indicating the stable MOR activity. In addition, the effect of UV light ($\lambda \sim 400$ nm) was examined during the MOR reaction, which led to improved current densities for all the catalysts; the highest value was 22 A cm^{-2} for the 4% Ni/CN sample. The obtained MOR catalytic activity of the synthesized Cu−Ni/g-C_3N_4 composites under visible-light irradiation was almost 2.7× higher than the activity under dark conditions in an alkaline electrolyte, and the catalysts exhibited oxidation peaks at a potential of 0.56 V. However, adding Cu to the hybrid damaged the efficiency due to irreversible reduction and oxidation of Cu^+ to Cu^0 and Cu^{2+}, respectively, which segregated copper oxide, affected the electron transfer, and finally gave rise to an increase in the redox potential. The stabilities of the modified electrodes with different nanocomposites were investigated. Their results showed that the Ni/CN catalyst had the most stable electrocatalytic performance compared to the Cu−Ni/CN and Cu/CN electrodes.[125]

Employing pyrolysis and acid leaching, ultrasmall Fe_2N nanocrystals were added to g-C_3N_4 spheres to form Fe_2N/MNGCS nanocomposites, as shown in Figure 14c. The sample (Fe_2N/MNGCS)-4 demonstrated optimized ORR activity, with high selectivity and stability (less than a 5% loss in the initial current after a 60 000 s operation), positive half-wave potentials (0.881 V vs. RHE), and a high methanol crossover tolerance (94.9% of the current was preserved when the concentration of methanol was increased from 0.5 to 4 M) in alkaline media. The electrocatalytic activity of the obtained composite was found to be superior to those of the commercial Pt/C (10 wt %) and carbon-encapsulated catalysts. This significant ORR activity arises from the synergistic effects of the mesoporous structure of the composite material, its high surface area with high-performance active sites for catalysis, and its proper conductivity. Compared to Pt/C, Fe_2N/MNGCS exhibited a positive oxygen reduction peak potential (0.9 V), indicating facile O_2 transport by Fe_2N/MNGCS. Chronoamperometry tests were carried out, and an almost 5% decrease in the current retention ratio was observed when 0.5−4 M methanol was injected into the alkaline electrolyte. This was attributed to the special structure of Fe_2N/MNGCS avoiding aggregation during the catalysis and preserving the active sites in addition to the highly carbonized MNGCS accelerating the transfer of the electrons, reactants, products, and intermediates.[84] The results are depicted in Figure 14a−f.

A core−shell composite material (TaO_xN_y@C_mN_n) was fabricated as an active Pt-free oxidation−reduction reaction (ORR) catalyst using spherical carbon nitride as the core and tantalum (oxy) nitride as the shell (Figure 15a−d). The aim of using CN was to synthesize a core capable of increasing the electrical conductivity. In return, the (oxy) nitride shell was formed in order to preserve the core in case of electrochemical corrosion. In comparison with pure tantalum (oxy) nitrides, the as-prepared core−shell composites exhibited enhanced ORR activity, which was more obvious when the nitriding step was carried out at 1000 °C. However, the selectivity tests (four-electron pathway to H_2O) revealed that further improvement was needed. The electrochemical characterizations were performed in acidic (0.5 M H_2SO_4) and basic (0.1 M KOH) electrolytes. Cyclic voltammetry (CV) in acid electrolytes demonstrated higher charging current densities in the double layer for composites prepared under higher nitriding temperatures, which could be attributed to an improved conductivity of the material lowering resistance in the catalyst layer. The higher conductivity was ascribed to the thin layers with large areas of Ta_4N_5 and TaN. This was assumed to be the origin of the more efficient electric contact between the carbon cores, which resulted in the availability of more surface area for electrochemical activity. Similar behavior was observed for the alkaline media CV records. According to the CV tests, among the various TaON@CN catalysts synthesized, only TaON@CN-700 (treated under 700 °C) revealed signals of surface reactions in addition to the currents created by double-layer charging, which was the predominant process in other samples. This catalyst had the highest peak current density at 0.4 V toward the ORR. Based on the electrochemical stability assessments, Ta_4N_5 or TaN in TaON@CN-1000 was proposed to act as the active surface phase in the ORR instead of the more stable phase of Ta_3N_5. This was ascribed to

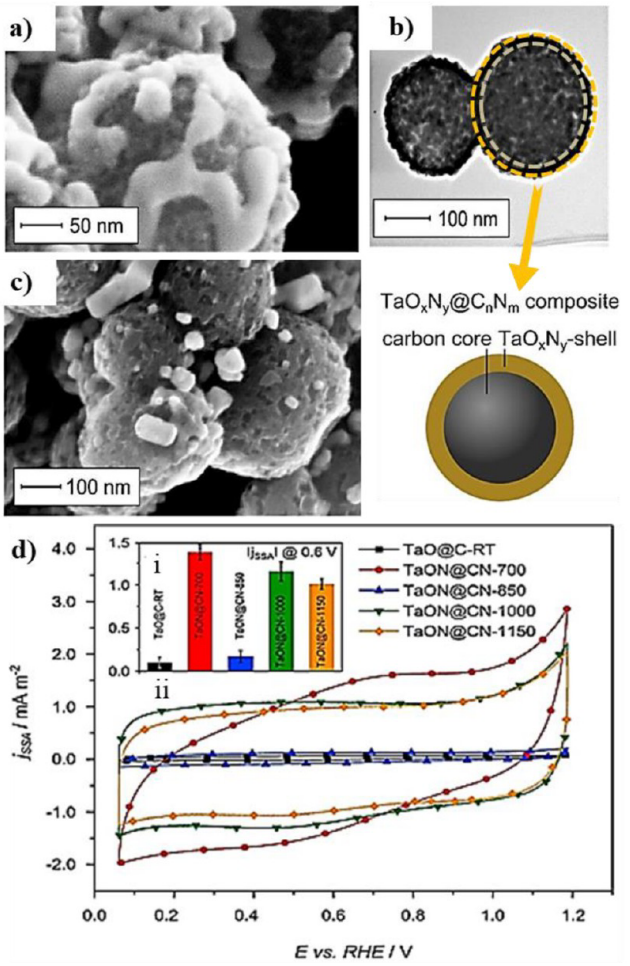

Figure 15. High-resolution SEM images of the surfaces of (a) TaON@CN-1000 and (b) TaON@CN-1150. (c) TEM image of the TaON@CN-1000 spheres. (d) Representation of (i) current densities and (ii) CV curves of TaON@CN nitrided at 0.6 V and at different temperatures in N_2-saturated 0.5 M H_2SO_4 (10 mV s^{-1}) with a catalyst loading of 0.28 mg cm^{-2}. Reproduced with permission from ref 174. Copyright 2017, Elsevier.

the almost complete dissolution of these unstable phases in acidic media together with the loss of the ORR activity.[174]

A strategy was applied to construct mesoporous structures based on the framework of g-C_3N_4 to produce potential metal-free hybrids as promising electrocatalysts for the acidic-medium oxygen reduction reaction (ORR). In this regard, hexagonally ordered mesoporous silica was employed as a template to fabricate ordered mesoporous carbon nitride (OMCN) architectures through a nanocasting synthesis route. The as-prepared OMCN demonstrated a supreme electrocatalytic activity toward the ORR with respect to the onset potential and the current density in comparison with ordered mesoporous carbon (OMC) and bulk carbon nitride (Figure 16a–d). The abundance of catalytically active nitrogen moieties in the OMCN architectures on the one hand and the high surface area of the structure on the other hand seemed to simultaneously improve the electrocatalytic performance of OMCN. In addition, the outstanding durability and higher tolerance to methanol in the ORR experiments compared to the Pt/C catalyst make this metal-free structure an ideal electrocatalyst for extensive use in proton-membrane fuel cells (PEMFCs) and DMFCs. The highest value for ORR activity was obtained for OMCN, although the reduction current was higher for OMC, specifically around the potential 0.9 V. This was attributed to the current from double-layer charging as a result of the large surface area of OMC instead of the current from oxygen reduction. In the ADT tests, a considerable loss of surface area was observed for commercial Pt/C, changing from 94 to 69 m^2 g^{-1} after 200 cycles due to the Ostwald ripening phenomenon in the cycling potential range. In comparison, no remarkable change was measured for OMCN in the cyclic voltammetry experiments, demonstrating its significant structural durability against acidic media compared to the Pt/C catalysts.[175]

Pursuing an innovative approach, a core–shell electrocatalyst structure was developed that contained carbon nitride as the "shell" and conducting carbon nanoparticles as the "core". In addition to uniformly enclosing the carbon nanoparticle core, the carbon nitride shell was developed as a matrix to accommodate alloy nanoparticles of PdCoNi. Since the ORR activity of the active sites could increase significantly based on platinum-group metals, Co and Ni were adopted as cocatalysts for Pd. The alloy nanoparticles were bonded to the carbon nitride shell through the "nitrogen coordination nests". As nitrogen atoms acted as coordination nests in the matrix shell for the palladium alloy, their concentration effect on the ORR efficiency of the prepared electrocatalyst was studied. The outcomes indicated that nitrogen and the alloy nanoparticles interacted with each other, influencing the active sites in terms of bifunctional and electronic mechanisms in the ORR as well as which adsorption or desorption activities the contaminants and oxygen molecules undertook. Furthermore, a higher surface activity (388 μA cm_{Pd}^{-2}) was observed for the PdCoNi electrocatalyst in comparison that of the Pt-based reference electrode (153 μA cm_{Pd}^{-2}), which further revealed a higher efficiency for the ORR at an applied potential of 0.9 V (versus RHE). On the basis of the results, effective features were determined to be the PdCoNi alloy-phase parameters, specifically the grain size and the cell constant, and the interactions between the carbon nitride "shell" and the nanoparticle alloy. Accordingly, it was demonstrated that the highest ORR activity was related to the PdCoNi alloy, which had the shortest cell constant and a low content of N in the shell. It was concluded that the N-based ligands not only hampered the growth of the alloy nanoparticles and led them to form fine grain sizes but also increased the electrocatalyst's tolerance to Cl anion contamination[176] (Figure 16e–g).

Fabricated CN_x/PVA nanostructures were compared to pristine carbon nitride, which revealed that the CN nanoparticles were dispersed in the PVA nanofibers and their ORR electrocatalytic performance was remarkably enhanced. This was confirmed by means of characterizations showing the existence of pyridine N and the formation of active amino N groups from small amounts of pyrrole N during high-voltage electrospinning. CV analysis indicated the improved peak current density and onset potential of these CN_x/PVA nanofibers, which were evaluated as comparable candidates to Pt/C (40:60 wt %) catalysts. The onset potential of the as-synthesized nanofibers was 0.88 V, while that for Pt/C was 0.97 V. Rotating ring disk electrode (RRDE) analysis demonstrated that the desired four-electron pathway was followed within the ORR. Besides, voltammetry studies combined with FTIR confirmed the high stability of the CN_x/PVA nanofibers toward the ORR after 5000 repetitions and the preservation of their active sites. It was observed that

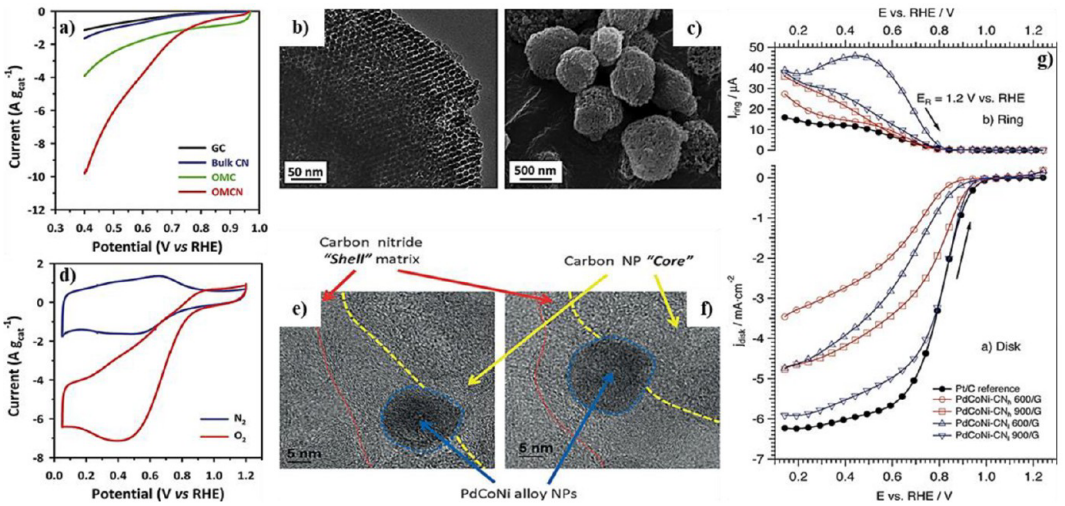

Figure 16. (a) ORR performance of ordered mesoporous carbon nitride (OMCN), bulk carbon nitride, OMC, and glassy carbon,. (b) TEM and (c) SEM images of OMCN. and (d) CV curves of OMCN in nitrogen- and oxygen-saturated $HClO_4$ electrolytes. Reproduced with permission from ref 175. Copyright 2012, American Chemical Society. High-magnification micrographs showing the core−shell structure of the (e) PdCoNi-CN(high N%wt.)-900 °C/G and (f) PdCoNi-CN(low N%wt.)-900 °C/G electrocatalysts. (g) Positive sweeps of Pt/C and PdCoNi-CN electrocatalysts in pure oxygen in a 0.1 M $HClO_4$ solution. Curves were recorded with a sweep rate of 5 mV s^{-1} for current densities using a glassy-carbon disk (a) and oxidation currents on a platinum ring (b). Reproduced with permission from ref 176. Copyright 2014, Wiley-VCH.

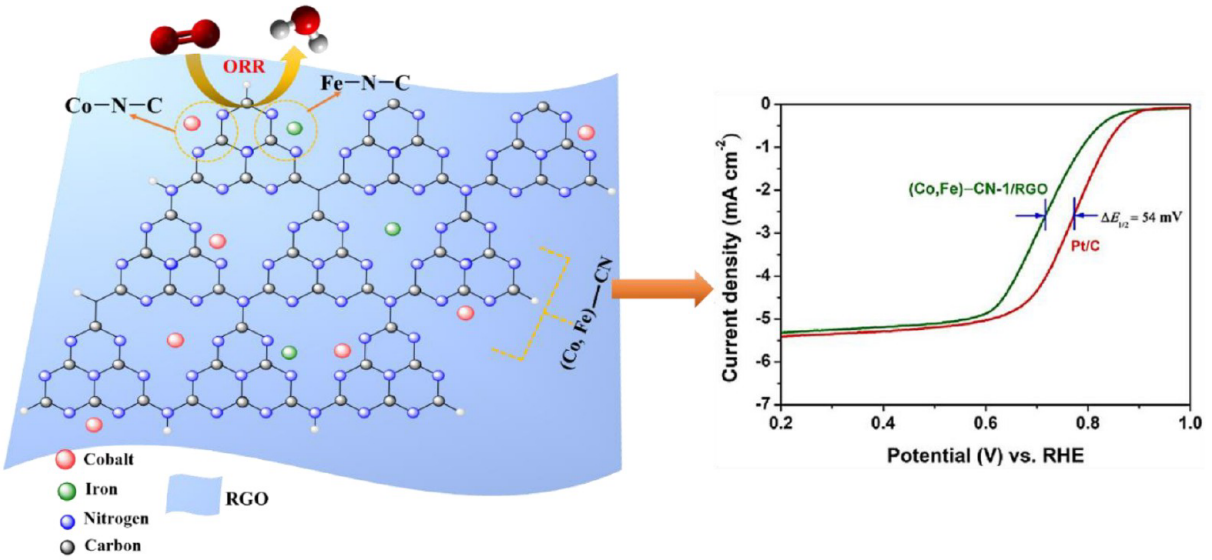

Figure 17. Illustration of cobalt- and iron-coupled carbon nitride as an electrocatalyst for the cathodic ORR and a comparison the LSV polarization curves of a 20 wt % Pt/C catalyst and the (Co, Fe)-CN-1/RGO sample in an oxygen-saturated 0.5 M H_2SO_4 electrolyte. Curves were recorded at a scan rate of 10 mV s^{-1}. The CN-based electrocatalyst reveals an ORR performance very close to that of the commercial Pt one. Reproduced with permission from ref 178. Copyright 2020, Elsevier.

the PVA nanofibers broke apart after the 5000 cycles were complete.[94] A molecular scaffold of g-C_3N_4 that hosted different transition metals was mounted on a carbon nanotube as a support to form a new category of catalysts for CO_2 reduction in an aqueous medium. The bimetallic structures of NiMn and NiCu coupled with g-C_3N_4 could create more efficient catalysts than their monometallic rivals. In particular, the activity of the Ni/C_3N_4 catalyst was improved considerably by the addition of a second metal. That was attributed to the g-C_3N_4 atomic modification in the presence of metal atoms, which gave rise to a high faradaic efficiency of about 90% (ηF(CO) ∼ 90%) for the CO evolution reaction in a wide potential range (−0.6 to −0.9 V versus RHE) and a low overpotential of 0.39 V.[177] A cost-effective bimetallic (Co, Fe)-CN/rGO electrocatalyst was fabricated as an efficient alternative to the use of Pt catalysts in the ORR. The fabricated M-N_x-C-class catalyst exhibited a high porosity, a large surface area, rapid charge transfer (at the (Co, Fe)-CN−rGO interface) in acidic media with its 2D−2D interface, and numerous Co-N_x-C and Fe-N_x-C active sites. The composite was reported to have an outstanding cathodic ORR reaction activity, with an 875 mV onset potential (41 mV more negative than that of Pt/C) and an efficient four-electron reaction route. The catalyst demonstrated an excellent methanol tolerance and a high durability, making it an ideal nonprecious bimetallic electrocatalyst in fuel cell applications[178] (Figure 17).

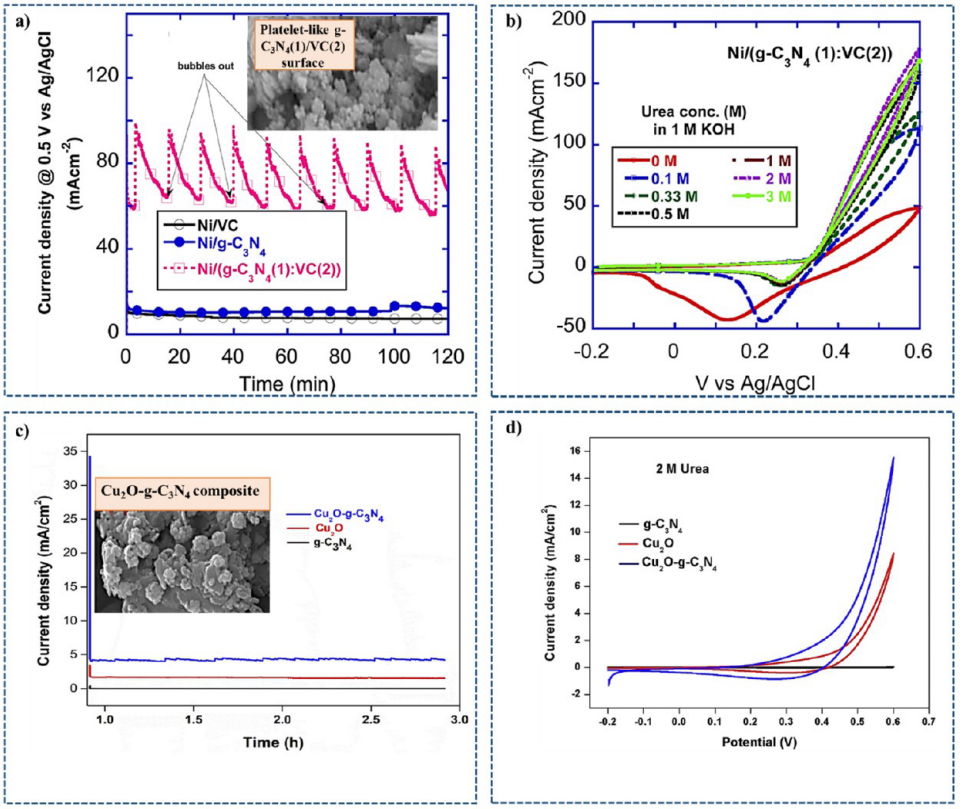

Figure 18. (a) CV curves of plate-like surface Ni/(g-C_3N_4 (1)/VC(2))-supported $Ni(OH)_2$ NPs and (b) the Ni/(g-C_3N_4 (1)/VC(2)) catalyst support effect on the current discharge at 0.5 V vs Ag/AgCl. Reproduced with permission from ref 182. Copyright 2020, Elsevier. (c) CV curves of g-C_3N_4, Cu_2O, and the Cu_2O-g-C_3N_4 composite recorded by applying 2 M urea. (d) Chronoamperometry data of g-C_3N_4, Cu_2O, and Cu_2O-g-C_3N_4 recorded by applying 2 M urea in 1 M KOH. Reproduced with permission from ref 183. Copyright 2021, Elsevier.

Electrocatalysts based on noble metals such as Pt,[179] Au, Pd, Ir, and Ru are recognized as highly efficient ORR catalysts. Sadhukhan et al.[180] developed a platinum nanoparticle−carbon nitride (Pt/CN_x) composite through the ultrasound-assisted reduction of H_2PtCl_6 by sodium borohydride in a medium that included CN_x nanosheets. In acid media, the as-prepared platinum carbon nitride (Pt/CN_x) demonstrated a supreme electrocatalytic performance for CH_3OH, HCOOH, and HCHO oxidation. Compared to the Pt/C catalyst, the Pt/CN_x composites had higher mass activities and onset potentials, a stronger carbon monoxide poisoning resistance, and better durability for the oxidation of the three compounds mentioned previously. The methanol oxidation mass activity of the Pt/CN_x composite (at 0.64 V), which was measured through forward scans, was 2.7× higher than that of the Pt/C commercial catalyst. On the Pt/CN_x composites, the HCOOH electro-oxidation mechanism exhibited a significantly improved efficiency through the dehydrogenation pathway. Besides, at 0.3 V (versus NHE), the Pt/CN_x composite exhibited a mass activity 25× higher than that of Pt/C. The superior electrocatalytic activity and reasonable durability were ascribed to the high level of dispersion of the Pt NPs, which provided a high surface area as well as a robust metal−support interaction.[180] Carbon nitride was dispersed on polyacrylonitrile (PAN) nanofibers by the electrospinning method in order to improve the oxygen reduction reaction efficiency. Both cyclic and linear voltammetry were applied to compare the ORR activities of the CN_x/PAN nanofibers and the native CN_x nanoparticles, and the results revealed an enhancement by the as-prepared composites. The ORR current density (5.82 mA cm^{-2}) and the onset potential (0.93 V) of Pt/C (40:60 wt %) were found to be slightly higher than those of the CN_x/PAN nanofibers. The electrocatalytic mechanism of the synthesized nanofibers was investigated by RRDE voltammetry, which indicated a four-electron reduction pathway for the ORR as well as water formation and inconsiderable H_2O_2 generation. The continuous formation of water as the ORR product was observed by in situ FTIR and voltammetry (0.93 to 0.63 V). Measurements were conducted using linear sweep voltammetry (LSV) with 6000 repetitions coupled with FTIR spectroscopy, which determined the increased stability of the CN_x/PAN catalytic activity for the ORR. An improved water content (4000 LSV cycles) and zero CO_2 evolution (2000 LSV cycles) were also specified.[181]

6.3.2. C_xN_y-Based Materials as Support. A composite of graphitic carbon nitride and Vulcan carbon (g-C_3N_4/VC) was synthesized hydrothermally with various ratios of VC and g-C_3N_4 and was used a support for $Ni(OH)_2$ nanoparticles to form novel Ni/(g-C_3N_4/VC) composites for urea oxidation purposes. The Ni deposited on different supports exhibited an excellent activity compared to those of the single supports. Among the multiple composite ratios of VC to g-C_3N_4, the sample with a ratio of 2:1 demonstrated the highest performance, with a current density nine-times higher than that of Ni over VC for with 2 M urea in 1 M KOH at 0.5 V. A high stability was achieved for the as-prepared Ni over the composite support, and the current density degradation for durations longer than 2 h was not considerable. EIS results exhibited an increased charge transfer rate due to the synergistic effect of the nanoparticles and g-C_3N_4 as well as

the VC support, which assisted the urea oxidation to a great extent[182] (Figure 18a and b). Cu_2O-g-C_3N_4 nanocomposites were successfully fabricated using a straightforward additive-free solution chemistry route in which glucose was applied as the reducing agent. Besides, the Cu_2O-*g*-C_3N_4 composites demonstrated outstanding performance in the electrochemical oxidation, and the activity was about two-times higher than those of the single-component catalysts (Cu_2O and g-C_3N_4). Such an increase was attributed to the synergy between the g-C_3N_4 support and Cu_2O. This synergy also led to a high stability, as determined from the lack of noticeable degradation after 3 h of constant current discharge[183] (Figure 18c and d).

A one-step simple solvothermal process was applied to prepare a graphitic carbon nitride−titanium oxide (g-C_3N_4/TiO_2) nanocomposite to act as a support for the Pt-based catalysis of the electrochemical oxidation of methanol. On the basis of the resultant high mass activity of 210 mA mg^{-1} for the MOR in acidic media (0.1 M H_2SO_4) compared to that of commercial Pt/C at a peak potential of 1.03 V, the supporting catalyst was determined to play a beneficial role. The adaptable architecture of the hybrid on the one hand and Ti−OH surface bonds on the other hand led to synergistic effects that were exhibited by the catalyst support. It was observed that the oxidation of the adsorbed intermediates like CO and their consequent removal was facilitated by Ti−OH groups on the surface, which thus weakened the poisoning effect of platinum. The catalytic performance of the g-C_3N_4/TiO_2 composite declined about 73% after the calcination step at 400 °C. Based on the reduction in the activity after the application of heat, it was concluded that the surface −OH bonds played a significant role in decreasing the activation energy for the adsorption of methanol, which was fruitful for both the final electrocatalytic activity and detaching the species adsorbed on Pt in the form of CO_2 and H^+. Therefore, the active sites on Pt were preserved for further MORs. Chronoamperometry analysis of g-C_3N_4/TiO_2/Pt revealed a relatively slow current density decay rate and an appropriate tolerance level toward intermediate species, thus indicating a high stability.[184]

In Pt-based catalysts, the introduction of Au can improve the ORR performance;[185] integrating the two approaches of developing Pt-based bimetallic catalysts and applying a catalyst support, a 3D Pt−Au/CN structure was fabricated on the surface of carbon nitride nanosheets to evaluate photoassisted reactions in fuel cells. For this purpose, a simple single-step hydrothermal technique was applied to deposit Pt and Au on the surface of a 2D g-C_3N_4 semiconductor (produced by urea thermal condensation) as the catalyst support. The as-prepared composite was then used as the working electrode in the electrocatalytic MOR. The electrocatalytic efficiency reported for 3D bimetallic Pt on a Au core joint with a 2D g-C_3N_4 support was nearly 14× higher than that of monometallic Pt-CN in the electro-oxidation reaction of methanol. This enhancement was reported to originate from the highly available active sites as well as the synergistic electronic effects of the two metals. Under visible-light irradiation, the Pt−Au/CN composite exhibited current density and stability levels higher than those typical for electrocatalysis processes in the MOR. It was also reported that the Pt_{10}-Au_1/CN-modified electrode exhibited the highest current density of 1.52 mA cm^{-2}, being 13.8× larger than that of Pt-CN at similar conditions. That was considered to be strong proof of the generation of bimetallic Pt and Au in the composites in addition to the Pt−Au alloy. The MOR electrocatalytic activity exhibited by Pt−Au/CN under visible-light irradiation was 1.70× and 23.5× higher than those exhibited by Pt−Au/CN and conventional Pt/CN, respectively, under dark conditions; the electrocatalytic activity was also accompanied by improved electrochemical stability. All the improvements were ascribed to the formation of a bimetallic structure, the growth of exposed catalytic active sites on 3D Pt−Au/CN, the simplicity of methanol adsorption on the surface of the 2D CN support, and finally the synergistic effect born from the combination of electro- and photocatalytic processes. The chronoamperometry (CA) and chronopoentiometric (CP) analyses were used to consider the electrocatalyst's stability. According to the CA analysis, the stability of the Pt−Au/CN electrode was greater than that of Pt/CN under both visible-light and dark situations. In addition, it was clearly detected that the Pt−Au/CN electrode had a higher electrocatalytic activity than the Pt/CN electrode in relation to both the initial and steady-state current density under similar conditions. The CP results demonstrated the antipoisoning effect with the application of visible light illumination, with Pt−Au/CN exhibiting a maintenance time of 12080 s under light and that of 8387 s under a dark environment (rather than 37 s for Pt/CN).[85]

A core@shell configuration was developed as a stable and electrochemically efficient support through the integration of 2D layered polymeric graphitic carbon nitride (pg-CN) and amorphous carbon black (a-CB). Due to its special molecular structure and unique electronic function, the as-prepared composite was suggested to be an ideal candidate for the electrocatalytic ORR. The novel a-CB@pg-CN composite was found to improve the stability of fuel cell devices, particularly at high potentials (1.2−1.7 V), as it did not undergo more alterations.[168] Compared to commercial a-CB-based electrodes in PEMFCs, where H_2 and O_2 are given as the reagents at the anode and cathode, respectively, and heat and electricity are produced from the electrochemical reaction energy,[186] the Pt catalyst electrodes based on the novel a-CB@pg-CN support displayed much higher stabilities and comparable ORR electrocatalytic activities while maintaining sufficiently high energy and power densities. Density functional theory (DFT) calculations were conducted, which clarified that the fantastic electrocatalytic characteristics of the as-prepared a-CB@pg-CNs were due to an inherent junction of the chemical and electronic features of the components. This junction surpassed the electrochemical corrosion kinetics and synergistically fostered interactions between the catalyst and the support. Unlike amorphous C, g-CN possesses a crystalline structure in which carbon and nitrogen atoms are bonded as fully oxidized atoms with satisfied valence states. Such a band gap characteristic was assumed to bracket the potentials of H^+/H_2 and O_2/H_2O, implying that the corrosion of the C−N structure was thermodynamically unfavorable in PEMFC devices;[168] this is an important feature, especially in duplicate start-up and shut-down conditions.[187]

A straightforward and quick combustion process was developed for the photoassisted chemical reduction-based synthesis of a palladium−graphitic carbon nitride (Pd-g-C_3N_4) nanocomposite through the room temperature deposition of palladium nanoparticles on a porous graphitic carbon nitride support for application as an efficient electrocatalyst in the oxygen reduction reaction (ORR). Using a 0.1 M KOH solution, the as-prepared Pd/g-C_3N_4 nanocomposite revealed a strong electrocatalytic performance for the ORR, satisfying the clear four-electron pathway. Pd-g-C_3N_4 showed a more

positive onset potential of 0.9 V than Pt/C (0.72 V). The improved ORR activity was presumed to originate from the simultaneous positive effects of the combination of g-C_3N_4 and Pd and the homogeneous dispersion of the nanosized Pd particles. Moreover, in comparison with the commercial Pt/C catalysts, a considerably higher tolerance and an improved stability toward methanol crossover were achieved by the developed nanocomposite. As nitrogen doping is considered to promote the formation of bonds between metal nanoparticles and the carbon of the support, the durability of the Pd-g-C_3N_4 nanocomposite was examined for long-term usage through CA analysis and compared to that of Pt/C at the applied potential of 0.61 V. Over 45 000 s, the Pd-g-C_3N_4 nanocomposite demonstrated around 8% activity loss, which was much lower than that of over 45% demonstrated by commercial 10 wt % Pt/C. Hence, it was concluded that the robust interaction between g-C_3N_4 frameworks and Pd nanoparticles could induce a premier stability higher than that of the benchmark Pt/C. Considering the kinetics of the ORR, the porous structure of the g-C_3N_4 support could effectively assist O_2 diffusion at the interface between the electrode and the electrolyte. Besides, the efficient dispersion of fine-sized Pd nanoparticles directly in contact with the g-C_3N_4 structure played a positive role in the significant electrocatalytic behavior of the Pd-*g*-C_3N_4 hybrids.[86]

The electrocatalytic properties of a ternary Pd/g-C_3N_4/rGO nanocomposite were measured and compared with those of both Pd/rGO and commercial Pd-activated carbon (Pd/AC) catalysts. The outcomes revealed the considerable improvement of properties toward the electrocatalytic oxidation of formic acid and methanol. The obtained signs of progress included a significantly larger surface area for the electrochemical activity, measured as ECSA values; strongly advanced forward current densities; and long-term stability. The synergy achieved among the individual components, together with the unique characteristics of the Pd-*g*-C_3N_4-rGO nanostructure, was reported to be responsible for the exceptional electrochemical activity of the material. The excellent electrical conductivity of rGO, the high specific surface areas obtained for the mesoporous structure that aid the access of fuel molecules, the appropriate structural stability of the composite induced by the covalent links between g-C_3N_4 and rGO, and finally the uniform distribution of Pd nanoparticles on the support as a consequence of planar group effects on the g-C_3N_4 layers were obtained. Theoretical studies applying DFT also revealed desirable interactions between palladium adatoms and carbon through the exchange-transfer mechanism. Additionally, g-C_3N_4 on the graphene sheets was able to harness the agglomeration of both fine and larger Pd nanoparticles.[92] Reduced graphene oxide (rGO) and nanoflakelets of g-C_3N_4 were combined via a facile two-step approach to design a novel support material (CNNF-G) that was nitrogen-rich and suitable for the deposition of Pd nanoparticles. The nanoflakelets were formed through the polymer splitting decomposition of bulk g-C_3N_4 on rGO at high temperatures. The produced CNNF was then coupled closely with the rGO sheets. When high dispersions of Pd nanoparticles were applied, the resulting CNNF could deliver more accessible edge sites and a higher number of active nitrogen groups. Pd nanoparticles with an average diameter of 3.92 nm were evenly dispersed on the CNNF-G layers. The Pd-CNNF-G nanocomposite catalyst revealed an outstanding electrocatalytic activity toward the oxidation reactions of formic acid and methanol. High ECSA values and substantial forward peak current densities were obtained. Reliable stability, durability, and an unusual poison tolerance were also achieved, which were highly ahead of those reported for Pd/carbon nanotubes, Pd/graphene, and commercial Pd/activated carbon catalysts. The attained distinctive properties were promising for rapid electrolyte diffusion through the induced swift and obstacle-free channels. Moreover, the nanocomposite could effectively contribute to the elimination of carbonaceous intermediates produced from the unfinished oxidization of the fuel from the catalyst surface.[188]

For a better understanding of the importance of the carbon nitride-based materials in fuel cells, a comparison table of C_xN_y-based electrocatalysts and other types of electrocatalysts is presented in Table S1.

6.4. C_xN_y-Based Materials for Metal−Air Batteries. Metal−air batteries are highly efficient energy storage and conversion devices due to their large specific energy and low expenses. They normally consist of a pure metal (alloy) electrode for discharge processes and a metal compound for charge processes, plus an air electrode coated with an electrocatalyst for the ORR (discharge) and the OER (charge). Typically, the air electrode is a matrix composed of catalyst particles (alone or carbon-particle-supported). However, combining systems of carbon and nitride compounds has emerged as promising strategy for increasing the recharging efficiency of such batteries in the OER and the ORR.[189] It is assumed that the low diffusion length in nanoscale dimensions relative to that in the bulk materials considerably decreases the travel distance for ions and electrons while cycling, giving rise to improved battery capacities and lifetimes.[190]

6.4.1. C_xN_y-Based Materials as Electrocatalysts. Pd nanoparticle-modified graphitic carbon nitride cathode catalysts (Pd-CN) were prepared for Li−O_2 batteries. Pd nanoparticles were loaded onto g-C_3N_4 with a high specific surface area (239.56 $m^2\ g^{-1}$) and a porous layered structure, which was obtained via thermal polymerization. According to the results, the maximum primary discharge specific capacity for the sample Pd-CN was 26614 mAh g^{-1} at a current density of 100 mA g^{-1}. This capacity remained high at high current densities, revealing a remarkable rate capability. After 70 cycles, the cathodes showed unchanged capacities with no terminal voltage alterations. Based on the electrochemical outcomes, the Pd nanoparticles efficiently increased the specific capacity and the cyclic stability while favorably reducing the overpotential. Those results proved that Pd-CN composites are promising future cathodes in Li−O_2 batteries.[191]

A CoS_x@PCN/rGO catalyst was developed with enhanced conductivity and activity compared to the pristine g-C_3N_4. The structure exhibited significant electrocatalytic activity and stability in both the OER and the ORR, which reportedly outmatched the electrocatalytic function exhibited by Pt, RuO_2, and other precious-metal electrocatalysts. The remarkable electrocatalytic activity of the composite material was assumed to originate from both its special nanomesh-like structure and the CoS_x nanoparticle modification. The long recyclability and the bifunctional activity of the as-prepared CoS_x@PCN/rGO were concluded to be appropriate for use in zinc−air battery systems. Accordingly, an effective rechargeability, as well as a good level of practicality, was obtained when CoS_x@PCN/rGO was utilized in a rechargeable Zn/air coin cell battery. The improved electrocatalytic efficiency of CoS_x@PCN/rGO was ascribed to the high porosity of the

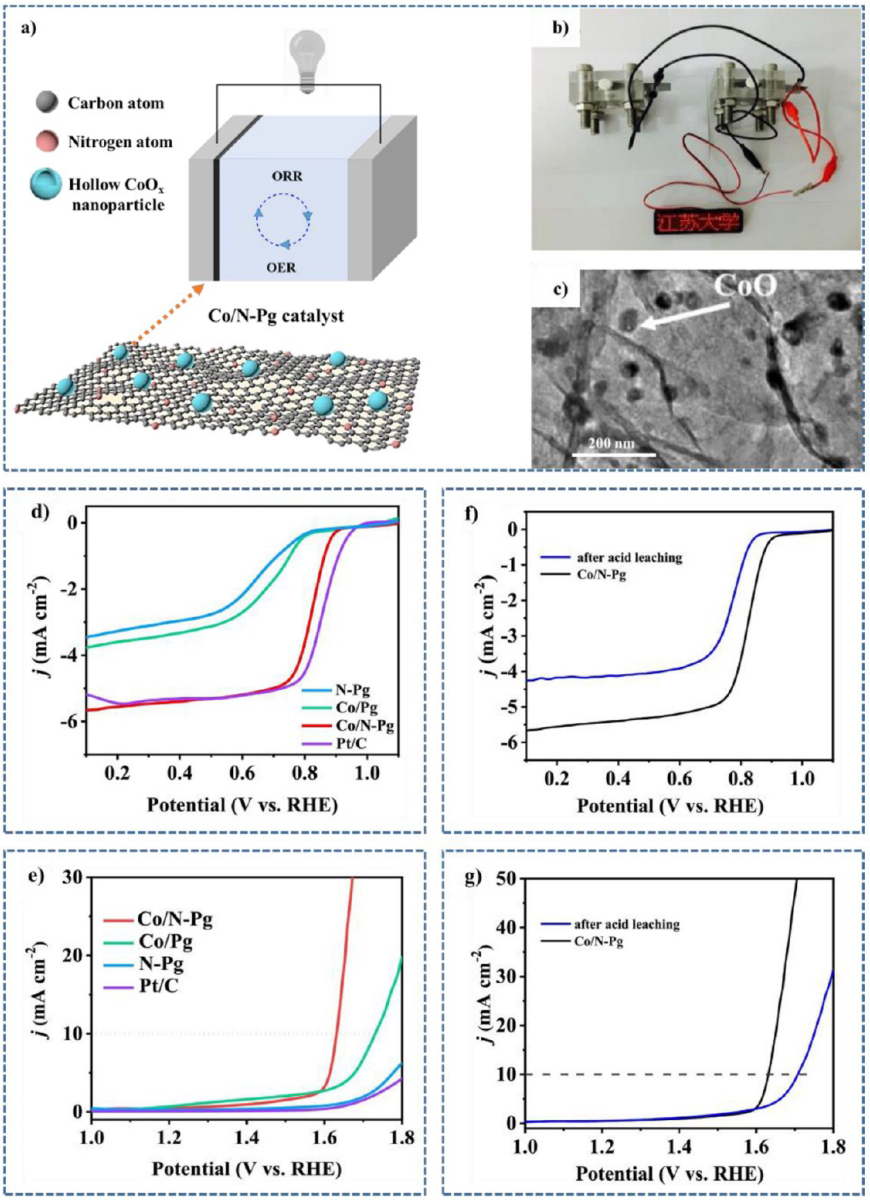

Figure 19. (a) Schematic representation of hollow cobalt oxide nanoparticles embedded in nitrogen-doped carbon nanosheets prepared from a peach gum (Co/N-Pg) catalyst in a Zn−air battery. (b) optical image of a LED plane powered by two Zn−air batteries in series with the Co/N-Pg air cathode. (c) TEM image of Co/N-Pg. (d) ORR and (e) OER (at 1600 rpm) polarization curves of Co/N-Pg, N-Pg, Co/Pg, and Pt/C in an oxygen-saturated 0.1 M KOH solution. (f) ORR and (g) OER polarization curves of Co/N-Pg at 1600 rpm in 0.1 M KOH before and after acid treatment. Reproduced with permission from ref 192. Copyright 2019, Elsevier.

synthesized morphology simplifying the transport of catalysis intermediates and increasing the internal accessibility of the exposed active nitrogen sites, both of which were desirable for the ORR and OER processes. The CoS_x@PCN/rGO electrocatalyst demonstrated a more positive ORR onset potential of 0.89 V compared to Pt/C (0.95 V). The Faradaic efficiency (FE) of the CoS_x@PCN/rGO electrode was found to be 95.7%, and the electrode exhibited a high selectivity for the oxidation of water to O_2. The stabilities of the CoSx@PCN/rGO electrode and the RuO_2 counterpart catalyst for the OER were tested. According to the chronoamperometric tests, the CoS_x@PCN/rGO electrode was able to preserve 93% of its primary current by completing 15 000 s operation, while its RuO_2 counterpart exhibited an almost 35% decline in the current density. In fact, CoSx@PCN/rGO is a highly stable electrode for OER reactions. Besides, a narrower and more stable potential gap was achieved for the CoS_x@PCN/rGO electrode compared to those achieved for Pt/C in long-term cycles, confirming the high catalytic activity and outstanding chemical stability.[89] An effective bifunctional cobalt oxide nanoparticle-based electrocatalyst was prepared for use in Zn−air batteries through a hydrothermal step followed by a pyrolysis phase. The hollow nanoparticles were inserted into carbon nanosheets doped with nitrogen, and the composite was denoted as Co/N-Pg due to the cheap biomass peach gum utilized in its structure. Due to the exclusive structure of the composite together with the synergy achieved from the proximity of the Co−N−C species and the hollow oxide nanoparticles, the offered Co/N-Pg catalyst demonstrated a dominant bifunctional electrocatalytic performance for the

ORR and the OER (Figure 19) and a significant stability. When Co/N-Pg was used as the air electrode, a small OER overpotential, a high four-electron selectivity in the ORR with a low charge−discharge voltage gap of 0.81 V, and a current density of 50 mA cm^{-2} were obtained for the tested Zn−air batteries. Additionally, the battery exhibited a remarkable peak power density of 119 mW cm^{-2} and long-term cycling durability. The nanoparticles could favor active sites with a short ion diffusion length. Moreover, Co−N−C bonds acted as bridges between the nanoparticles and the N-doped carbon lattice, which finally boosted the electroactivity of the material for the ORR and the OER. The cathodic peak potential of the Co/N-Pg (0.81 V) catalyst was approximately equal to that of Pt/C. Additional active sites were provided for the OER due to the Co_4N species in Co/N-Pg. Meanwhile, the charge transport in catalysis was also higher due to the N-doped carbon shell, which also prevented the dissolution and aggregation of cobalt oxide nanoparticles; thus, the Co/N-Pg catalyst exhibited considerable stability. The accelerated durability test results showed that the potential of Co/N-Pg at 10 mA cm^{-2} shifts positively by approximately 6 mV after 200 continuous cyclic voltammetry cycles due to the evolution of O_2 bubbles, which affected the exfoliation of the electrocatalyst from the electrode.[192]

A straightforward and scalable approach for the preparation of Fe-TCNQ MOFs as precursors was employed to fabricate bifunctional core−shell $Fe_3C@CN_x$ structures based on nitrogen-doped carbon. The obtained nonprecious electrocatalysts were produced through a one-step hydrothermal method, which led to hierarchical structures that possessed multimodal porosity. The numerous types of mesoporosity in the structure increased the accessibility of the active site, thus improving the mass transport during the reaction. Therefore, a high electrocatalytic yield was achieved by the optimized catalyst in the ORR and the OER in addition to the high stability and good methanol crossover resistance of the product. In an alkaline medium, the optimized Fe-TCNQ-900 catalyst revealed excellent ORR activites, reasonable OER activities, and proper durability compared to those of Pt/C. This electrocatalyst exhibited an oxygen reduction potential of −0.16 V in O_2. This advancement was attributed to the combination of the robust coupling of N-doped carbon shells with Fe_3C, $Fe-N_X$ active sites, the appropriate nitrogen doping , and the multimodal porosity (Figure 4a and c). The stability of the prepared Fe-TCNQ-900 was investigated for the OER after 1000 cycles. The results showed that the current density of Fe-TCNQ-900 declined approximately 27 mV at 10 mA cm^{-2}, which confirmed that Fe-TCNQ-900 is a stable and useful electrocatalyst for the OER. In addition, the Faradaic efficiency (FE) was 87.5% for the Fe-TCNQ-900 electrode, which displayed a high selectivity in the oxidation of H_2O to O_2.[82] A hybrid self-supported film of g-C_3N_4 overlapped with MXene-phase titanium carbide (Ti_3C_2) nanosheets was prepared via the $Ti-N_x$ interaction. These binder-free configuration films exhibited a remarkable catalytic activity toward the OER and a high durability in an alkaline aqueous solution. It was realized that the porous structure of the film, together with its conductive framework possessing the $Ti-N_x$ species as electroactive sites and the outstanding electrocatalytic performance of the flexible TCCN structures, was comparable to that of transition-metal-based catalysts. Besides, the function was found to be superior to plenty of other films reported so far, since the films were directly applied as cathodes in the aforementioned batteries. It was concluded that the interaction between 2D structures was responsible for the excellent oxygen electrochemistry, which is capable of revolutionizing clean energy devices. The ORR and the OER were located at potentials of 0.87 and 2.55 V, respectively.[193]

Utilizing a sandwich-like azulene-based polymer precursor, Fe/N doped mesoporous carbon nanosheets were prepared with topological defects. The as-synthesized electrocatalysts revealed a half-wave potential (841 mV) in an alkaline medium superior to those of other porous carbon materials, as well as promising methanol resistance, reasonable ORR activity, and stability. The ORR peak located at 0.78 V revealed that this electrocatalyst was more active than Pt/C. When applied in Zn−air batteries as the air cathode, the sample exhibited a peak power density (153 mW cm^{-2}) and a specific capacity (628 mAh g^{-1}) higher than those of Pt/C. The positive effect of the topological defects on the ORR was further proven using DFT.[194] Combining the advantages of g-C_3N_4 with those of spinel-type metal oxides, $CoFe_2O_4$/g-C_3N_4 composites with accelerated O_2 and Li^+ transport were prepared. The presence of $CoFe_2O_4$ facilitated Li_2O_2 decomposition and hindered the electrode polarization. $CoFe_2O_4$/g-C_3N_4 had a more positive ORR onset potential of 0.9 V compared to $CoFe_2O_4$ and g-C_3N_4. A higher specific capacity for discharge of 9550 mAh g^{-1} was observed when the $CoFe_2O_4$/g-C_3N_4 composite catalysts were employed in Li−O_2 batteries. Besides, the stability of 85 cycles indicated an improvement in the battery's cycling stability.[195] A Ag/g-C_3N_4 nanocomposite modified with Co_3O_4 was prepared as a cathode catalyst for use in Li−O_2 cells. Benefiting from the improved surface area of g-C_3N_4 in the presence of Ag NPs and the higher electronic conductivity, the oxygen evolution and reduction potentials of Co_3O_4 were enhanced considerably. The synergy between the constituents of the Ag/g-C_3N_4/Co_3O_4 nanocomposite led to its superior catalytic activity in Li−O_2 batteries and high electrochemical efficiency toward the ORR and the OER, including a reduced charge−discharge potential gap, a high discharge capacity, and a high cycling stability; the significant ORR catalytic activity of Ag/g-C_3N_4/Co_3O_4 was acquired at −0.245 V.[196] A composite of α-MnO_2 nanorods on porous g-C_3N_4 sheets was produced for use as the air cathode in Li−air batteries. The composite demonstrated activities toward the ORR and the OER superior to those of individual constituents of α-MnO_2 and g-C_3N_4. It was found that the α-MnO_2 nanorods were responsible for catalyzing the OER, while the porous g-C_3N_4 sheets were responsible for catalyzing the ORR. The g-C_3N_4/α-MnO_2 showed a more positive ORR onset potential of −0.105 V compared to g-C_3N_4 and α-MnO_2. The g-C_3N_4/α-MnO_2 composite also exhibited an efficiency higher than those of carbon catalysts due to its larger discharge capacity, cycling stability, and decreased voltage gap.[197]

Lithium−sulfur batteries are potential systems that have a high specific capacity and low cost. Host materials that hamper the dissolution of lithium polysulfides are used to solve the long-term cycling challenge in these batteries.[198] Concerning some further relevant C_xN_y applications in batteries, a composite anode of Li−C_3N_4 was fabricated for use in solid-state electrolyte (SSE) batteries. A Li_3N-modified Li anode was formed that exhibited a higher wettability at the interface with garnet SSE. Thanks to the formed Li_3N layer and the increased interface wettability, the Li−C_3N_4 electrode-symmetric cell exhibited a very low interfacial resistance of 11 Ω cm^{-2} and an enhanced critical current density (CCD) of 1500 μA cm^{-2}.

Additionally, a full cell fabricated with a Li−C_3N_4 anode, a $LiFePO_4$ cathode, and a garnet SSE demonstrated a function comparable to those of liquid cells.[199] A 3D porous N-deficient g-C_3N_4 (NDCN) architecture with abundant macro and meso pores was developed as the cathode for Li−S batteries. The prepared structure with active sites for the adsorption of Li polysulfides could host S and accelerate ion transport. As a result, a Li−S cell that used the S@NDCN cathode exhibited a high cycling stability and a low decay rate of 0.045% per cycle after 300 cycles.[198] A number of sustainable materials derived from waste with carbon nitride grafted on them were prepared to be applied as sulfur cathodes in Li−S batteries. The waste-derived carbons included melamine−urea−formaldehyde resins (MUF-C-1100), carbonizing coals (PM), and luffa cylindrical sponges (SG). The Li−S cell containing the sample cathodes exhibited improved activities in terms of the specific capacity, the capacity retention, and the Coulomb efficiency, which was predominantly attributed to the modified S hosts possessing micrometer meso pores and the high affinity of the N sites of C_3N_4 for lithium polysulfides. The S-PM-CN, MUF-CN, and SG-CN sample cathodes demonstrated specific capacities of 1269.8, 1335.6, and 953.9 mAh g^{-1} at 0.05 C together with capacity retentions of 75.9%, 66.7%, and 95.1% and Coulomb efficiencies of 97.3% after 200 cycles, 93.6% after 300 cycles at 0.5 C, and 98.2% after 125 cycles at 1 C, respectively.[200] DFT was applied to evaluate the ORR process on g-C_3N_4 and the S-, O-, and P-doped g-C_3N_4 surfaces. Accordingly, the reaction was determined to start with the adsorption of Li, the first atom of which was trapped on the substrates. The ORR process was investigated on such surfaces, and discharge overpotentials of 0.41 and 0.84 V were obtained for g-C_3N_4S and g-C_3N_4S/Li, respectively, making g-C_3N_4S an ideal candidate for Li−O_2 batteries.[201]

For a better understanding of the the importance of C_xN_y-based materials in metal−air batteries, a comparison table of C_xN_y-based electrocatalysts and other types of electrocatalysts is presented in Table S2.

6.5. C_xN_y-Based Materials for Water Splitting Devices. In contrast to carbon-emitting technologies for H_2 production, water electrolysis demands water as an input material and applies a reproducible electricity driving force with no environmental pollution. However, its low energy conversion performance overshadows its functionality for industrial purposes. Water electrolysis includes two half-reactions, the HER and the OER, between which the OER needs a higher overpotential and thus has slower kinetics due to the four-electron transfer path to pass the energy barrier of the reaction. Furthermore, different energy storage devices like metal−air batteries and fuel cells also deal with the OER.

6.5.1. C_xN_y-Based Materials as Electrocatalysts. Molybdenum carbide nanoparticles were homogeneously embedded in a N-doped carbon matrix (NCS) by employing g-C_3N_4 as a template to prepare the material from the polyaniline-molybdate monolith, which was generated via the direct carbothermal reduction of a self-polymerized aniline species. In this regard, a highly porous molybdenum carbide−carbon composite (MoC@NCS) was obtained as an efficient and cost-effective electrocatalyst with a high electrical conductivity and good corrosion resistance for use in water reduction half-reactions. When used in alkaline (1 M KOH) and acidic (0.5 M H_2SO_4) media, the MoC@NCS hybrid catalyst indicated an extremely high hydrogen evolution activity, producing a current density of 10 mA cm^{-2} with low overpotentials of 89 and 81 mV, respectively. Such proper electrochemical behavior was even analogous to that of the Pt/C benchmark. Furthermore, in the case of long-term period tests, the MoC@NCS catalyst exhibited significant durability in both alkaline and acidic electrolytes. Besides, its excellent catalytic performance in the alkaline-medium oxygen evolution reaction was attributed to the high concentration of N heteroatoms in the structure and the hierarchically porous architecture of the carbon matrix. For overall water splitting purposes, the prepared NCS was coupled with MoC@NCS and used as both the anode and cathode electrodes at 1.69 V. The double-electrode alkaline electrolyzer demonstrated strong durability and a 10 mA cm^{-2} current density, with a slight current deterioration over 24 h. Different factors, including the high nitrogen content in the porous carbon matrix, the uniform dispersion of molybdenum carbide nanoparticles, and the ordered arrangement of the material's structure with abundant available active sites, were assumed to be the reasons for the remarkable electrocatalytic HER efficiency.[202]

Utilizing g-C_3N_4 nanosheets, graphene, and few-layered MoS_2, a bottom-up method based on a solvothermal coassembly approach was examined for the large-scale preparation of 3D cross-linked ternary structures through a straightforward self-assembly technique. The macropores formed between the GO sheet galleries could host the g-C_3N_4 and MoS_2 nanosheet, and the 3D architectures were fixed through freeze-drying, inhibiting the restacking of the sheets. Owing to their unique structural properties, such as a high specific surface area, a small charge-transfer resistance, and extremely thin walls, the MoS_2−CN/G hybrid catalysts exhibited an excellent HER efficiency. Accordingly, the as-prepared composites displayed appropriate long-term durabilities and a small onset potential around 140 mV with a Tafel slope of 79 mV dec^{-1}, all of which led to composites highly outperforming the functionalities of pristine catalysts of MoS_2, graphene, and g-C_3N_4. DFT calculations showed that the conductive interconnected network of graphene provided rapid electron and ion transportation that was coincident with the accessibility of both the edge sites in the 2D MoS_2 as catalytic active sites for the HER and the hydrogen binding sites in g-C_3N_4 nanosheets, which could speed up the process.[203] A new multicomponent electrocatalyst containing g-C_3N_4 and metal phosphide (Cu_3P) on 3D graphene was synthesized that exhibited an excellent electrocatalytic activity and long-term durability, as depicted in Figure 4b. This splendid electrocatalytic performance was evaluated with respect to the current density, which was 10 mA cm^{-2}, the overpotentials for the hydrogen evolution reaction and the oxygen evolution reaction, which were 67 and 255 mV, and the very small Tafel slopes, which were 45 and 40 mV dec^{-1}, respectively. The corresponding onset potentials for the HER and the OER were 5 mV and 1.28 V, respectively. It was proven that decorating g-C_3N_4 nanoflakes or hexagonal Cu_3P nanoplatelets on the graphene network greatly contributed to the rapid electron transport against a low transfer resistance of around 8.5 ohms. Therefore, superior stabilities (25 h for HER and 15 h for OER) were obtained in the electrochemical reactions with negligible current losses. It was reported that the aforementioned behavior chiefly originated from the availability of more active sites, the intrinsic binary catalytic properties of g-C_3N_4, the superior bifunctional catalytic feature of the copper phosphide as a transition-metal-based material, and the synergistic effect contributed by the highly conductive

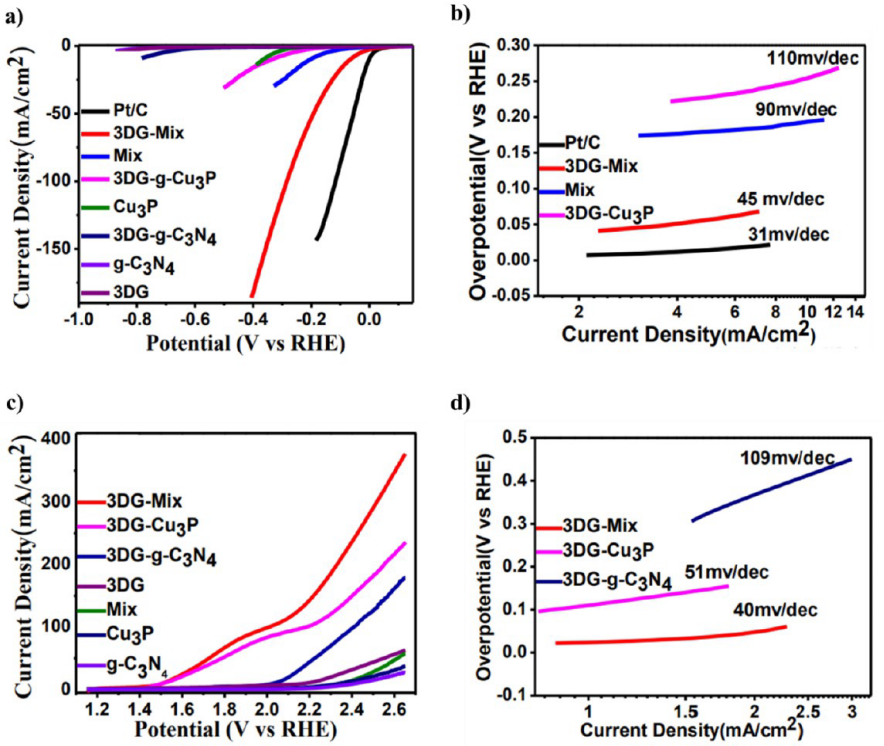

Figure 20. HER (a) polarization curve and (b) Tafel plot and OER (c) polarization curve and (d) Tafel plot of the $Cu_3P/g\text{-}C_3N_4$/3D graphene electrocatalyst compared to Pt/C and the other component rivals. Reproduced with permission from ref 83. Copyright 2020, Wiley-VCH.

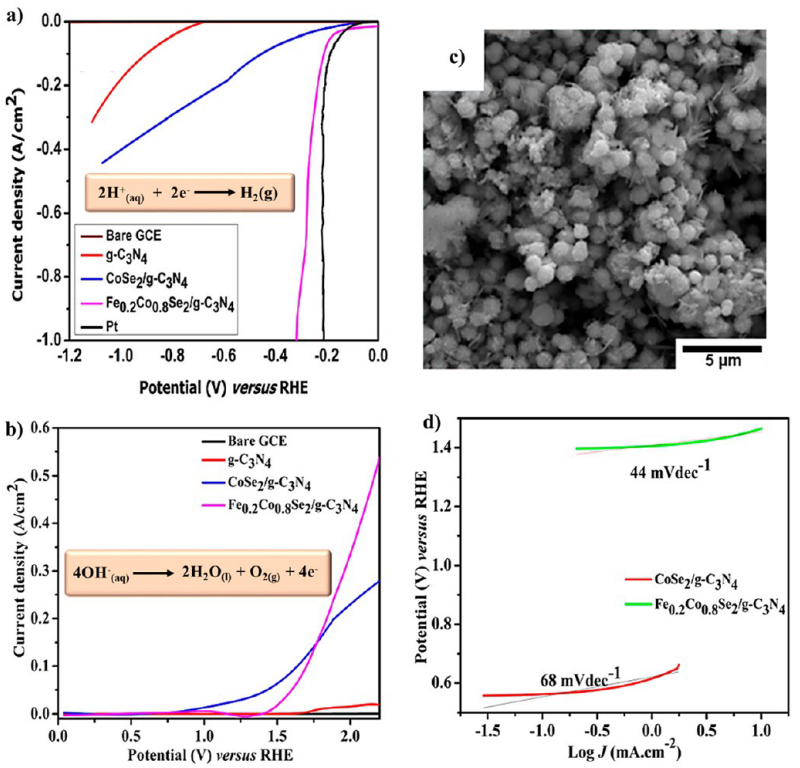

Figure 21. (a) HER activity of GCE, $g\text{-}C_3N_4$, $CoSe_2/g\text{-}C_3N_4$, $Fe_xCo_{1-x}Se_2/g\text{-}C_3N_4$, and Pt after *iR* compensation in 0.5 M H_2SO_4. (b) OER activity of GCE, $g\text{-}C_3N_4$, and $Fe_xCo_{1-x}Se_2/g\text{-}C_3N_4$ in 1 M KOH. (c) SEM image of $Fe_{0.2}Co_{0.8}Se_2/g\text{-}C_3N_4$. (d) Tafel plots for $CoSe_2/g\text{-}C_3N_4$ and $Fe_{0.2}Co_{0.8}Se_2/g\text{-}C_3N_4$ in a 1 M KOH solution. Reproduced with permission from ref 205. Copyright 2020, Springer Nature.

graphene matrix. The overall performance of the $Cu_3P/g\text{-}C_3N_4$/3D graphene nanohybrid was tested in terms of water splitting in a 1 M KOH electrolyte. Based on the results, the catalyst displayed a very small cell voltage equal to 1.54 V, reaching a 10 mA cm^{-2} current density and a minimum stability of 35 h without potential loss. This was attributed to

the chemical inertness of the material nature as well as the low level of agglomeration due to proper surface anchoring[83] (Figure 20).

Using a silica nanotemplate, a nanoconfinement synthesis method was applied for the production of an ordered mesoporous carbon nitride electrocatalyst (gMesoCN) possessing rich contents of C and N (48%) and a large surface area (406 m^2 g^{-1}). Uniform pore size channels with a 4.56 nm diameter were obtained. A high OER electrocatalytic activity and desirable kinetics, including a Tafel slope of 52.4 mV dec^{-1}, were achieved in an alkaline medium. In particular, in alkaline electrolytes, good durability after 24 h with the maintenance of 98.4% of the current density was exhibited by the gMesoCN hybrid, which was found to be a low-cost, ecofriendly, and facile-production electrocatalyst. The stability of the prepared gMesoCN was tested using chronoamperometric analysis. The results showed that the performance of gMesoCN decreased by about 1.6% after 24 h. According to mentioned results, the gMesoCN is a promising material for electrocatalytic applications. The good stability of the catalyst could be connected to the existence of the many nitrogen atoms (48.08%) in a conjugated aromatic ring.[204] $FeCoSe_2$ spheres were dispersed on g-C_3N_4 for the hydrothermal fabrication of HER and OER catalysts (Figure 21) with considerably low overpotentials. Improved electrocatalytic stabilities and activities were exhibited by the as-constructed strong and inexpensive catalysts for H_2 production, which were ascribed to the composite's distinctive structure. Iron incorporation gave rise to an enhanced turnover frequency (TOF_{min}). Various solutions, including phosphate-buffered saline, artificial seawater, and acidic and alkaline electrolytes, were examined for the HER using $Fe_{0.2}Co_{0.8}Se_2$/g-C_3N_4 with significantly low overpotentials, which demonstrated current densities of −3.24, −7.84, −14.80, and −30.12 mA cm^{-2} at 0 V (versus RHE), respectively. Such high current densities at low potentials (e.g., −20 mA cm^{-2} at 83 mV in 0.5 M H_2SO_4), the small Tafel slope, and the high proton conductivity explain the natural catalysis properties of the prepared bifunctional catalyst, which was also accompanied by a constant −1000 mA cm^{-2} current density at only 317 mV. Additionally, chronopotentiometric tests were conducted to evaluate the catalyst's stability, and a stable current density of −30 mA cm^{-2} was obtained even after 24 h at −0.2 V, which demonstrated the high catalytic stability of the sample.[205]

The electronic and structural changes in g-C_3N_4 were investigated regarding the incorporation of manipulated nanomaterials under prompt cooling techniques, including room-temperature, ice, and liquid N_2 quenching . The quenching approach was found to increase the absorbance and band gap potential and decrease the particle scale. Various structural and morphological analyses confirmed the presence of a distortion in g-C_3N_4 quenched in liquid nitrogen. Reactive dye degradation was used to study the photocatalytic properties of the as-engineered g-C_3N_4 nanostructures, which were analyzed using total organic carbon (TOC) measurements and UV−vis spectroscopy analysis. The measured degradation efficiencies were reported to be 4.2% for the room-temperature operation, 14.7% for ice quenching, and 82.33% for the liquid nitrogen conditions, respectively; these efficiencies were improved compared to those of samples prepared by pyrolysis alone. Following the pseudo-first-order model, the reaction rate for the nitrogen-quenched g-C_3N_4 was found to be nine-times higher than that for the one quenched in ice. Moreover, the electrocatalytic efficiency of the manipulated g-C_3N_4 was evaluated with respect to the hydrogen evolution reaction under acidic conditions. The lowest overpotential together and a high H_2 evolution efficiency were demonstrated by the liquid nitrogen-quenched g-C_3N_4 electrocatalyst.[206]

Bismuth oxychlorides were integrated with TiO_2 and g-C_3N_4 to fabricate a water oxidation heterostructure through low-temperature calcination. To investigate the material's photoelectrocatalytic properties, the electrocatalytic function toward the oxygen evolution reaction was recorded in a 1 M KOH solution. The produced amorphous BiOCl/TiO_2-g-C_3N_4 nanocomposite exhibited an 81 mV dec^{-1} Tafel slope and could generate a 10 mA cm^{-2} current density at a 376 mV overpotential; however, under light illumination, the overpotential declined to 366 mV without a loss of the current density and the Tafel slope decreased to 70 mV dec^{-1}. The abundant cavities and active sites in the catalyst gave rise to a stable and excellent water oxidation activity. Such an effective performance was ascribed to the synergy created by the heterostructure and the visible-light responses of the nanocomposite.[207] A HER descriptor was developed for the precise prediction of the electrocatalytic performance of heteroatom-doped g-C_3N_4. This novel principal design qualifies the highly active catalysts and leads to rational design improvements based on the characteristics and bonding periphery properties of the dopant, including electronegativity, electron numbers, and affinity. A "volcano" relationship was developed to describe the HER activity of the modified graphitic carbon nitride, which could result in the determination of the most appropriate dopants and structures. O, S, and Se were found to be the most active dopants. Accordingly, doping close to the g-C_3N_4 edge was recognized as a potential approach for the fabrication of high-efficiency catalysts containing metal-free g-C_3N_4. Additionally, the source of the inherent catalytic properties of doped g-C_3N_4 was demonstrated for various active sites.[143] A low-temperature N_2 plasma treatment was performed on g-C_3N_4 to modify the electrocatalytic activity toward the HER. Remarkable chemical and morphological variations were induced on the g-C_3N_4 surface, and nitrogen atoms were incorporated on the surface by active species. Consequently, the hydrophilicity of the surface and the HER electrocatalytic performance improved, and great stability was achieved within 2000 runs of HER, all of which confirmed that plasma processing is a potential technique for the preparation of carbonaceous layered nanostructures in HER applications.[208] NiO nanoparticles were coupled with carbon nitride through Ni−N bonds to produce a conductive interface. The NiO/CN composite revealed an OER efficiency higher than those of separate NiO and CN as well as NiO/C and RuO_2 in alkaline and buffer saline systems. The NiO/CN-2:1 sample exhibited a current density of 10 mA cm^{-2} at an overpotential of 261 mV in 1 M KOH and a current density of 1 mA cm^{-2} at an overpotential of 580 mV in 0.05 M PBS. The low Gibbs energy of formed nickel−nitrogen links was beneficial for both the adsorption of the OER intermediate and charge transfer and mass transmission in OER. Moreover, the NiO/CN composite was examined in a photovoltaic water electrolyzer for high-energy conversion production. An efficiency around 5.35% was achieved, proving that conductive interface construction is an effective strategy for OER catalyst fabrication. The stability of these materials for the OER was tested using chronopotentiometry (CP). The potential of

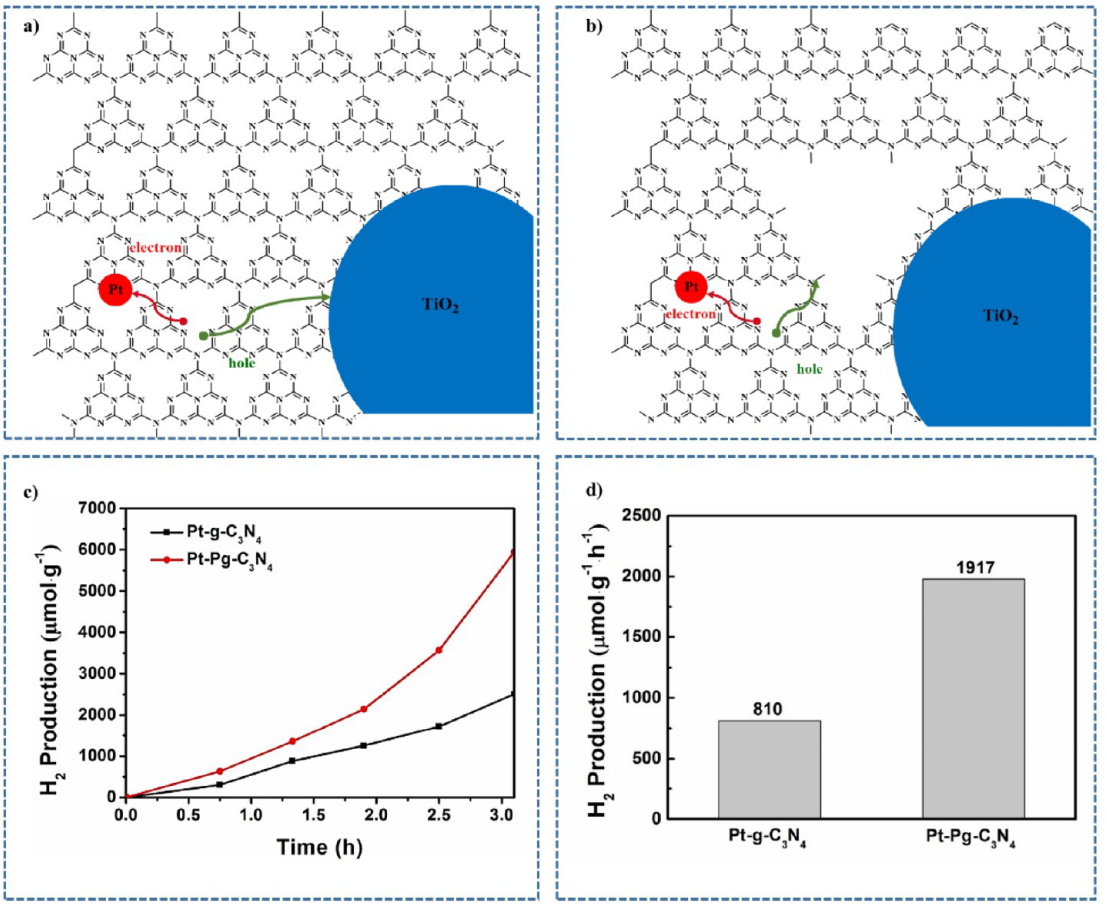

Figure 22. Schematic illustrations of photogenerated electron−hole transportation on (a) Pt-g-C_3N_4−TiO_2 and (b) Pt-porous graphitic C_3N_4−TiO_2 (the Pg-C_3N_4 has a "defective" porous structure). (c) Photocatalytic hydrogen evolution (PHE) kinetics for Pt-g-C_3N_4 and Pt-Pg-C_3N_4 under visible light. (d) Comparison of the PHE rates of Pt-g-C_3N_4 and Pt-Pg-C_3N_4. Reproduced with permission from ref 212. Copyright 2018, Elsevier.

NiO/CN-2:1 could be retained to the extent of approximately 1.49 V at 10 mA cm^{-2} for 16 h, indicating NiO/CN-2:1 had a higher stability than commercial RuO_2 (8 h) and NiO/C (6 h). This was related to the synergetic effects of NiO and CN. Accordingly, g-C_3N_4 showed a good mechanical strength and could be applied as support material for NiO nanocrystals, avoiding their aggregation and loss from the glassy carbon electrode.[209]

6.5.2. C_xN_y-based materials as support. 2D supports, including g-C_3N_4, were hydrothermally prepared and investigated in terms of their effect on the electrochemical activity of CoS_2 nanoparticles in overall water splitting. Compared with their unsupported counterparts, the supported nanohybrids, namely CoS_2/g-C_3N_4, presented more effective water reduction and oxidation and a better overall water splitting performance in a 1 M KOH solution. The specific surface area of the CoS_2/g-C_3N_4 nanocomposites was 20.976 m^2 g^{-1}, and the HER onset potential value was 123 mV versus RHE. The overpotential needed to deliver a current density equal to 10 mA cm^{-2} was 322 mV, and a Tafel slope value of 156 mV dec^{-1} was also obtained for the composite. Concerning the OER activity, an anodic overpotential of 417 mV and a Tafel slope of 138 mV dec^{-1} were measured for this nanocomposite.[210] A composite of $NiSe_2$@g-C_3N_4 that resembled nanocoral was fabricated for highly efficient water oxidation catalysis (OER) under alkaline conditions. Employing a g-C_3N_4 multilayered structure as support, the resultant $NiSe_2$@g-C_3N_4 composite revealed an amazing electrocatalytic activity at a low overpotential value of about 290 mV at a 40 mA cm^{-2} current density and a small onset potential equal to 1.38 V. Moreover, at a 2 V potential the composite generated a higher current density than either of the components alone, exhibiting a current density of 199 mA cm^{-2} versus 142 and 112 mA cm^{-2} exhibited by $NiSe_2$ and g-C_3N_4, respectively. In addition, the composite had a significant electrochemical stability of 10 h.[211] To develop oxidation capabilities at the interface of porous g-C_3N_4, defects were introduced into the structure, and the investigation confirmed that the photocatalytic HER improved under visible light. This edge-site-defected porous g-C_3N_4 was prepared by the confined formation of g-C_3N_4 on a kaolinite template. An enhanced electrocatalytic activity was observed for the as-prepared g-C_3N_4 due to the added contribution of defect-born electrons on the basal plane toward the oxidation process rather than the reduction process. Such characteristics assisted the electron transfer, thus quenching the generated holes during photocatalysis. Results from the visible-light-irradiated HER demonstrated a rate of 1917 μmol^{-1} g^{-1} h^{-1} for the porous g-C_3N_4, which was almost 2.4× that of g-C_3N_4 (Figure 22). Therefore, the engineered defects could facilitate the oxidation of holes in photoinduced water splitting, qualifying the 2D solar fuel generation catalysis.[212]

For a better understanding of the importance of carbon nitride-based materials in water splitting devices, a comparison

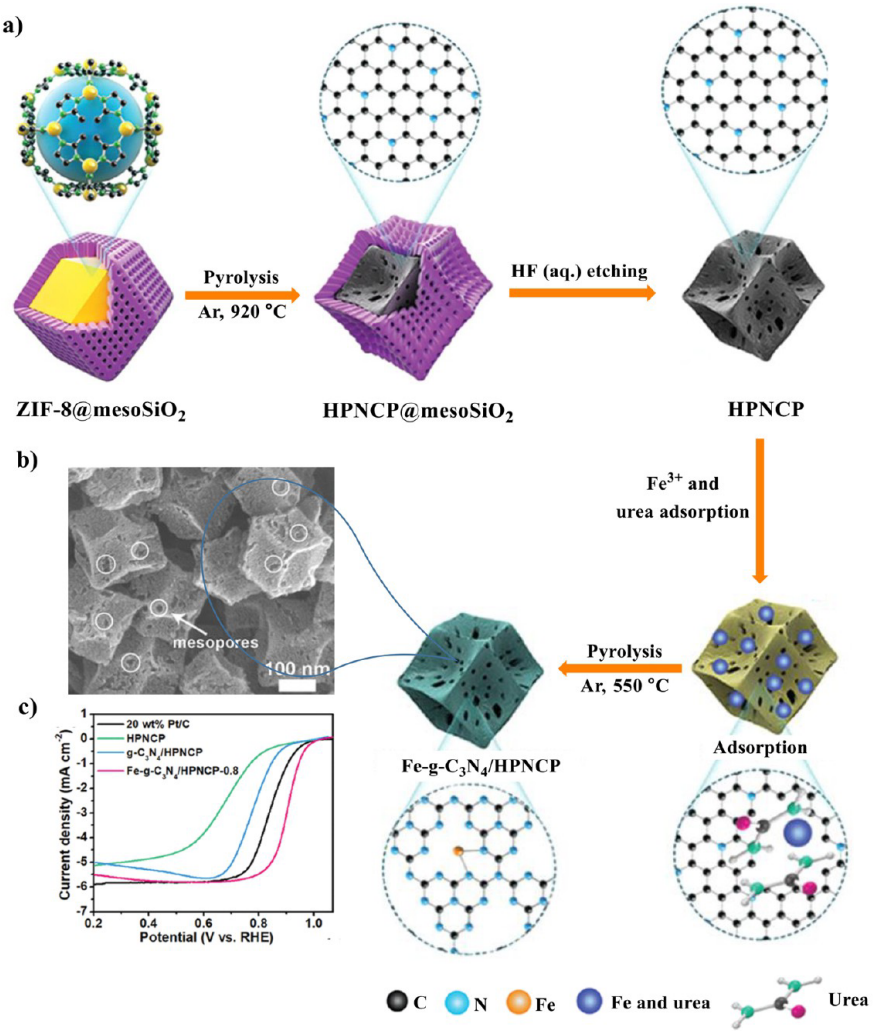

Figure 23. (a) Representation of the fabrication of Fe-g-C_3N_4/HPNCP catalysts through the coordination of iron to carbon nitride. (b) SEM image of the Fe-g-C_3N_4/HPNCP-0.8 sample. (c) Comparative LSV curves for the ORRs of the Fe-g-C_3N_4/HPNCP-0.8, g-C_3N_4/HPNCP, HPNCP, and Pt/C electrocatalysts. Curves were recorded at scan rate of 5 mV s^{-1} and with a rotation rate of 1600 rpm. Reproduced with permission from ref 217. Copyright 2020, Royal Society of Chemistry.

table of C_xN_y-based electrocatalysts and other types of electrocatalysts is presented in Table S3.

6.6. Multipurpose Applications. *6.6.1. C_xN_y-Based Materials as Electrocatalysts for Fuel Cells or Batteries.* As Fe- and N-enriched precursors, hybrid nanostructures of Fe- and N-codoped CNT/Fe-based nanoparticles were prepared with the aid of Zn powder through the direct carbonization of Fe-doped g-C_3N_4. A sufficient level of N doping in CNTs was guaranteed by the presence of zinc. During the formation of the CNTs, Fe and N were doped concomitantly. Fe nanoparticles acted as catalysts for CNT growth at high temperatures during calcination. Due to the abundance of Fe and N, the even and high doping of Fe and N was successfully achieved in CNTs. In the as-synthesized Fe,N-CNT/FeNP nanostructures, a number of different classes of active species were involved in the ORR as follows: the homogeneously dispersed coordinating moieties of Fe such as FeC_xN_y or FeN_x and the $CFe_{15.1}$ nanoparticles encapsulated in Fe,N/CNTs. The Fe,N-CNT/FeNP nanohybrids exhibited an extreme electrocatalytic performance toward the ORR. The results indicated that the nanostructures produced at 800 °C with an Fe source of 0.15 mmol exhibited the best ORR electrocatalytic behavior. It was reported that the nanostructures were able to provide the benefits of both nanoparticles and CNTs. The presence of nanoparticles with different loadings assisted the dispersion of CNTs, while CNTs could increase the stability of the Fe nanoparticles within the ORR. The abundant multiply active components in the heavily Fe- and N-doped nanohybrids led them to express an ORR catalytic activity superior to that of commercial Pt/C, presenting a half-wave potential of 0.82 V, an onset potential of 0.95 V, and a fantastic resistance against methanol crossover.[213]

The impact of sulfur doping on the electrocatalytic activity of CN supported by mesoporous carbon materials was studied in terms of the ORR and the HER. When sulfur was added to mesoporous carbon, a significant improvement in the ORR performance of the SCN-MPC composite catalyst was realized in terms of both its initial potential and its kinetic current regarding the selectivity of the more effective four-electron ($4e^-$) pathway, outperforming the dopant-free mesoporous carbon-supported CN (CN-MPC) with a high durability and a high crossover tolerance. The SCN-MPC electrocatalyst had an oxygen reduction peak potential at −0.22 V in an O_2-saturated electrolyte. Besides, the HER efficiency of the

composite catalyst was superior to those of plenty of other metal-free electrocatalysts and was found to be comparable to those of non-noble metal materials, which were highly active toward the HER. A HER onset potential of 60 mV, a Tafel slope of 51 mV dec^{-1}, and a low overpotential of 145 mV to reach a current density of 10 mA cm^{-2} were demonstrated. Regarding DFT calculations, the supreme performance of the sulfur-doped composites originated from the high spin and charge densities in the C_3N_4 species as well as the modified Gibbs free energy for the adsorption of intermediates. Concerning the chronoamperometric measurements, the SCN-MPC composite maintained 78% of its primary current value over the 50 h test, which was almost 70% higher than that of Pt/C. Besides, the morphology of the SCNMPC structure barely changed over the 50 h stability tests, which confirmed its advanced durability.[214]

Melamine and cyanuric acid were used as the carbon nitride precursors together with green and low-cost glucose as a carbon source for the template-free fabrication of porous hierarchical composite spheres of graphitic carbon nitride–carbon. The 3D (g-C_3N_4/C) composites were able to markedly catalyze the ORR such that the g-C_3N_4/C-2 sample with 33.75 wt % nitrogen exhibited a 0.90 V onset potential with a current density of 23.92 mA cm^{-2}. These properties originated from the high content of nitrogen in the composites, the high specific surface area, and the multisize macropores and micropores, favoring numerous ORR active sites and providing simple charge transfer in the promising as-obtained metal-free hybrids. Mass transfer facilitated through the micropores in addition to the intimate contact between g-C_3N_4 and carbon assisted the electron conductivity, favoring the efficiency of the ORR in the end. The long-term durability results were compared to those of g-C_3N_4. The obtained ORR current in the case of the g-C_3N_4/C-2 composite presented a lower decay rate than the g-C_3N_4 sample. Besides, over 20 000 s, a continuous polarization current retention of 80% eventually resulted in the g-C_3N_4/C-2. Moreover, an evaluation of the composite's morphology after the stability test revealed that it remained almost unchanged and similar to that of the pristine g-C_3N_4/C-2.[215]

A straightforward and cost-effective method was adopted to develop a highly nitrogen-doped (23.54%) porous carbon (NOC-800) with oxygen functionalization (6.11%) using a framework of zinc zeolitic imidazolate as the nitrogen source and graphitic carbon nitride as the template. The designed electrocatalyst was produced with a high degree of graphitization, a large surface area, and a high total pore volume. Electrochemical experiments showed that the as-prepared NOC-800 material had abundant multifunctional electrocatalytic features in alkaline media, owing to its oxygen-based sections. Under an O_2-saturated atmosphere, the NOC-800 exhibited a redox peak at −0.325 V that was more positive than those of other samples, indicating a higher catalytic activity toward the ORR. In this regard, an onset potential of −0.141 V versus Ag/AgCl and a half-wave potential of −0.249 V were obtained for the ORR, while an overpotential of 377 mV at 10 mA cm^{-2} and overpotential of 448 mV at 50 mA cm^{-2} were eventually attained for the OER. Besides, favorable stability was achieved for the NOC-800 sample in the ORR and the OER. Since catalyst stability is an important issue for large-scale commercial applications, the NOC-800 sample and Pt/C catalysts were compared at a voltage of −0.6 V versus Ag/AgCl for 10 h. The NOC-800 sample and Pt/C catalysts exhibited losses of 19% and 34%, respectively, which showed that the NOC-800 sample was more stable than Pt/C catalyst. The oxygen functional groups generated more inherent OER active sites. Meanwhile, the high volume of nitrogen contributed to the creation of more sites for the ORR. Those were accompanied by enhanced electron transfer and mass transport as a result of the high graphitization degree in the product and its high surface area.[216]

To fabricate a porous Fe-*g*-C_3N_4/HPNCPs electrocatalyst, dispersed atomic Fe was coordinated to g-C_3N_4 and anchored on a MOF-derived porous carbon polyhedral support that had previously been doped with nitrogen, as presented in Figure 23. The hierarchical catalyst was synthesized through the absorption of iron precursors on carbon particles, followed by a thermal treatment under an argon atmosphere. Using a 0.1 M KOH electrolyte, the optimum Fe-*g*-C_3N_4/HPNCP-0.8 sample exhibited a supreme electrocatalytic performance toward the ORR. Additionally, a very positive half-wave potential of 0.902 V was achieved, about 60 mV higher than that of the commercial Pt/C catalyst, along with a high durability and strong methanol tolerance. The synergy between the dispersed Fe–N_2 sites and the hierarchical porous structure of the electrocatalyst was realized to be responsible for the considerable ORR activity and the increased availability of the Fe–N_2 active sites, which enhanced the mass and charge transfer.[217]

The galvanic exchange method was used to synthesize CoAg alloy nanoparticles on carbon nitride as an electrocatalyst for the ORR and CO_2 conversion. The lower reduction potential of cobalt compared to that of Ag simplifies the replacement of Co^0 by Ag^+. Primarily, Co nanoparticles were produced through adsorption and reduction steps on the carbon nitride surface to obtain Co/CN, and CoAg/CN nanoparticles were produced via partial galvanic exchange on the solid surface. Both Co/CN and CoAg/CN catalysts were examined for both the ORR in a 1 M KOH solution and CO_2 conversion in a 0.5 M $KHCO_3$ solution. The oxygen reduction potential of this catalyst was at 0.7 V, which was more positive than that of Co/CN (0.47 V). The CoAg/CN catalyst exhibited both a better ORR activity, with a 0.93 V onset potential, and a higher electrocatalytic CO_2 conversion than Co/CN. A decline in the cathodic current to lower than −0.9 V demonstrated the high CO_2 conversion efficiency. The synergy between alloy-type CoAg nanoparticles and the surface morphology alteration resulted in such an improvement of the electrocatalytic performance.[218]

Carbon nanotubes with a bamboo-like morphology coupled with Co nanoparticles wrapped in carbon were fabricated as an electrocatalyst using g-C_3N_4 via a facile pyrolysis method at high temperatures to transform bulk graphitic carbon nitride into a high-surface-area BCNT/Co composite structure. In an O_2-saturated electrolyte, the oxygen reduction peak was observed at 0.857 V, suggesting its ORR catalytic activity. Regarding the ORR process, the as-prepared catalyst outperformed commercial Pt/C in an alkaline medium, with the BCNT/Co sample prepared at 800 °C exhibiting an onset potential of 1.12 and a half-wave potential of 0.881 V. The excellent ORR performance, high stability, and strong methanol resistance of the catalyst resulted from the presence of Co nanoparticles covered by carbon increasing the conductivity, the bamboo-like carbon nanotubes, and the Co–N_x active sites and defects formed in the composite structure, respectively.[219]

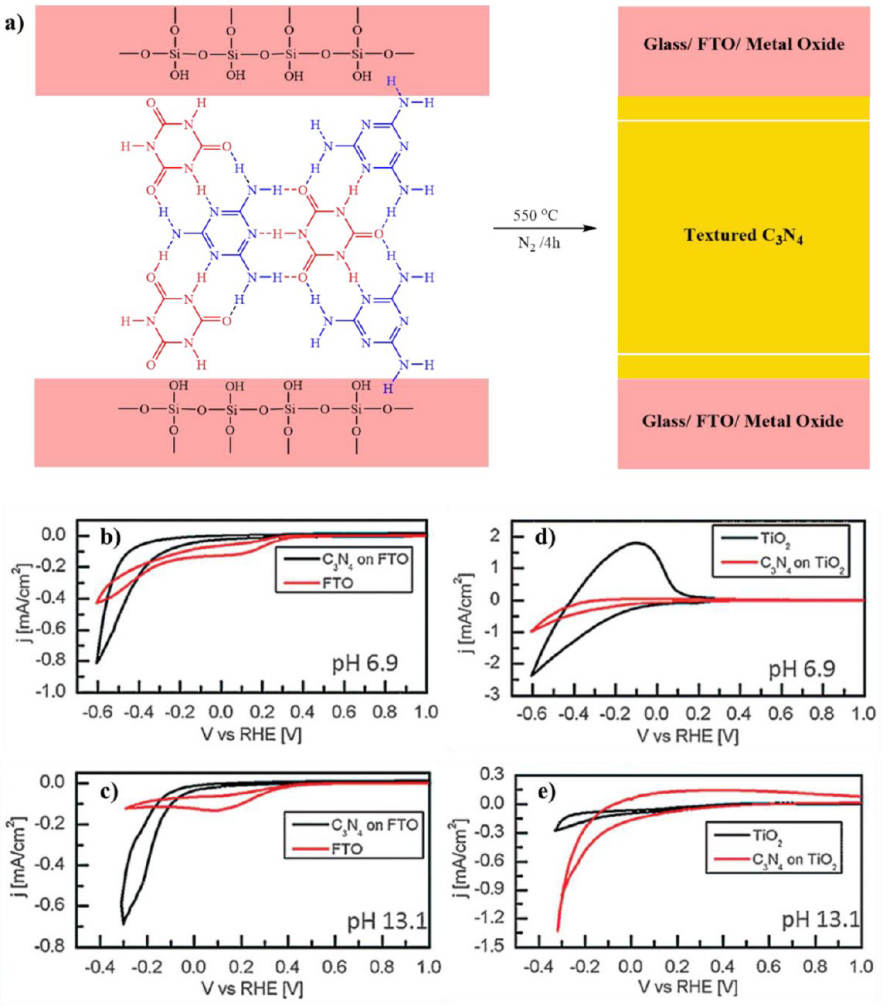

Figure 24. (a) Design of the synthetic process for growing perfectly ordered C_3N_4 on glass substrates. CV measurements of C_3N_4/FTO in (b) a 0.1 M phosphate buffer solution and (c) a 0.1 M KOH solution. CV measurements of C_3N_4/TiO_2 (d) a 0.1 M phosphate buffer solution and (e) a 0.1 M KOH solution. The scan rate was 25 mV s^{-1}. Reproduced with permission from ref 228. Copyright 2014, Wiley-VCH.

6.6.2. C_xN_y-Based Materials as Supports for Fuel Cells or Water Splitting. Uniformly dispersed bimetal AuPd nanoclusters were coordinated to a g-C_3N_4 support to develop a AuPd NCs/g-C_3N_4 electrocatalyst through a simple aqueous method with no special additives. The nanocomposites revealed a remarkable active surface area for electrochemical activities such as the ORR and the HER. The attained nanoscale catalyst demonstrated a higher positive onset potential of 1.09 V and a half-wave potential at 0.98 V (versus NHE) for the ORR in an acidic medium. Besides, an improved current density of 1.86 mA cm^{-2} was obtained. Moreover, enhanced catalytic hydrogen evolution reaction activity was observed for the nanocatalyst, which had a low Tafel slope of 47 mV dec^{-1} and an onset potential of −29 mV. Compared to commercial Pt/C and Pd/C catalysts, the as-prepared nanocomposite exhibited a superior electrocatalytic efficiency.[220]

Porous Au-aerogel-CN_x and AuNPs-CN_x composites were synthesized by dispersing ultrafine gold nanoparticles and a high-surface-area gold aerogel on a carbon nitride support. A supreme ORR electrocatalytic activity was observed for the as-prepared composites in both alkaline and acidic solutions. When the glassy carbon electrode was decorated with Au-aerogel-CN_x and AuNPs-CN_x, two strong peaks appeared at 0.8 and 0.61 V, respectively, indicating the ORR capability of composites. Onset potentials of 0.92 V in 0.5 M KOH and 0.43 V in 0.5 M H_2SO_4 were attained for the Au-aerogel-CN_x composite, which followed the $4e^-$ reduction process. In an alkaline solution, a more positive onset potential of about 30 mV was achieved for the Au-aerogel-CN_x catalyst compared to the commercial Pt/C, and both composites demonstrated a great methanol tolerance and reasonable durability. Besides, in an acidic solution, Au-aerogel-CN_x exhibited a high catalytic HER activity at a low onset potential (−30 mV), a 53 mV dec^{-1} Tafel slope, a high stability, and a 10 mA cm^{-2} current density at an overpotential of −185 mV (with 0.130 mg cm^{-2} Au loading), all of which confirmed the high ORR and HER efficiencies of Au-aerogel-CN_x composites compared to those of AuNPs-CN_x.[221]

6.7. C_xN_y-Based Materials for Other Electrocatalytic Oxidation or Reduction Reactions (ORR, CO_2RR, and NRR). *6.7.1. C_xN_y-Based Materials As Electrocatalysts.* Recently, the electrochemical applications of N-doped mesoporous carbons (NMCs) have attracted a lot of attention, especially in electrochemical applications. In a study, researchers used nitrogen-doped mesoporous carbon nanospheres as a template material.[222] In fact, a colloidal two-step amphiphile-templating technique was reported for the

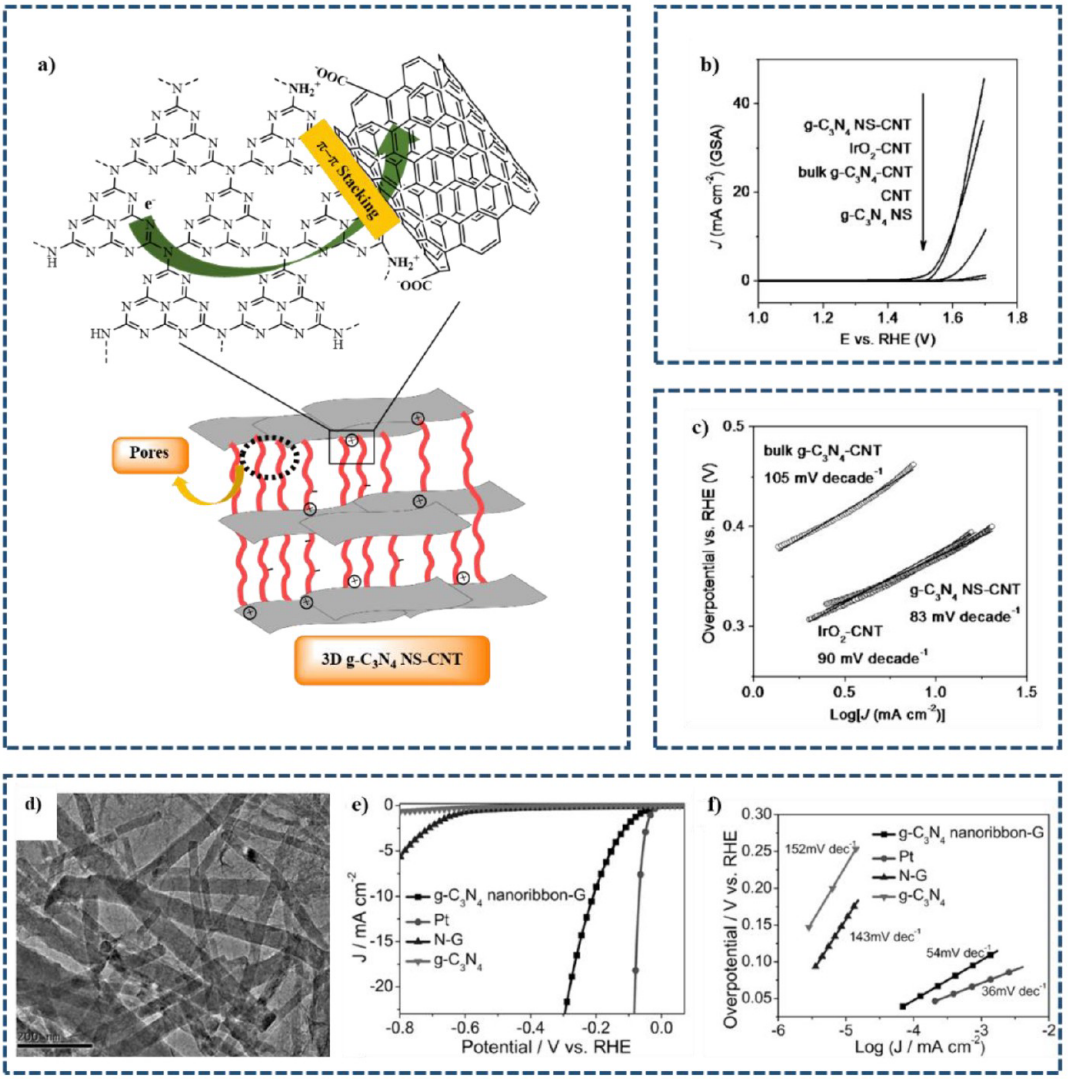

Figure 25. (a) Self-assembly-induced manufacture of the 3D g-C_3N_4 NS-CNT electrocatalyst composite with a porous structure. (b) linear sweep voltammograms and (c) Tafel plots for g-C_3N_4 NS-CNT, IrO_2−CNT, bulk g-C_3N_4−CNT, purified oxidized CNTs, and g-C_3N_4 NSs on a rotating disk electrode (1500 rpm) in an O_2-saturated 0.1 M KOH solution (scan rate of 5 mV s^{-1}). Reproduced with permission from ref 149. Copyright 2014, Wiley-VCH. (d) TEM image of the prepared g-C_3N_4 nanoribbon graphene. (e) HER polarization curves and (f) the corresponding Tafel plots of various catalysts (g-C_3N_4 nanoribbon-G, Pt wire, N-doped graphene (N-G), and g-C_3N_4 in 0.5 M H_2SO_4). The scan rate was 50 mV s^{-1}. Reproduced with permission from ref 232. Copyright 2014, Wiley-VCH.

preparation of a nanosized Fe_3C@mCN nanocomposite, as presented in Figure 4e, which consisted of Fe_3C encapsulated in mesoporous N-doped carbon nanospheres. Along with fine Fe_3C nanocrystals, the produced Fe_3C@mCN hybrids presented an outstanding catalytic performance and excellent durability toward the ORR, owing to their large surface area. Colloidal amphiphilic-template-fabricated composites (CAMs) contained cores of inorganic nanoparticles, which were bound to the hydrophilic polyethylene glycol (PEG) hairs. The nanosized Fe_3C with a 14 nm diameter exhibited multiple vital active sites for enhancing the ORR performance of the produced Fe_3C@mCN electrocatalysts, including the graphite shell of the nanocrystals and the Fe-coordinated nitrogen sites. Among the prepared samples, the Fe_3C@mCN-800 catalyst (pyrolyzed at 800 °C) exhibited a superior durability compared to the commercial Pt/C catalyst. A current retention of 90% was preserved for the catalyst after 10 h, while this value was only 43% in the case of Pt/C. Accordingly, due to its high onset potential (0.9 V), high current density, and strong stability, the Fe_3C@mCN-800 catalyst exhibited one of the highest ORR activities among various Pt-free electrocatalysts. It was concluded that mesoporous CN spheres could be also be loaded with other nanosized metal compounds (oxides, sulfides, and carbides) with the help of the method, and the resultant potent electrocatalysts could be integrated with relevant ORR devices.[88]

Fe/Ni@g-C_3N_4 nanocomposites were developed through an environmentally friendly treatment for application in trichloroethylene (TCE) hydrodechlorination and successive ORRs. An improved TCE hydrodechlorination rate (about eight-times higher at −0.4 V) and efficiency were obtained by decorating lamellar g-C_3N_4 with bimetallic Fe/Ni due to the provision of a large surface area and the small internal resistance for rapid electron transfer. Additionally, an excellent ORR activity with an electron transfer number 3.9 was observed, which arose from the iron oxides produced on the Fe/Ni@g-C_3N_4 surface after dechlorination. A current density of 3.6 mA cm^{-2} and an onset potential of 0.84 V were also achieved for Fe/Ni@g-

C_3N_4.[223] Pd-g-C_3N_4/NCQD composites were prepared for application as a macrocyclic electrocatalyst in the ORR in an alkaline electrolyte by decorating palladium-doped g-C_3N_4 with N-doped carbon quantum dots. The formation of Pd−N bonds and chemical linkages between Pd-g-C_3N_4 and NCQD was confirmed. Based on the electrochemical investigations, the ORR activity of the as-prepared Pd-g-C_3N_4/NCQD was demonstrated to occur via a four-electron path. The Pd−N_x reaction sites together with the accelerated electron transfer at the Pd-g-C_3N_4 and NCQD interface could enhance the ORR kinetics. Compared to commercial Pt/C, the nitrogen-rich Pd-g-C_3N_4/NCQD composite exhibited a comparable catalytic performance and excellent methanol resistance in addition to long-term activity, suggesting it was an appropriate framework for DMFCs.[224]

A Fe−N−C material was developed as the cathode catalyst for DMFC electrocatalysis to cut the high costs of precious-metal-based catalysts. Due to the additives with rich C and N sources, plenty of Fe−N_x and N−C sites were formed, increasing the ORR efficiency in alkaline and acidic media. The ORR efficiency experienced a very slight drop after 2000 cycles. Those active sites mentioned for ORR electrocatalysis also exhibited outstanding performance regarding their stability and durability in methanol, confirming their prospects for use in DMFCs and PEMFC devices.[225]

Researchers have used the hydrogen-bonded cyanuric acid melamine (CM) supramolecular complex as a novel and effective path for the preparation of ordered structures of carbon nitride (C_3N_4).[226,227] Shalom et al. reported an efficient, simple, and novel method of growing high ordered C_3N_4 on diverse substrates from surface-bound CM complexes.[228] In addition, they investigated the catalytic activity of the synthesized materials for the HER and indicated that the synthesized C_3N_4 could be grown on various porous metal oxide electrodes such as ZnO, TiO_2, etc. For this purpose, they examined the deposition of the ordered C_3N_4 rods on glass and fluorine-doped tin oxide (FTO) (Figure 24) and showed the favorable electrochemical properties of C_3N_4 on FTO and TiO_2 using cyclic voltammetry techniques in different media, including basic and neutral electrolytes.

A Cu_2O/g-C_3N_4 composite composed of cuprous oxide enfolded by graphitic carbon nitride was produced as an electrode for the HER. With the aid of CV, EIS, LSV, and other analyses, this nanocomposite was shown to have a large surface area and thus an improved electrocatalytic performance toward the HER in alkaline media. A low onset potential and an internal resistance of 25 mV and 3.42 Ω, respectively, were observed, and the Volmer−Heyrovsky HER mechanism was confirmed. An overpotential of 148.7 mV was measured along with an exchange current density of 12.8 mA cm^{-2}, while the Tafel slope was determined to be 55 mV dec^{-1}.[229]

A defect-engineered electrocatalyst of carbon nitride (DCN) was fabricated and further loaded with low contents of Ru nanoparticles. The as-prepared DCN catalyst exhibited a remarkable catalytic performance toward the electrochemical hydrogen evolution reaction. At a current density of 10 mA cm^{-2}, the Ru-DCN electrocatalyst exhibited an overpotential of 51 mV and a Tafel slope of 59.5 mV dec^{-1}, which was smaller than that of Ru-CN. The enhanced properties originated from the increased surface area and the abundant defect sites.[230] Mesoporous exfoliated nanocomposites of g-C_3N_4/NiO were fabricated. The samples reformed from an alcohol−water medium, and it was realized that the electrochemical hydrogen evolution activity of the composite increased with the amount of nickel oxide. Among the different samples, g-C_3N_4/NiO (7.5%) demonstrated the best HER results such that at 10 mA cm^{-2} the overpotential was 215 mV and the Tafel slope was 95 mV dec^{-1}. The high stability by the composite was also indicated during voltammetry tests.[231] In another study, Qiao et al. investigated the efficient and simple self-assembly of graphitic carbon nitride nanosheets (NSs) and CNTs (g-C_3N_4 NS-CNT)[149] (Figure 25). In the study, the g-C_3N_4 NS was applied instead of g-C_3N_4 alone, which created a simple and robust assembly of a 3D interconnected network with advantages that included an improved porous structure, a high surface area, and a high N content. The synthesized composite was employed as an efficient electrocatalyst in the OER, and the lower Tafel slope value for the g-C_3N_4 NS-CNT (83 mV dec^{-1}) revealed its more favorable kinetics relative to the nanosized IrO_2 catalyst supported by CNTs (90 mV dec^{-1}) (Figure 25c). The stability of the g-C_3N_4 NS-CNT was evaluated using chronoamperometric tests, which showed a high stability through a slight anodic current attenuation of 13.3% in 10 h.

To enhance the conductivity and electrocatalytic properties of g-C_3N_4 for various reactions such as the OER, the HER, and the ORR, a combination of g-C_3N_4 and graphene is a desirable choice for the electrocatalytic performance, which is normally superior to those of metal-based catalysts.[149,233−235] Qu et al. successfully demonstrated an efficient, modest, and one-step hydrothermal technique for the synthesis of 3D interconnected networks using the rational assembly of 1D g-C_3N_4 nanoribbons with 2D graphene sheets (g-C_3N_4 nanoribbon-G)[232] (Figure 25d). The prepared g-C_3N_4 nanoribbon-G exhibited a much lower onset overpotential (η = 80 mV) than other carbon-based materials and even non-noble metals or oxides. The results indicated that these graphene-modified g-C_3N_4 nanoribbons could be applied as high-performance HER electrocatalysts, providing benefits such as high available surface areas, multielectron transport channels, and a small diffusion space for an exceptional transfer and separation of charge.

In another study, Lee et al. developed a procedure for the synthesis of efficient and metal-free electrocatalysts using g-C_3N_4 coupled with S- and Se-doped nanoporous graphene (g-C_3N_4@S-Se-pGr).[236] The synthesized electrocatalyst showed a performance for the HER higher than those of metal-based electrocatalysts such as MoS_2 and Pt/C. Lee et al. demonstrated that the best catalytic activity could be achieved when the least amount of catalyst was loaded. In addition, their results showed the desirable stability and full tolerance in acidic and alkaline media of the synthesized catalysts.

In another study in the same year, Amal et al. investigated the fabrication of novel composites using covalently bonded g-C_3N_4/multiwall carbon nanotube (g-C_3N_4/MWCNTs) hybrids.[237] For this purpose, they used a two-step method, including coprecipitation and polycondensation. The synthesized g-C_3N_4/MWCNT was applied as an efficient new electrocatalyst for the electrocatalytic reduction of CO_2 to CO. The experimental results showed that the prepared composite had a high stability and selectivity as well as a maximum Faraday efficiency of 60%. In addition, the composites did not experience a decrease in catalytic activity even over 50 h of reaction. The obtained improvement in the catalytic activity could be due to several reasons, including the formation of an active carbon−nitrogen bond and large specific

surface area and high conductivity of the composites. In 2016, Liu and co-workers demonstrated an efficient and simple in situ interfacial engineering technique for the synthesis of molybdenum disulfide−graphitic carbon nitride (MoS_2/g-C_3N_4) van der Waals (vdW) ultrathin layers.[238] The prepared MoS_2/g-C_3N_4 vdW layers displayed a high catalytic performance toward the HER. Moreover, the synthesized compound had a higher catalytic activity than Pt catalysts. This activity could be attributed to the interfacial connections between MoS_2 and g-C_3N_4 layers, particularly the electronic coupling between Mo and N atoms, as a result of which the hydrogen adsorption and reduction kinetics for the HER would be improved.

Graphitic carbon nitrides have abundant nitrogen groups, which provide more coordination sites for different metals. In addition, they provide exact data for the characterization of the active sites in catalytic reactions. Since g-C_3N_4 alone may not have sufficient electrocatalytic properties, many studies have been conducted, revealing that a metal-g-C_3N_4 complex (M-C_3N_4) can perform well in electrocatalytic reactions. Qiao et al. developed the synthesis of a novel series of metal−nitrogen−carbon (M-N/C) complex materials, including M-C_3N_4 organometallic complexes.[239] For this goal, they used g-C_3N_4 as a platform. Co−C_3N_4 was applied as an electrocatalyst for the ORR and OER in an alkaline environment. The results confirmed a high catalytic performance related to the accurate M-N_2 coordination in the g-C_3N_4 matrix. In 2018, Huang and colleagues successfully reported an efficient and one-pot approach for the synthesis of porous B-doped g-C_3N_4 nanosheets.[240] Accordingly, they used urea and H_3BO_3 as precursors for thermal polymerization. The prepared B-doped g-C_3N_4 nanosheets had two functionalities, including photocatalytic and electrocatalytic performances. In other words, the B-doped g-C_3N_4 nanosheets could be applied for the photodegradation of methylene blue (MB) under visible-light irradiation as well as the ORR and the OER. The high catalytic performance of the synthesized catalyst was assumed to be related to the increased number of exposed active sites created during the exfoliation of g-C_3N_4 in the nanosheets, the resulting porous structure, and the high conductivity due to B-doping. Thus, the use of heteroatoms, such as boron, sulfur, etc., in doping can increase the conductivity of g-C_3N_4, which can in turn lead to an increase in the HER and ORR electrocatalytic activity.[241]

Recently, the utilization of salt templates instead of traditional compounds such as silica, sodium dodecyl sulfate, and anodic alumina, has received a lot of attention, as salt templates have several privileges, including simple movability, the possibility of scalable manufacturing, and a safer preparation procedure.[242] In 2019, Zhu and co-workers demonstrated an efficient and novel method for the synthesis of 3D porous g-C_3N_4 using a facile NaCl-assisted ball-milling approach.[243] The synthesized porous material were shown to have a bifunctional role in both the electrocatalytic OER and photocatalytic hydrogen evolution. The 3D cubic NaCl particles were applied as an easy-to-move template to modify the production of 3D porous g-C_3N_4 networks and to avoid g-C_3N_4 agglomeration during the calcination procedure.

A novel g-C_3N_4/Cu_2O-FeO nanocomposite was reported as an electrocatalyst for the reduction of CO_2 to CO. The highest Faradaic efficiency of 84.4% was obtained at a low onset overpotential equal to −0.24 V versus NHE. At −1.60 V versu Ag/AgCl, a turnover frequency of 10 300 h^{-1} was achieved for the conversion of CO_2 to CO along with a great selectivity of 96.3% regarding thermodynamic overpotential of −0.865 V versu NHE. Such a significant CO_2 to CO reduction in a neutral aqueous medium was ascribed to the close interactions at the interface between g-C_3N_4 and Cu_2O-FeO as well as to the larger active surface area.[244] A great CO_2 electroreduction was investigated for cobalt phthalocyanine (CoPc)/g-C_3N_4-CNT composites, which exhibited the selective transformation of CO_2 to CO with a turnover frequency of 4.9 ± 0.2 s^{-1} and a Faradaic efficiency of 95 ± 1.8%. Besides, no degradation was observed at −0.8 V versus RHE after 24 h. As the polymeric catalyst was fixed on g-C_3N_4−CNTs to form an interconnected network, the active surface area for electrocatalysis became enlarged, leading to structural and operational strength.[245] An Mn−C_3N_4/CNT composite for the electrochemical CO_2RR was synthesized by embedding Mn with a Mn−N_3 site into graphitic carbon nitride on carbon nanotubes. In an aqueous electrolyte, the prepared catalyst successfully exhibited a 98.8% Faradaic efficiency and a 14 mA cm^{-2} current density at an overpotential of 0.44 V. However, in an ionic liquid electrolyte, the current density was 29.7 mA cm^{-2} at an overpotential of 0.62 V. The presence of Mn−N_3 sites contributed to the formation of COOH* intermediates with a reduced free energy barrier and thus to the enhanced CO_2RR performance.[246] Cu−C_3N_4 was produced as a single-atom catalyst that offeredasymmetrical active sites, including Cu, C, and N, to reduce CO_2 and generate C_2 products. Multiple reaction pathways for the conversion of CO_2 to ethylene were investigated theoretically, among which 1.08 eV at the open circuit was realized to be the most probable reaction route with the help of the C and Cu active sites. When dealing with C/N and Cu/N active sites, the carbon atoms are settling sites for the initial reduced CO_2, leaving Cu vacant to reduce the next CO_2 molecule.[247] The reduction of CO_2 to formic acid was studied through the fabrication and use of Sn/CN-*x* electrocatalysts. Due to the electron-rich Sn structure originating from metal (Sn)−support (N atoms) interactions, features such as CO_2 adsorption and activation and charge transfer were enhanced. An excellent formic acid Faradaic efficiency (96% ± 2%) at −0.9 V versus RHE was obtained for the composite, which had a high stability (maintained above 92%) over 10 h of reaction.[248] A ZnO/g-C_3N_4 nanocomposite was synthesized for the electrochemical reduction of CO_2 to formate in an aqueous $KHCO_3$ solution at −0.504 V versus RHE. Faradaic yields of 40.20, 53.60, and 80.99% were obtained by bulk electrolysis at −0.504, −0.734, and −0.934 V versus RHE, respectively.[249]

A Pd/g-C_3N_4@rGO hybrid was developed for methanol electro-oxidation. The electrochemical results revealed that the hybrid had a high current density of 0.131 mA cm^{-2} and long-term stability, suggesting its great electrocatalytic efficiency toward methanol oxidation. Such features were attributed to the favorable rGO conductivity and the complete exposure of Pd nanoparticles to methanol molecules.[250] Atom-pair catalysts (APCs) were produced using transition-metal-doped g-CN monolayers for the nitrogen reduction reaction (NRR), and the electrochemical mechanism was theoretically defined. In the case of the Fe_2@CN and Co_2@CN catalysts, the limiting potentials were −0.47 and −0.78 V, respectively. Co_2@CN was more efficient for N_2 fixation because it suppressed the HER. Additionally, stable Fe_2@CN with an improved selectivity and an almost low overpotential was acceptable for the NRR. A two-way charge transport mechanism was

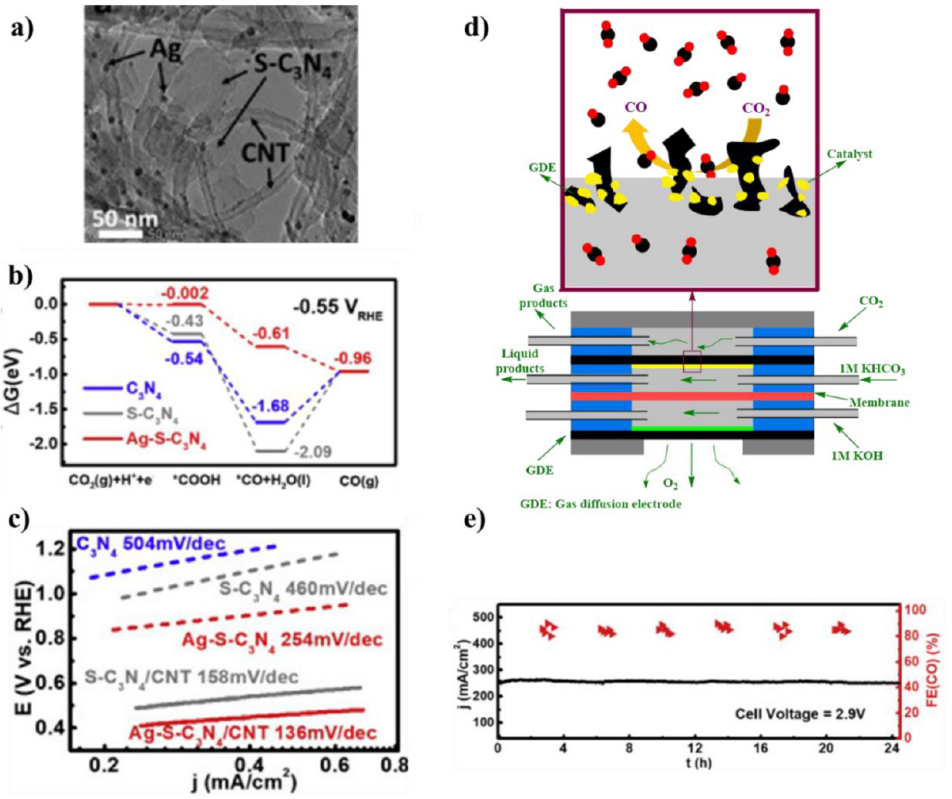

Figure 26. (a) TEM image of the Ag−S−C_3N_4/CNT nanocomposites. (b) The calculated Gibbs free-energy diagram for the CO_2RR to CO catalyzed by C_3N_4, S-C_3N_4, and Ag-S-C_3N_4. (c) Tafel plots for the C_3N_4, S−C_3N_4, Ag−S−C_3N_4, S−C_3N_4/CNT, and Ag−S−C_3N_4/CNT nanocomposites at different applied potentials. (d) schematic of a CO_2 flow cell electrolyzer applied to evaluate the electrocatalytic activity of the prepared Ag−S−C_3N_4/CNT composite. (e) Long-term electrolysis tests under a cell voltage of 2.9 V. Reproduced with permission from ref 258. Copyright 2020, Elsevier.

observed for each synthesized catalyst and N_2, which could activate the inert N≡N bonds.[251] A number of boron−carbon nitride composites (BCN) with Lewis acid sites, which were adjusted by tuning the nitrogen and boron contents, were synthesized for nitrogen reduction electrocatalysis. The composites exhibited significant NRR activity, with a −9.87% Faradaic efficiency, a −41.9 μg h^{-1} mg_{cat}^{-1} ammonia yield, andh noticeable stability. Theoretical calculations revealed that the BCN boron sites lowered the energy barrier for NRR rate-determining steps and enabled nitrogen adsorption spontaneity.[252]

The NRR is an emerging field toward sustainable ammonia (NH_3) production that provides a promising opportunity to replace the Haber−Bosch process. Despite some progress, this research field is still in its infancy and remains largely unexplored. There are lots of challenges to the use of NRR catalysts, and it is still challenging to prevent low selectivities and Faraday efficiencies from impeding the development of the electrochemical NRR.[253−256] According to the results obtained in the literature,[256] the reported yields of NH_3 and the Faraday efficiencies of g-C_3N_4-based catalysts are still far from satisfactory and also uncompetitive with state-of-the-art NRR catalysts due to poor N_2 activation, the limited density of active sites, the high reaction energy barrier, and unsatisfactory HER suppression.[257] In addition, it can be clearly seen from the recent reports that the activity for most NRR catalysts comes from impurities. The metal impurities are present in the reaction media in trace amounts. However, the impact of metal impurities on the catalytic prowess is still unclear; therefore, further research is required to understand the overall mechanism and to develop efficient electrocatalysts to improve the selectivity and Faradaic efficiency.

In 2020, Feng et al. investigated a cost-effective method for the synthesis of Ag-decorated sulfur-doped graphitic carbon nitride−carbon nanotube nanocomposites (Ag-S-C_3N_4/CNT)[258] (Figure 26a). The synthesized nanocomposites were applied as efficient electrocatalysts for the CO_2RR. The DFT results showed that the interfacial electron transfer from Ag to S-C_3N_4 contributes to the conductivity of the catalytic system, while decorated Ag nanoparticles tune the *COOH binding energy and lead to the high selectivity for CO production (Figure 26b). The experimental results and DFT calculations revealed that the efficient CO_2RR performance originated from the synergetic effect of Ag nanoparticles, sulfur elements, the g-C_3N_4 scaffold, and CNT supports, where the enhanced intrinsic electrical properties and CO_2 reactivity have promoted the electron transfer and stabilized the reaction intermediates (Figure 26c). In addition, it was reported that the Ag-S-C_3N_4/CNT nanocomposite could be applied with an industrial-scale current density in flow cell configurations, revealing its high stability and selectivity (Figure 26d and e).

There are a number of studies on the high performance of metal phosphides in the HER, where the phosphorus applied exists as a hypophosphite, a phosphate, or a phosphite. Phosphorus acts like nitrogen in g-C_3N_4, bringing about active sites. The application of elemental red phosphorus (P) in electrocatalytic reactions is limited due to its low conductivity; however, hydrothermal treatments at shorter durations reduces

Table 1. Research Conducted on Fabrication and Electrocatalytic Reactions Using Various Carbon Nitride Composites

electrocatalyst	reaction	surface area ($m^2\ g^{-1}$)	current density	onset potential	FE	yield ($\mu g\ h^{-1}\ mg^{-1}_{cat.}$)	ref
polymeric carbon nitride (PCN)	NRR				11.59%	8.09	267
2D C_3N_4@MoN hybrid	HER		10 mA cm^{-2}				268
exfoliated g-C_3N_4	HER from a water−alcohol solution	136.7					269
Pd-supported C@C_3N_4	ORR, HOR	527	8.5 A mg_{Pd}^{-1}, 0.14 A mg$_{Pd}^{-1}$	0.67 V			270
Pt-supported C@C_3N_4	HER, HOR	527	−6.9 A mg_{Pt}^{-1}, 0.03 A mg_{Pt}^{-1}				270
MGCN	HER		10 mA cm^{-2}	197 mV			271
C/g-C_3N_4	NRR						272
C_3N_4/($Co(OH)_2$/$Cu(OH)_2$	CO_2 reduction		8.94× higher than C_3N_4				273
CN/C600	NRR				16.8−62.1%	1.7−2.9	274
nitrogen-deficient g-C_3N_4	HER	66.40	10 mA cm^{-2}				275

its size and surface oxidation increases its conductivity, making P an appropriate additive for improving the electrocatalytic activity of nonmetallic g-C_3N_4.[259−263] Prakash et al. reported the synthesis of red P-embedded binary rGO-*g*-C_3N_4 via a hydrothermal treatment.[264] The prepared composite was applied as an efficient electrocatalyst for the HER, the results of which exhibited that a catalyst prepared using 30 wt % red P, reduced graphene oxide (with a fixed weight percentage of 5% in all composites), g-C_3N_4 could have a high performance toward the HER of water in an acidic environment.

6.7.2. C_xN_y-Based Materials as Support. Support materials are very important in electrocatalyst fabrication as they can increase the noble-metal activity by improving the surface area, conductivity, and surface interactions. Carbon supports are popular for various Pd-based catalytic applications. Among these supports, graphitic carbon nitride has received significant attention as a support due to its rich surface features and consistent C−N bonds with a nonlocalized π-electron structure.[265] Through the investigation of g-C_3N_4 as a support material for palladium, a Pd−Ni/g-C_3N_4 nanocomposite was synthesized and evaluated for its HER electrochemical activity. The characterizations confirmed the structure-improving effect of the support material. The HER performance was evaluated in 0.5 M H_2SO_4, and the electrocatalyst revealed a superior catalytic activity with a Tafel slope of 56 mV dec^{-1}, a current density of 10 mA cm^{-2}, and a low overpotential of 55 mV. This activity was associated with the high dispersion of nanopalladium onto the support and the tight interaction between g-C_3N_4 and Pd−Ni. Further, according to stability measurements there was a negligible current density loss over 12 h, a slight change in the polarization curve was observed by 10 000 cycles.[265] Gascon et al. reported the preparation of a novel structure of silver nanoparticles supported by g-C_3N_4 (Ag on g-C_3N_4).[266] They applied the synthesized Ag on g-C_3N_4 hybrid as an effective catalyst for the electrocatalytic reduction of CO_2 in the synthesis process of syngas ($CO + H_2$). In addition, they indicated that the prepared electrocatalyst had a high stability and high selectivity in the presence of buffers like phosphate. Finally, the synthesized catalyst could be recycled and reused for several cycles without any significant loss of performance.

In the following, a number of studies focused on the preparation and application of carbon nitride compounds in different electrocatalytic reactions are listed in Table 1.

For a better understanding of the importance of the carbon nitride-based materials in a number of oxidation and reduction reactions, a comparison table of C_xN_y-based electrocatalysts and other types of electrocatalysts is presented in Table S4.

6.8. C_xN_y-Based Materials for Supercapacitors. The structural features of carbon nitride turn it into a promising electrode material for application in supercapacitors. The small specific surface area of bulk nitrides and their weak conductivity are usually solved through modification or by mixing them with other compounds, which improves their electrochemical activity for use as supercapacitors.[276]

6.8.1. C_xN_y-Based Materials As Electrocatalysts. A g-C_3N_4/PPy nanocomposite was prepared as a supercapacitor. At the current density of 0.4 mA cm^{-2}, its maximum areal capacity was 289.6 mF cm^{-2}, which was higher than pristine PPy (194.8 mF cm^{-2}). This heterostructure electrode exhibited a low resistance and maximum life cycles of 99% approaching 10 000 cycles, which arose from the synergy between g-C_3N_4 and PPy with good adhesion on the surface.[276] TGCN/PANI electrodes composed of template-free prepared g-C_3N_4 and optimized polyaniline nanofibers were evaluated as efficient supercapacitor materials. At a scan rate 0.02 V s^{-1}, the optimized TGCN/PANI nanocomposites (TCP50) developed a large specific capacitance (298.31 F g^{-1}) and a high cycling stability, losing very small capacitance levels after 5000 cycles. Besides, low self-discharge and current leakage were observed, and the sample electrode TCP50 demonstrated a high energy density equal to 33.57 Wh kg^{-1} at a 400 W kg^{-1} power density. It was concluded that PANI nanofibers on g-C_3N_4 nanosheets could provide good surface area, porosity, and charge transfer features.[277] Carbon self-doped g-C_3N_4/NiS composites were prepared for electrochemical performance through thermal oxidation, which improved the fluidity of charge through self-doping and, after being thermally etched, accommodated NiS particles. At a current density of 1 A g^{-1}, the produced composite retained a high specific capacitance of 1162 F g^{-1}, with an 82% capacitance retention for up to 8000 cycles. Moreover, a high energy density of 27 Wh kg^{-1} was obtained for the TC-g-C_3N_4/NiS/AC device, with a 87.9 capacitance retention after the same cycles.[278] A new PPy/C_3N_4 composite was prepared through the incorporation of polypyrrole on carbon nitride. As a supercapacitor, the material exhibited an 810 F g^{-1} capacitance at 0.2 A g^{-1}, with 92% capacitance retention after 6000 cycles at 6 A g^{-1}. Furthermore, a capacitance of 610 F g^{-1} was obtained at 9 A g^{-1}, which was ascribed to the stabilized structure of the material due to Ppy

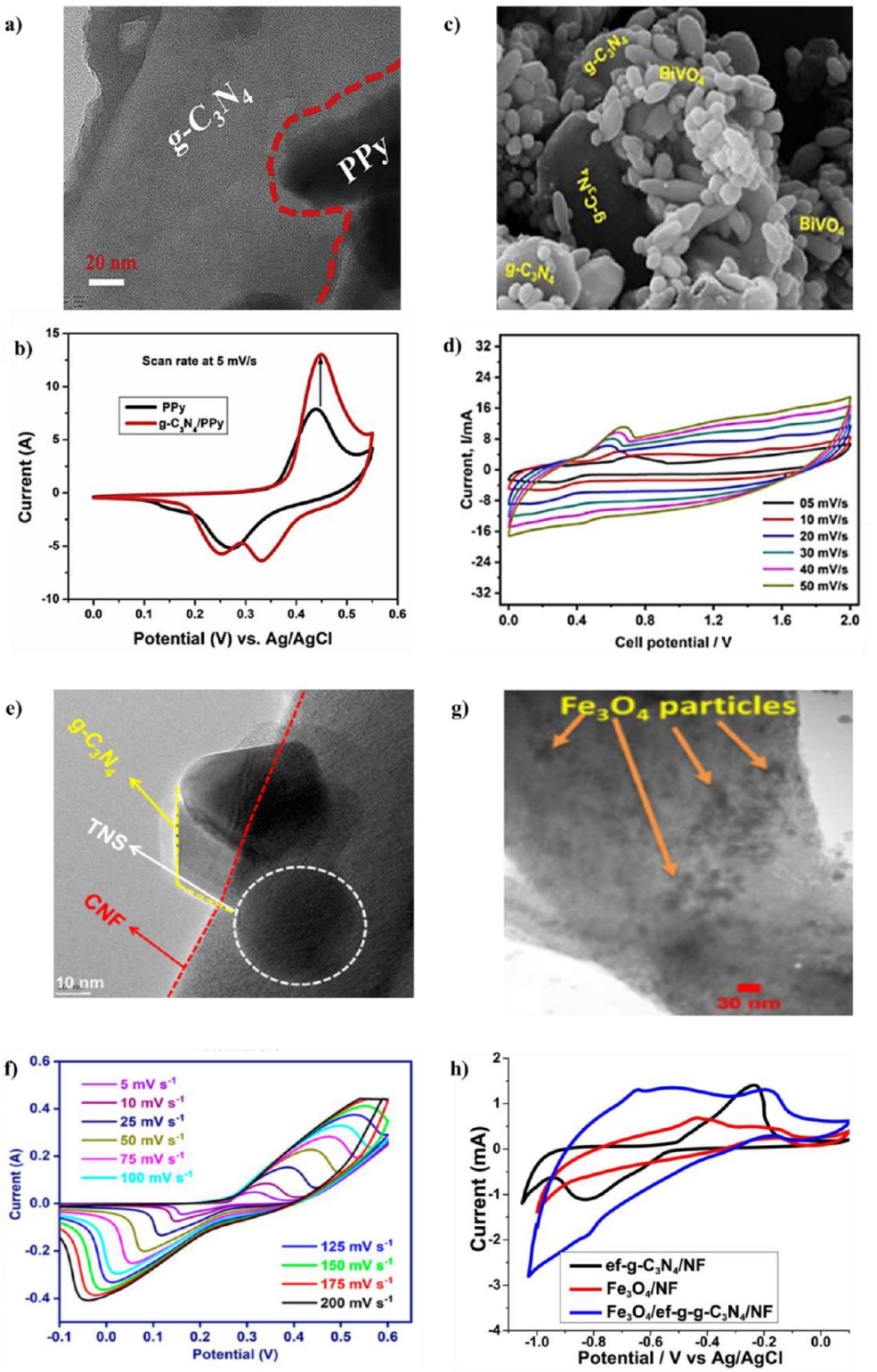

Figure 27. (a) TEM image and (b) cyclic voltammetry results reported for pristine PPy and its g-C_3N_4 composite. CV curves were recorded at a scan rate of 5 mV s^{-1}. Reproduced with permission from ref 276. Copyright 2020, Elsevier. (c) Image of g-C_3N_4–bismuth vanadate nanocomposite-based supercapacitor materials and (d) CV curves recorded at various scan rates. Reproduced with permission from ref 285. Copyright 2020, American Chemical Society. (e) Image of the functionalized carbon nanofiber/g-C_3N_4/TiO_2 nanosphere electrode and (f) CV curves at different scan rates. Reproduced with permission from ref 282. Copyright 2021, American Chemical Society. (g) Image of the binder-free synthesized Fe_3O_4–edge-functionalized-*g*-C_3N_4 composite and (h) CV curves recorded at 5 mV s^{-1}. Reproduced with permission from ref 289 Copyright 2020, Elsevier.

N–H bonds, the C_3N_4 π-system, and the planarization effect over polypyrrole chains.[279]

Graphite carbon nitride-coated carbon cloth (CC@g-C_3N_4-900) electrodes were fabricated that exhibited an excellent

specific capacitance of 499 F g^{-1} at 1 A and showed a high rate capability equal to 292 F g^{-1} at 20 A g^{-1}. Besides, after 10 000 cycles, a capacitance loss of 4.4% was observed. Additionally, an energy density of 10.1 W h kg^{-1} was obtained at 10000 W kg^{-1}. All the superior electrochemical activity of this electrode originated from its binder-free self-supported feature as well as the strong C−C and g-C_3N_4 coupling and rich nitrogen doping.[280] A Co_3O_4/g-C_3N_4 composite electrode that included Co_3O_4 dispersed on graphitic carbon nitride was synthesized for electrochemical supercapacitance measurements. Compared to pure Co_3O_4, the electrode revealed a higher specific capacitance of 1071 F g^{-1} in a 6 M KOH solution and a 1 A g^{-1} current density. About 80% of the capacitance was preserved after 4000 cycles. Further, the asymmetric Co_3O_4/g-C_3N_4/AC device delivered an energy density of 20.4 Wh kg^{-1} at a power density of 0.8 kW kg^{-1}.[281] The carboxyl-modified surfaces of g-C_3N_4 and carbon nanofibers were coupled with TiO_2 nanospheres, and g-C_3N_4−CNF/TiO_2 composite electrodes were prepared. At 0.25 A g^{-1} in a 4 M KOH electrolyte, the electrodes showed a specific capacitance of 817 F g^{-1} and good stability for 2000 cycles while maintaining 89.2% of the capacitance. The great conductivity, surface functionalization, accessibility, chemical interface, and composition synergy were reported to be responsible for the improvement of the supercapacitance.[282] g-C_3N_4 nanosheets were synthesized through chemical and thermal oxidations and exhibited different electrochemical performances. At a current density of 0.5 A g^{-1}, a specific capacitance of 170.1 F g^{-1} was obtained via thermal oxidation at 580 °C, which was higher than those of both ordinary g-C_3N_4 (127.7 F g^{-1}) and 12 M sulfuric acid-treated g-C_3N_4 (133.6 F g^{-1}). In 2 M KOH, the cyclic stability was accompanied by 95.9% capacity retention after 1000 cycles.[283] Nanocomposites of Fe_3O_4/O-functionalized g-C_3N_4 were fabricated by the electrophoretic−electrochemical method. Based on the electrochemical evaluations, the Fe_3O_4@O-*g*-C_3N_4/Ni foam exhibited a 710 F g^{-1} specific capacitance at 0.5 A g^{-1}, and 94.6% of it was retained after 8000 cycles at a current load 5 A g^{-1}. That reached 80.15% at 3 A g^{-1}, which was explained the superior synergism by Fe_3O_4 nanoparticles and O-functionalized g-C_3N_4 sheets.[284] A nanocomposite of g-C_3N_4/$BiVO_4$ was synthesized as a supercapacitor in aqueous electrolytes. Since rice pellet-formed $BiVO_4$ decorated the g-C_3N_4 nanosheets, the wettability was enhanced, leading to better electrolyte ion permeability in the electrodes and increasing the specific capacity. At a current density of 2 A g^{-1}, the 6 wt % g-C_3N_4/$BiVO_4$ nanocomposite exhibited a large specific capacity of 2171 C g^{-1}. At a maximum cell potential of 2 V, the symmetric supercapacitor configuration of the 6 wt % g-C_3N_4/$BiVO_4$ electrode delivered power and energy densities of 16.2 kW kg^{-1} and 61 W h kg^{-1}, respectively. For over 20 000 cycles, the nanocomposite exhibited 130% stability at a current density of 20 A g^{-1} together and a 98.8% Columbic efficiency. The capacitive and noncapacitive charge storage processes in the composite were found to deliver such superior properties.[285]

The g-C_3N_4/TiO_2 nanocomposites were prepared through thermal spreading. Among various carbon nitride loadings, the composite with 33 wt % g-C_3N_4 showed a high specific capacitance with a reasonable electrochemical behavior in the charge−discharge cycling tests. Examining the composite in terms of the supercapacitance, a higher specific capacitance of almost 864.5 F g^{-1} was measured. For 2000 cycles at a current density of 6 A g^{-1}, the g-C_3N_4/TiO_2 nanocomposite demonstrated excellent retention.[286] An O-functionalized-g-C_3N_4/$Ni(OH)_2$/nickel foam electrode was prepared. The electrochemical charge storage of the fabricated composite electrode was studied in a KOH, and the electrode's specific capacity was calculated to be 967 C g^{-1} along with an excellent stability of 94.4% for 5000 cycles at 3 A g^{-1}. The synthesized O@g-C_3N_4/$Ni(OH)_2$/NF electrode showed smaller internal and charge transfer resistance, verifying its larger rate of charge transfer and higher conductivity compared to pristine Ni-$(OH)_2$/NF.[287] A hybrid asymmetric S-doped g-C_3N_4/CoS_2 material was prepared as a supercapacitor that was workable at a 30 A g^{-1} current density. A high electrochemical stability (89% for over 100 000 cycles) and a Coulombic efficiency of 99.6% were achieved. Additionally, a specific capacitance of 180 C g^{-1} at a 1 A g^{-1} current density was obtained by the electrode working with a negative bioderived carbon electrode in a cell with 1.6 V potential, where high energy density and power density values of 26.7 W h kg^{-1} and 19.8 kW kg^{-1}, respectively, were measured in the aqueous electrolyte.[288] Fe_3O_4/g-C_3N_4 was deposited on Ni foam, and Fe_3O_4/edge-functionalized-*g*-C_3N_4/NF nanocomposite electrodes were created to be investigated as binder-free supercapacitors. Based on the results, the electrodes obtained a specific capacitance of 197.2 mAh g^{-1} at 0.5 A g^{-1}, and cycle lives of 96.1% and 88.5% were obtained at 0.5 and 3 A g^{-1}, respectively, for 4000 cycles, confirming the synergetic effect in the structure.[289] Mesoporous 3D Zn−Ni−Co−S nanowire-like arrays were grown on Ni foam for use as electrode supercapacitors and demonstrated a capacity of 418.2 mAh g^{-1} at a current density 4.6 mA cm^{-2}. Moreover, after 10 000 cycles, the arrays demonstrated a cycle life around 89%. In an asymmetric supercapacitor, the Zn−Ni−Co−S arrays were used as the cathode while graphitic carbon nitride/graphene was applied as the anode, and a cell capacity of 110.7 mAh g^{-1} was achieved at 5 mA cm^{-2} with 54% capacity retention at 75 mA cm^{-2}. After 10 000 cycles, 93% cyclic behavior was also observed in addition to an 88.6 Wh kg^{-1} current density at a 419.4 W kg^{-1} power density.[290] A number of images of the g-C_3N_4-based structures, adopted from the above reports, and their cyclic voltammetry analysis graphs are depicted in Figure 27.

6.8.2. C_xN_y-Based Materials as Supports. A g-C_3N_4@$ZnCo_2O_4$ composite was synthesized to work as an electrode in the energy storage field. The composite presented a remarkable specific surface area and specific capacity (157 mAh g^{-1}) at a current density of 4 A g^{-1}. In addition, the hybrid composite electrode preserved its considerable capacity retention (about 90%) for 2500 cycles. A specific capacity of 121 mAh g^{-1} was observed for the g-C_3N_4@$ZnCo_2O_4$/g-C_3N_4@$ZnCo_2O_4$ symmetric device, which exhibited an energy density of 39 W h kg^{-1} and and a power density of 1478 W kg^{-1}. Moreover, a capacity retention of 71% and an energy efficiency of 75% were obtained after 10 000 cycles. The above properties were attributed to the increased surface area and increased number of active sites that originated from the g-C_3N_4 support providing chemical stability toward electrochemical applications.[291]

For a better understanding of the importance of the carbon nitride-based materials in supercapacitors, a comparison table of C_xN_y-based electrocatalysts and other types of electrocatalysts is presented in Table S5.

6.9. Further Electrochemical Devices. TiO_2 nanotubes were bonded on g-C_3N_4/rGO nanosheets to form a TiO_2NT/

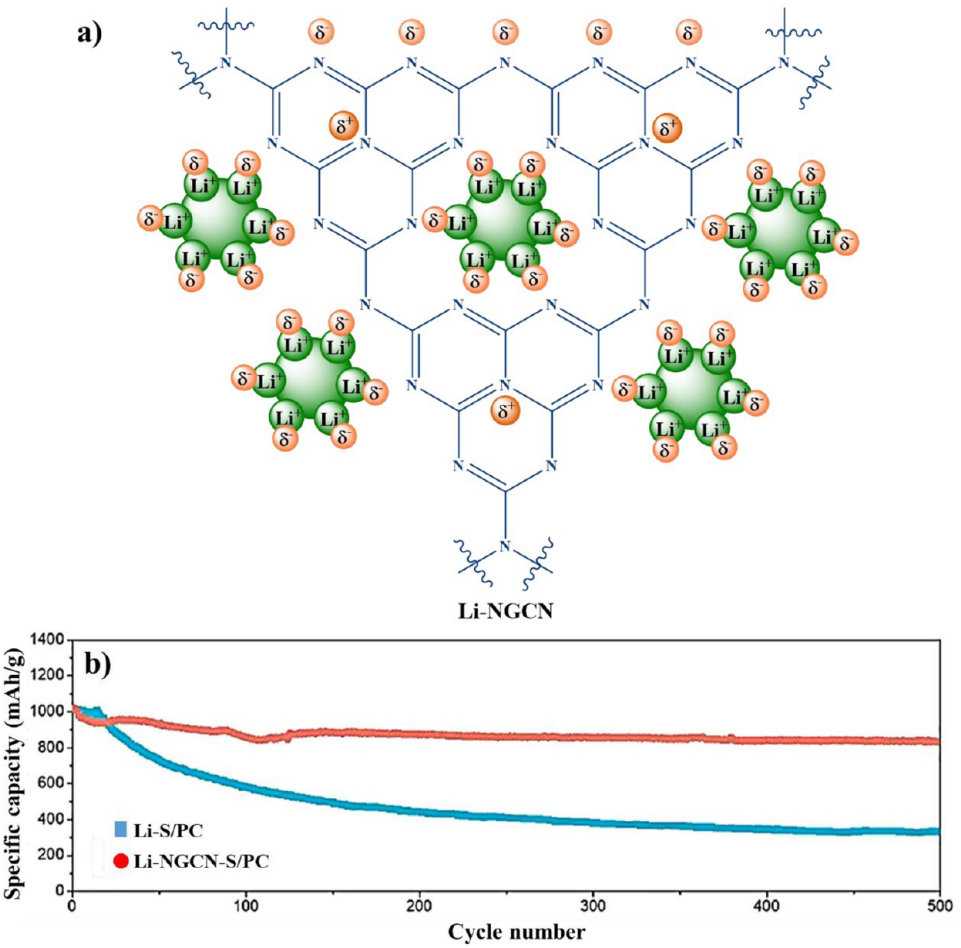

Figure 28. (a) Schematic illustration of Li ions deposited on nitrogen-defective g-C_3N_4-sulfur/porous carbon and (b) cycling performance of Li-S/porous carbon and Li-N-defective g-C_3N_4-S/porous carbon batteries. Reproduced with permission from ref 298. Copyright 2021, Elsevier.

g-C_3N_4/rGO composite as an anode for Na-ion batteries. At 0.1 A g^{-1}, a high reversible capacity of 138.5 mAh g^{-1} was obtained after 244 cycles, with a high rate capability of 103.3 mAh g^{-1} at 0.8 A g^{-1}. Such outstanding sodium storage was due to the double coating of TiO_2 nanotubes by g-C_3N_4/rGO nanosheets, which prevented the cycle from changing the volume.[292] 3D structures composed of $Na_2Ti_3O_7$ nanotubes anchored to g-C_3N_4/rGO composites were fabricated to measure the electrochemical sodium storage performance. More active sites for Na^+ transfer were offered through the integration of g-C_3N_4 and graphene. The $Na_2Ti_3O_7$ nanotube shortened the Na^+ transport paths, leading the $Na_2Ti_3O_7$NT/g-C_3N_4/rGO electrodes to exhibit high rate capabilities and cycling efficiencies. Additionally, their reversible capacity as an anode in a sodium half-cell was 210.8 mAh g^{-1} at 0.1 A g^{-1} after 300 cycles. The preservation of up to 98% of the Coulomb efficiency after the 50 cycles showed the good stability of the electrode, with a 364 Wh kg^{-1} energy density at a 0.048 W kg^{-1} power density.[293] N-Doped graphene derived from g-C_3N_4 and synthesized by polyvinylpyrrolidone was investigated as an anode in lithium and sodium ions batteries, revealing specific capacities of 1236 and 300 mAh g^{-1}, respectively, at a current density of 0.05 A g^{-1}. Moreover, a great cycling stability and a satisfying rate capability were achieved. The interplanar spacing played the main role in the electrochemical performances of the lithium-ion batteries and sodium-ion batteries.[294] Phosphorus-doped g-C_3N_4 (xP-g-C_3N_4) was prepared as a sulfur host in LIS batteries. The 0.1P-doped sample with improved conductivity exhibited a specific surface area of 19.66 m^2 g^{-1}, and after 100 cycles this composite presented a 1344 mAh g^{-1} initial discharge specific capacity and an 882 mAh g^{-1} reversible specific capacity. Besides, its 0.34% capacity decay per cycle demonstrated its outstanding cycling behavior due to the higher conductivity, stronger physical adsorption, and polysulfide chemisorption.[295] Composite anodes of ZnS/g-C_3N_4 were fabricated for lithium- and sodium-ion batteries. The ZnS nanoparticles presented a large capacity when embedded in g-C_3N_4 nanosheets. A long-term reversible capacity of about 596.9 mAh g^{-1} was obtained for the 0.7ZnS:0.3 g-C_3N_4 composite at a current density of 1 A g^{-1} after 1150 cycles in the Li^+ system, and that near 432.6 mAh g^{-1} was obtained after 750 cycles in the Na^+ half-cell configuration. Due to capacitive charge storage, an increased rate capability was seen for the 0.7ZnS:0.3 g-C_3N_4 electrode. The volume change during Li^+ or Na^+ ion shuttling was attenuated in ZnS in the presence of g-C_3N_4, which led to the great reversible capacity and primary Columbic efficiency of the composite anodes.[296] Porous sulfur host (Co/NC) nanostructures fabricated for lithium−sulfur batteries were studied and shown to enable fast electron or ion transport, effective sulfur trapping, and electrolyte penetration. As chemisorption sites and electrocatalytic sites for sulfur, the N heteroatoms and Co nanocatalysts embedded in the g-C_3N_4 played significant roles. The redox conversion kinetics was

simplified by such Co−N active sites alleviating the polysulfides. Thus, improved cycling performance was observed for the LIS batteries. Therefore, a high primary specific capacity of 1505 mAh g^{-1} was exhibited by the S/Co@NC cathode at 0.1 C in addition to an outstanding cycling stability of up to 300 cycles at 1 C, leading to 91.7% capacity retention and a capacity decay of 0.03% per cycle.[297] Using nitrogen-defective graphitic carbon nitride (NGCN), Li deposition was adjusted for the performance of symmetrical Li-NGCN||Li-NGCN cells. Accordingly, long-term cycling and a high capacity of 822.1 mAh g^{-1} were observed for Li-NGCN-S/PC pouch cells, with a 67.4% capacity retention rate for 100 cycles[298] (Figure 28).

Carbon nitride was prepared at different temperatures as an improved anode material for use in lithium-ion batteries. Based on the results, at a 0.1 C rate, the anode material exhibited a remarkable specific capacity of 2221 mAh g^{-1} at 600 °C (g-C_3N_4-600 °C) in addition to an improved cycling stability and rate capability.[299] The g-C_3N_4/Mo_2CT_x hybrid was synthesized for lithium storage. As expected, the rich exposed MXene layers provided fast ion diffusion and abundant active sites for Li storage. Hence, a high Coulumbic efficiency of 70.8% and an excellent lithium storage of 525.8 mAh g^{-1} were delivered by the g-C_3N_4/Mo_2CT_x hybrid.[300] P-Doped mesoporous g-C_3N_4 (P-MCN) was synthesized as an anode for use in high-energy and high-power Li-ion batteries. At a current density of 1 A g^{-1}, the P-MCN-1 anode sample delivereda 963 mAh g^{-1} reversible discharge capacity after 1000 cycles. Moreover, after 2500 cycles, excellent rate capabilities of 685, 539, and 274 mAh g^{-1} were demonstrated by the electrode at current densities of 5, 10, and 20 A g^{-1}, respectively.[301]

In a subsequent study, hydrogenated thin films (or N-DLC electrodes) of amorphous carbon-nitride (a-CN) were deposited on FTO and glass by the dielectric barrier discharge plasma method in a CH_4/N_2 gas mixture. In a $K_3Fe(CN)_6$ electrolyte, the optimized nitrogen-rich electrodes exhibited electrochemical reversibility with ΔEp = 125 mV and Jpa/Jpc = 1.03 and a rapid charge transfer constant of 6.59×10^{-4} cm s^{-1}, all of which were ascribed to the high N-doping level, the high surface area, the multitude holes, and the high number of nanopores with great electron transfer for the redox reaction.[302]

For a more comprehensive overview of energy systems based on carbon nitride structures utilized as electrocatalysis materials, some relevant studies are summarized in Table S6.

7. FUTURE SCOPE AND CHALLENGES

Currently, C_xN_y-based materials are mainly being investigated for clean energy production processes, including water oxidation, water splitting, the ORR, the HER, and the production of hydrogen as a carbon-neutral fuel, and the conversion of CO_2 into useful compounds.[303−311] The appropriate features of carbon nitride together with the typical modifications and functionalizations generate new prospects for its future use in global clinical and sustainable energy fields. Delivering synergistic effects by offering more active sites and developed mass and charge transfer toward hydrogen and oxygen evolution processes and oxygen reduction reactions, the improved carbon nitride-based materials present higher electrocatalytic activities and higher durabilities. Mesoporous structures and improved specific surface areas are two key factors that make the electrical conductivity and mass transfer properties of C_xN_y-based nanostructures particularly appropriate for their electrocatalytic performance, as they facilitate the role of active sites for the transfer of reactant or product molecules in addition to the diffusion mechanisms. These features can be satisfied by the rational design of C_xN_y structures in terms of fabrication strategies (namely choosing appropriate precursors and methods) and surface modifications with a targeted approach based on the application field. Besides, to obtain g-C_3N_4-based structures with efficient functionalities, it is necessary to engineer their compositions and structures, especially for environmental remediation purposes where g-C_3N_4-based structures are employed in a photocatalytic capacity.[312,313] This can be accomplished through the optimization of defect and heterojunction formation and the use of organic protocols and modification routes, e.g., the addition of organic compounds such as carbonates and thiocyanates, which would benefit the final electron transport, stability, and active site performance in both purification and fuel resource compensation purposes. Moreover, since bifunctional electrocatalysts capable of two concomitant reactions (HER and OER or ORR and OER) are of growing interest, efficient composites of g-C_3N_4 may be required to be fabricated for use in new energy storage and conversion devices. Thus, C_xN_y compounds with sufficient stabilities together with significant activities are expected to cut the prices and durations of relevant processes.

Nevertheless, there are still unclear points that require further evaluations. On the basis of merged theoretical and experimental analyses, details of charge transfer paths and catalytic mechanisms in special carbon nitride structures may be clarified. Any alterations induced in the crystalline structure demand optimization to avoid the attenuation of the electronic configuration. Considering all operative aspects related to the environment and economics, feasible production and functionality at the highest yield are highly essential. Thus, further endeavors should be devoted toward the efficient fabrication of carbon nitride structures with engineered properties, which may contribute to their possible utilization in advanced drug storage and delivery, sensing, electronic devices, and environmental applications. In a word, there are enormous opportunities concerning the synthesis of g-C_3N_4 and g-C_3N_4-based materials and their application for photocatalytic water splitting, fuel cells, metal−air batteries, etc. However, the studies are preliminary, and the correlations between the structure, catalytic prowess, kinetics, and shape selectivity are still not very clear, which may require further research efforts.

Although the applications of g-C_3N_4 have been extended for metal−air batteries, some challenges need to be addressed in future studies to develop metal−air batteries with performances better than the Li-ion batteries. In recent years, due to the disadvantages of carbon supports such as corrosion in the operating fuel cell environment and the loss of catalyst activity, g-C_3N_4 has emerged as an attractive material and catalyst support in fuel cells. After reviewing the past research works on this unique family of materials for the development of an electrocatalyst toward fuel cells, we believe that a deeper understanding of the catalyst−support interactions and the role of the carbon nitride phases will be necessary to determine the ORR and OER reaction kinetics. Indeed, combining g-C_3N_4 with novel conductive supports (e.g., graphene or mesoporous carbon) may enhance the path toward ORR electrocatalysis to promote fuel cell technology. Thus, an understanding of g-C_3N_4 and g-C_3N_4-based materials is vital for the new catalysts,

opening a new avenue for the development of fuel cell technology and metal−air batteries.

One of the applications of C_xN_y-based materials is as efficient electrocatalysts in the NRR. Although many studies have reported the use of C_xN_y-based materials for the NRR, either experimentally or theoretically, it is still in its infancy stage, and some challenges need further study. Despite all the aforementioned efforts to investigate the use of C_xN_y materials in NRR processes, there is still a considerable gap between the calculation-based and expected NRR yields and Faradaic efficiencies of these materials and those amounts obtained through actual studies, which requires further profound evaluations in future attempts in this field. This is due to various issues such as a high reaction energy barrier, the finite density of active sites, limited N_2 activation, etc., which would be better to examine more in future works. In addition, efficient methods for modifying the surface of CN should be further explored in the future, one of the most important of which is heteroatom doping to obtain C_xN_y-based catalysts whose performance is expected for NRR reactions.

In recent years, due to the low efficiency and selectivity of photocatalytic hydrogen production under solar energy, graphitic carbon nitrides have been investigated as attractive materials for solar hydrogen production. However, non-defective g-C_3N_4 as water splitting photocatalysts present disadvantages, including a low charge carrier mobility and a relatively large band gap, which limit the electron and hole separation and transport and therefore limit the effective use of visible light and the rate of hydrogen evolution. Thus, there is an urgent need to develop modification methodologies by creating defects within C_xN_y-based materials. Indeed, noble-metal and nonmetal doping may resolve this issue and enhance solar-energy conversions.

In photocatalytic applications of C_xN_y-based materials, the development of a plausible mechanism using defective CN photocatalysts is relatively unclear, which would be better addressed in the future. Finally, one of the things that should be addressed in the future is that the carbon nitride itself contains nitrogen; therefore, we must be careful during its analysis so that it does not contain nitrogen-containing contaminants. Novel techniques need to be advanced to controllably synthesize vacancy-defect-modified CN using materials that are inexpensive, highly efficient, and stabile.

8. CONCLUSIONS

Lately, C_xN_y-based materials have gained increased attention for their supreme properties such as non-toxicity, low-expense preparation, abundance, facile processing, and high chemical, thermal, and physical stabilities. For years, metal-based electrocatalysts have been considered as suitable options for use in electrochemical systems due to their high catalytic performance in energy-related technologies such as fuel cells, electrolyzers, etc. However, their drawbacks, including low stability, poor selectivity, high expenses, and rare resources, threaten both their survival and future chances to improve energy systems. Instead, nonmetallic catalysts in energy generation and storage technologies, including C_xN_y-based nanomaterials, are free of such impediments and have revealed considerable success in the field of sustainable energy development. This review summarizes the most relevant improvements of the carbon nitride functionality for electrochemical catalysis purposes. In this account, carbon nitride's energy applications in fuel cells, batteries, supercapacitors, and water splitting equipment have been reviewed. Various C_xN_y structures, properties, modification routes, fabrication techniques, and electrocatalytic applications were assessed in detail. In brief, regarding synthesis and functionalization, much focus is paid to the significance of precursors, processing paths, including vapor deposition routes, pyrolysis, microwave-assisted processes, electrodeposition, hydrothermal and solvothermal synthesis, sol−gel, and polymerization, and modification techniques, including inducing mesoporous structures, controlling diverse morphologies, coupling with noble or transition metals and bimetallic structures, doping methods, etc.. Based on the consensus of the reviewed electrochemical results, the efficiency of g-C_3N_4-derived materials in the reported ORR, OER, HER, and other electrochemical reactions could be attributed to their surface and structure characteristics in terms of functional groups, defects, pores, doping states, geometries, and morphologies. Overall higher electrocatalytic activities and larger stabilities were noticed for nitrogen-doped carbon-based materials used as either electrode modifiers or electrocatalysts in cells, which were attributed to their unique characteristics, such as the 2D polymeric composition of N, C, and H atoms providing a high surface area and surface effects; specific semiconductor photo- and electroproperties; and simple and cost-effective synthesis routes.

AUTHOR INFORMATION

Corresponding Authors

Mahmoud Nasrollahzadeh − *Department of Chemistry, Faculty of Science, University of Qom, Qom 37185-359, Iran;* orcid.org/0000-0002-4539-3544; Email: mahmoudnasr81@gmail.com

Manoj B. Gawande − *Department of Industrial and Engineering Chemistry, Institute of Chemical Technology, Jalna, Maharashtra 431203, India;* orcid.org/0000-0003-1575-094X; Email: mb.gawande@marj.ictmumbai.edu.in, mbgawande@gmail.com

Authors

Farzaneh Besharat − *Department of Chemistry, Faculty of Science, University of Qom, Qom 37185-359, Iran*

Fatemeh Ahmadpoor − *Department of Chemistry, Faculty of Science, University of Qom, Qom 37185-359, Iran*

Zahra Nezafat − *Department of Chemistry, Faculty of Science, University of Qom, Qom 37185-359, Iran*

Nilesh R. Manwar − *Department of Industrial and Engineering Chemistry, Institute of Chemical Technology, Jalna, Maharashtra 431203, India;* orcid.org/0000-0002-4619-546X

Paolo Fornasiero − *Department of Chemical and Pharmaceutical Sciences, Center for Energy, Environment and*

Transport Giacomo Ciamiciam, *INSTM Trieste Research Unit, ICCOM-CNR Trieste Research Unit, University of Trieste, I-34127 Trieste, Italy;* orcid.org/0000-0003-1082-9157

Notes

The authors declare no competing financial interest.

■ ACKNOWLEDGMENTS

We gratefully acknowledge the Iranian Nano Council and the University of Qom for the support of this work. M.B.G. acknowledges the DST-SERB (CRG/2021/001738) core research grant.

■ REFERENCES

(1) Barrio, J.; Volokh, M.; Shalom, M. Polymeric Carbon Nitrides and Related Metal-Free Materials for Energy and Environmental Applications. *J. Mater. Chem. A* **2020**, *8* (22), 11075−11116.

(2) Popović, S.; Smiljanić, M.; Jovanovič, P.; Vavra, J.; Buonsanti, R.; Hodnik, N. Stability and Degradation Mechanisms of Copper-Based Catalysts for Electrochemical CO_2 Reduction. *Angew. Chem., Int. Ed.* **2020**, *59* (35), 14736−14746.

(3) Tackett, B. M.; Lee, J. H.; Chen, J. G. Electrochemical Conversion of CO_2 to Syngas with Palladium-Based Electrocatalysts. *ACS. Chem. Res.* **2020**, *53* (8), 1535−1544.

(4) De Gregorio, G. L.; Burdyny, T.; Loiudice, A.; Iyengar, P.; Smith, W. A.; Buonsanti, R. Facet-Dependent Selectivity of Cu Catalysts in Electrochemical CO_2 Reduction at Commercially Viable Current Densities. *ACS Catal.* **2020**, *10* (9), 4854−4862.

(5) Stamenkovic, V. R.; Strmcnik, D.; Lopes, P. P.; Markovic, N. M. Energy and Fuels from Electrochemical Interfaces. *Nat. Mater.* **2017**, *16* (1), 57−69.

(6) Becknell, N.; Lopes, P. P.; Hatsukade, T.; Zhou, X.; Liu, Y.; Fisher, B.; Chung, D. Y.; Kanatzidis, M. G.; Markovic, N. M.; Tepavcevic, S.; et al. Employing the Dynamics of the Electrochemical Interface at Aqueous Zinc-Ion Battery Cathode. *Adv. Funct. Mater.* **2021**, *31* (35), 2102135.

(7) Niu, W.; Yang, Y. Graphitic Carbon Nitride for Electrochemical Energy Conversion and Storage. *ACS Energy Lett.* **2018**, *3* (11), 2796−2815.

(8) Sakaushi, K.; Antonietti, M. Carbon-and Nitrogen-Based Organic Frameworks. *ACS. Chem. Res.* **2015**, *48* (6), 1591−1600.

(9) Siegmund, D.; Metz, S.; Peinecke, V.; Warner, T. E.; Cremers, C.; Grevé, A.; Smolinka, T.; Segets, D.; Apfel, U.-P. Crossing the Valley of Death: From Fundamental to Applied Research in Electrolysis. *JACS Au* **2021**, *1* (5), 527−535.

(10) Zinola, C. F.; Martins, M. E.; Tejera, E. P.; Neves, N. P. Electrocatalysis: Fundamentals and Applications. *Int. J. Electrochem.* **2012**, *2012*, No. 874687.

(11) Voiry, D.; Shin, H. S.; Loh, K. P.; Chhowalla, M. Low-Dimensional Catalysts for Hydrogen Evolution and CO_2 Reduction. *Nat. Rev. Chem.* **2018**, *2*, No. 0105.

(12) Barrio, J. S.; Lin, L.; Wang, X.; Shalom, M. Design of a Unique Energy-Band Structure and Morphology in a Carbon Nitride Photocatalyst for Improved Charge Separation and Hydrogen Production. *ACS Sustain. Chem. Eng.* **2018**, *6* (1), 519−530.

(13) Lyu, X.; Zhang, W.-N.; Li, G.; Shi, B.-W.; Zhang, Y.-N.; Chen, H.; Li, S.-C.; Wang, X. Two-Dimensional Porous PtPd Nanostructure Electrocatalysts for Oxygen Reduction Reaction. *ACS Appl. Nano Mater.* **2020**, *3* (9), 8586−8591.

(14) Jin, H.; Guo, C.; Liu, X.; Liu, J.; Vasileff, A.; Jiao, Y.; Zheng, Y.; Qiao, S.-Z. Emerging Two-Dimensional Nanomaterials for Electrocatalysis. *Chem. Rev.* **2018**, *118* (13), 6337−6408.

(15) Rosso, C.; Filippini, G.; Criado, A.; Melchionna, M.; Fornasiero, P.; Prato, M. Metal-Free Photocatalysis: Two-Dimensional Nanomaterial Connection toward Advanced Organic Synthesis. *ACS Nano* **2021**, *15* (3), 3621−3630.

(16) Xiao, F.; Li, H.; Yan, X.; Yan, L.; Zhang, X.; Wang, M.; Qian, C.; Wang, Y. Graphitic Carbon Nitride/Graphene Oxide ($g\text{-}C_3N_4$/GO) Nanocomposites Covalently Linked with Ferrocene Containing Dendrimer for Ultrasensitive Detection of Pesticide. *Anal. Chim. Acta* **2020**, *1103*, 84−96.

(17) Wang, Y.; Nian, Y.; Biswas, A. N.; Li, W.; Han, Y.; Chen, J. G. Challenges and Opportunities in Utilizing Mxenes of Carbides and Nitrides as Electrocatalysts. *Adv. Energy Mater.* **2021**, *11* (3), 2002967.

(18) Lu, Q.; Eid, K.; Li, W.; Abdullah, A. M.; Xu, G.; Varma, R. S. Engineering Graphitic Carbon Nitride ($g\text{-}C_3N_4$) for Catalytic Reduction of CO_2 to Fuels and Chemicals: Strategy and Mechanism. *Green Chem.* **2021**, *23*, 5394−5428.

(19) Mousavi, S. S.; Jaleh, B.; Nasrollahzadeh, M.; Ahmadpoor, F.; Azizi, M.; Nasri, A.; Khazalpour, S. Hardystonite/Palladium Nanocomposite as a High Performance Catalyst for Electrochemical Hydrogen Storage and Cr(VI) Reduction. *Int. J. Hydrog. Energy* **2021**, *46* (49), 25175−25188.

(20) Eslamipanah, M.; Jaleh, B.; Mohazzab, B. F.; Khazalpour, S.; Nasrollahzadeh, M.; Shokouhimehr, M. Facile Synthesis and Electrochemical Hydrogen Storage of Bentonite/TiO_2/Au Nanocomposite. *Int. J. Hydrog. Energy* **2020**, *45* (58), 33771−33788.

(21) Hu, C.; Xiao, Y.; Zou, Y.; Dai, L. Carbon-Based Metal-Free Electrocatalysis for Energy Conversion, Energy Storage, and Environmental Protection. *Electrochem. Energy Rev.* **2018**, *1* (1), 84−112.

(22) Gong, Y.; Li, M.; Wang, Y. Carbon Nitride in Energy Conversion and Storage: Recent Advances and Future Prospects. *ChemSusChem* **2015**, *8* (6), 931−946.

(23) Bhat, V. S.; Hegde, G.; Nasrollahzadeh, M. A Sustainable Technique to Solve Growing Energy Demand: Porous Carbon Nanoparticles as Electrode Materials for High-Performance Supercapacitors. *J. Appl. Electrochem.* **2020**, *50* (12), 1243−1255.

(24) Wang, J.; Kong, H.; Zhang, J.; Hao, Y.; Shao, Z.; Ciucci, F. Carbon-Based Electrocatalysts for Sustainable Energy Applications. *Prog. Mater. Sci.* **2021**, *116*, 100717.

(25) Deng, Y.; Xie, Y.; Zou, K.; Ji, X. Review on Recent Advances in Nitrogen-Doped Carbons: Preparations and Applications in Supercapacitors. *J. Mater. Chem. A* **2016**, *4* (4), 1144−1173.

(26) Klingele, M.; Van Pham, C.; Fischer, A.; Thiele, S. A Review on Metal-Free Doped Carbon Materials Used as Oxygen Reduction Catalysts in Solid Electrolyte Proton Exchange Fuel Cells. *Fuel Cells* **2016**, *16* (5), 522−529.

(27) Salinas-Torres, D.; Navlani-García, M.; Mori, K.; Kuwahara, Y.; Yamashita, H. Nitrogen-Doped Carbon Materials as a Promising Platform toward the Efficient Catalysis for Hydrogen Generation. *Appl. Catal. A Gen.* **2019**, *571*, 25−41.

(28) Feng, X.; Bai, Y.; Liu, M.; Li, Y.; Yang, H.; Wang, X.; Wu, C. Untangling the Respective Effects of Heteroatom-Doped Carbon Materials in Batteries, Supercapacitors and the ORR to Design High Performance Materials. *Energy Environ. Sci.* **2021**, *14* (4), 2036−2089.

(29) Wu, J.; Pan, Z.; Zhang, Y.; Wang, B.; Peng, H. The Recent Progress of Nitrogen-Doped Carbon Nanomaterials for Electrochemical Batteries. *J. Mater. Chem. A* **2018**, *6* (27), 12932−12944.

(30) Wabo, S. G.; Klepel, O. Nitrogen Release and Pore Formation through KOH Activation of Nitrogen-Doped Carbon Materials: An Evaluation of the Literature. *Carbon Lett.* **2021**, *31* (4), 581−592.

(31) Daems, N.; Sheng, X.; Vankelecom, I. F.; Pescarmona, P. P. Metal-Free Doped Carbon Materials as Electrocatalysts for the Oxygen Reduction Reaction. *J. Mater. Chem. A* **2014**, *2* (12), 4085−4110.

(32) Li, M.; Xu, F.; Li, H.; Wang, Y. Nitrogen-Doped Porous Carbon Materials: Promising Catalysts or Catalyst Supports for Heterogeneous Hydrogenation and Oxidation. *Catal. Sci. Technol.* **2016**, *6* (11), 3670−3693.

(33) Pumera, M. Materials Electrochemists' Never-Ending Quest for Efficient Electrocatalysts: The Devil Is in the Impurities. *ACS Catal.* **2020**, *10* (13), 7087−7092.

(34) Gawande, M. B.; Fornasiero, P.; Zbořil, R. Carbon-Based Single-Atom Catalysts for Advanced Applications. *ACS Catal.* **2020**, *10* (3), 2231−2259.
(35) Sharma, P.; Kumar, S.; Tomanec, O.; Petr, M.; Zhu Chen, J.; Miller, J. T.; Varma, R. S.; Gawande, M. B.; Zbořil, R. Carbon Nitride-Based Ruthenium Single Atom Photocatalyst for CO_2 Reduction to Methanol. *Small* **2021**, *17* (16), 2006478.
(36) Li, S.; Yang, K.; Tan, C.; Huang, X.; Huang, W.; Zhang, H. Preparation and Applications of Novel Composites Composing of Metal-Organic Frameworks and Two-Dimensional Materials. *Chem. Commun.* **2016**, *52*, 1555−1562.
(37) Kumar, S.; Battula, V. R.; Kailasam, K. Single Molecular Precursors for C_xN_y Materials- Blending of Carbon and Nitrogen Beyond g-C_3N_4. *Carbon* **2021**, *183*, 332−354.
(38) Sakaushi, K.; Antonietti, M. Carbon- and Nitrogen-Based Porous Solids: A Recently Emerging Class of Materials. *Bull. Chem. Soc. Jpn.* **2015**, *88* (3), 386−398.
(39) Wood, K. N.; O'Hayre, R.; Pylypenko, S. Recent Progress on Nitrogen/Carbon Structures Designed for Use in Energy and Sustainability Applications. *Energy Environ. Sci.* **2014**, *7* (4), 1212−1249.
(40) Kessler, F. K.; Zheng, Y.; Schwarz, D.; Merschjann, C.; Schnick, W.; Wang, X.; Bojdys, M. J. Functional Carbon Nitride Materials — Design Strategies for Electrochemical Devices. *Nat. Rev. Mater.* **2017**, *2*, 17030.
(41) Jiang, L.; Yuan, X.; Pan, Y.; Liang, J.; Zeng, G.; Wu, Z.; Wang, H. Doping of Graphitic Carbon Nitride for Photocatalysis: A Reveiw. *Appl. Catal., B* **2017**, *217*, 388−406.
(42) Yang, J.; Wang, H.; Jiang, L.; Yu, H.; Zhao, Y.; Chen, H.; Yuan, X.; Liang, J.; Li, H.; Wu, Z. Defective Polymeric Carbon Nitride: Fabrications, Photocatalytic Applications and Perspectives. *Chem. Eng. J.* **2022**, *427*, 130991.
(43) Yi, J.; El-Alami, W.; Song, Y.; Li, H.; Ajayan, P. M.; Xu, H. Emerging Surface Strategies on Graphitic Carbon Nitride for Solar Driven Water Splitting. *Chem. Eng. J.* **2020**, *382*, 122812.
(44) Liang, Q.; Shao, B.; Tong, S.; Liu, Z.; Tang, L.; Liu, Y.; Cheng, M.; He, Q.; Wu, T.; Pan, Y.; et al. Recent Advances of Melamine Self-Assembled Graphitic Carbon Nitride-Based Materials: Design, Synthesis and Application in Energy and Environment. *Chem. Eng. J.* **2021**, *405*, 126951.
(45) Wang, Z.; Hu, X.; Liu, Z.; Zou, G.; Wang, G.; Zhang, K. Recent Developments in Polymeric Carbon Nitride-Derived Photocatalysts and Electrocatalysts for Nitrogen Fixation. *ACS Catal.* **2019**, *9* (11), 10260−10278.
(46) Shi, L.; Yin, Y.; Wang, S.; Sun, H. Rational Catalyst Design for N_2 Reduction under Ambient Conditions: Strategies toward Enhanced Conversion Efficiency. *ACS Catal.* **2020**, *10* (12), 6870−6899.
(47) Su, T.; Shao, Q.; Qin, Z.; Guo, Z.; Wu, Z. Role of Interfaces in Two-Dimensional Photocatalyst for Water Splitting. *ACS Catal.* **2018**, *8* (3), 2253−2276.
(48) Stavrou, E.; Lobanov, S.; Dong, H.; Oganov, A. R.; Prakapenka, V. B.; Konôpková, Z.; Goncharov, A. F. Synthesis of Ultra-Incompressible Sp^3-Hybridized Carbon Nitride with 1:1 Stoichiometry. *Chem. Mater.* **2016**, *28* (19), 6925−6933.
(49) Mahmood, J.; Lee, E. K.; Jung, M.; Shin, D.; Jeon, I.-Y.; Jung, S.-M.; Choi, H.-J.; Seo, J.-M.; Bae, S.-Y.; Sohn, S.-D.; Park, N.; Oh, J. H.; Shin, H.-J.; Baek, J.-B. Nitrogenated Holey Two-Dimensional Structures. *Nat. Commun.* **2015**, *6*, 6486.
(50) Dong, H.; Oganov, A. R.; Zhu, Q.; Qian, G.-R. The Phase Diagram and Hardness of Carbon Nitrides. *Sci. Rep.* **2015**, *5*, 9870.
(51) Hu, Q.; Wu, Q.; Wang, H.; He, J.; Zhang, G. First-Principles Studies of Structural and Electronic Properties of Layered C_3N Phases. *Phys. Status Solidi B* **2012**, *249* (4), 784−788.
(52) Lee, J. S.; Wang, X.; Luo, H.; Dai, S. Fluidic Carbon Precursors for Formation of Functional Carbon under Ambient Pressure Based on Ionic Liquids. *Adv. Mater.* **2010**, *22* (9), 1004−1007.
(53) He, F.; Chen, G.; Miao, J.; Wang, Z. X.; Su, D.; Liu, S.; Cai, W.; Zhang, L.; Hao, S.; Liu, B. Sulfur-Mediated Self-Templating Synthesis of Tapered C-PAN/g-C_3N_4 Composite Nanotubes towards Efficient Photocatalytic H_2 Evolution. *ACS Energy Lett.* **2016**, *1* (5), 969−975.
(54) Bu, H.; Yang, B.; Yuan, H.; Yuan, X.; Wang, H.; Qi, S.; Ma, X.; Zhao, M. New Spiral Form of Carbon Nitride with Ultrasoftness and Tunable Electronic Structures. *ACS Omega* **2021**, *6* (1), 516−522.
(55) Darkwah, W. K.; Ao, Y. Mini Review on the Structure and Properties (Photocatalysis), and Preparation Techniques of Graphitic Carbon Nitride Nano-Based Particle, and Its Applications. *Nanoscale Res. Lett.* **2018**, *13*, 388.
(56) Ashritha, M. G.; Hareesh, K. A Review on Graphitic Carbon Nitride Based Binary Nanocomposites as Supercapacitors. *J. Energy Storage* **2020**, *32*, 101840.
(57) Mittal, D.; Dutta, D. P. Synthesis, Structure, and Selected Photocatalytic Applications of Graphitic Carbon Nitride: A Review. *J. Mater. Sci.: Mater. Electron.* **2021**, *32* (14), 18512−18543.
(58) Mishra, A.; Mehta, A.; Basu, S.; Shetti, N. P.; Reddy, K. R.; Aminabhavi, T. M. Graphitic Carbon Nitride (g-C_3N_4)-Based Metal-Free Photocatalysts for Water Splitting: A Review. *Carbon* **2019**, *149*, 693−721.
(59) Suter, T.; Brázdová, V.; McColl, K.; Miller, T. S.; Nagashima, H.; Salvadori, E.; Sella, A.; Howard, C. A.; Kay, C. W. M.; Corà, F.; McMillan, P. F. Synthesis, Structure and Electronic Properties of Graphitic Carbon Nitride Films. *J. Phys. Chem. C* **2018**, *122* (44), 25183−25194.
(60) Jiang, J.; Yang, J.; Lin, J.; Huang, Z.; Wang, S. C. Carbon Nanomaterials and Related Nanostructures: Synthesis, Characterization, and Application. *J. Nanomater.* **2014**, *2014*, 319165.
(61) Luo, Y.; Yan, Y.; Zheng, S.; Xue, H.; Pang, H. Graphitic Carbon Nitride Based Materials for Electrochemical Energy Storage. *J. Mater. Chem. A* **2019**, *7* (3), 901−924.
(62) Dong, X.; Cheng, F. Recent Development in Exfoliated Two-Dimensional g-C_3N_4 Nanosheets for Photocatalytic Application. *J. Mater. Chem. A* **2015**, *3*, 23642−23652.
(63) Ajiboye, T. O.; Kuvarega, A. T.; Onwudiwe, D. C. Graphitic Carbon Nitride-Based Catalysts and Their Applications: A Review. *Nano-Struct. Nano-Objects* **2020**, *24*, 100577.
(64) Rono, N.; Kibet, J. K.; Martincigh, B. S.; Nyamori, V. O. A Comparative Study between Thermal Etching and Liquid Exfoliation of Bulk Graphitic Carbon Nitride to Nanosheets for the Photocatalytic Degradation of a Model Environmental Pollutant, Rhodamine B. *J. Mater. Sci.: Mater. Electron.* **2021**, *32* (1), 687−706.
(65) Li, Y.; Wang, M.-Q.; Bao, S.-J.; Lu, S.; Xu, M.; Long, D.; Pu, S. Tuning and Thermal Exfoliation Graphene-Like Carbon Nitride Nanosheets for Superior Photocatalytic Activity. *Ceram. Int.* **2016**, *42* (16), 18521−18528.
(66) Liu, W.; Yanase, T.; Iwasa, N.; Mukai, S.; Iwamura, S.; Nagahama, T.; Shimada, T. Post-Annealed Graphite Carbon Nitride Nanoplates Obtained by Sugar-Assisted Exfoliation with Improved Visible-Light Photocatalytic Performance. *J. Colloid Interface Sci.* **2020**, *567*, 369−378.
(67) Zhu, Y.; Feng, Y.; Chen, S.; Ding, M.; Yao, J. Carbon Nitride Nanotube-Based Materials for Energy and Environmental Applications: A Review of Recent Progresses. *J. Mater. Chem. A* **2020**, *8* (48), 25626−25648.
(68) Stroyuk, O.; Raievska, O.; Zahn, D. R. T. Graphitic Carbon Nitride Nanotubes: A New Material for Emerging Applications. *RSC Adv.* **2020**, *10* (56), 34059−34087.
(69) Wang, A.; Wang, C.; Fu, L.; Wong-Ng, W.; Lan, Y. Recent Advances of Graphitic Carbon Nitride-Based Structures and Applications in Catalyst, Sensing, Imaging, and LEDs. *Nano-Micro Lett.* **2017**, *9*, 47.
(70) Hao, Q.; Jia, G.; Wei, W.; Vinu, A.; Wang, Y.; Arandiyan, H.; Ni, B.-J. Graphitic Carbon Nitride with Different Dimensionalities for Energy and Environmental Applications. *Nano Res.* **2020**, *13* (1), 18−37.
(71) Chen, K.; Chai, Z.; Li, C.; Shi, L.; Liu, M.; Xie, Q.; Zhang, Y.; Xu, D.; Manivannan, A.; Liu, Z. Catalyst-Free Growth of Three-Dimensional Graphene Flakes and Graphene/g-C_3N_4 Composite for Hydrocarbon Oxidation. *ACS Nano* **2016**, *10* (3), 3665−3673.

(72) Ma, T. Y.; Tang, Y.; Dai, S.; Qiao, S. Z. Proton-Functionalized Two-Dimensional Graphitic Carbon Nitride Nanosheet: An Excellent Metal-/Label-Free Biosensing Platform. *Small* **2014**, *10* (12), 2382−2389.
(73) Tang, Y.; Su, Y.; Yang, N.; Zhang, L.; Lv, Y. Carbon Nitride Quantum Dots: A Novel Chemiluminescence System for Selective Detection of Free Chlorine in Water. *Anal. Chem.* **2014**, *86* (9), 4528−4535.
(74) Fidan, T.; Torabfam, M.; Saleem, Q.; Wang, C.; Kurt, H.; Yüce, M.; Tang, J.; Bayazit, M. K. Functionalized Graphitic Carbon Nitrides for Environmental and Sensing Applications. *Adv. Energy Sustain. Res.* **2021**, *2* (3), 2000073.
(75) Zhu, J.; Xiao, P.; Li, H.; Carabineiro, S. A. C. Graphitic Carbon Nitride: Synthesis, Properties, and Applications in Catalysis. *ACS Appl. Mater. Interfaces* **2014**, *6* (19), 16449−16465.
(76) Lau, V. W.-h.; Moudrakovski, I.; Botari, T.; Weinberger, S.; Mesch, M. B.; Duppel, V.; Senker, J.; Blum, V.; Lotsch, B. V. Rational Design of Carbon Nitride Photocatalysts by Identification of Cyanamide Defects as Catalytically Relevant Sites. *Nat. Commun.* **2016**, *7*, 12165.
(77) Kroke, E. gt-C_3N_4—the First Stable Binary Carbon(IV) Nitride. *Angew. Chem., Int. Ed* **2014**, *53* (42), 11134−11136.
(78) Chen, Z.; Zhang, S.; Liu, Y.; Alharbi, N. S.; Rabah, S. O.; Wang, S.; Wang, X. Synthesis and Fabrication of g-C_3N_4-Based Materials and Their Application in Elimination of Pollutants. *Sci. Total Environ.* **2020**, *731*, 139054.
(79) Nazarian-Samani, M.; Haghighat-Shishavan, S.; Nazarian-Samani, M.; Kashani-Bozorg, S. F.; Ramakrishna, S.; Kim, K.-B. Perforated Two-Dimensional Nanoarchitectures for Next-Generation Batteries: Recent Advances and Extensible Perspectives. *Prog. Mater. Sci.* **2021**, *116*, 100716.
(80) Guan, L.; Xu, N.; Liu, X.; Zhao, Y.; Li, H.; Sun, J.; Wu, J.; Ying, Z. Controlled Growth of Crystalline G-C_3N_4 Nanocone Arrays by Plasma Sputtering Reaction Deposition. *Carbon* **2014**, *79*, 578−589.
(81) Ahmad, R.; Tripathy, N.; Khosla, A.; Khan, M.; Mishra, P.; Ansari, W. A.; Syed, M. A.; Hahn, Y.-B. Recent Advances in Nanostructured Graphitic Carbon Nitride as a Sensing Material for Heavy Metal Ions. *J. Electrochem. Soc.* **2020**, *167*, 037519.
(82) Wei, L.; Sun, H.; Yang, T.; Deng, S.; Wu, M.; Li, Z. Iron Carbide Encapsulated by Porous Carbon Nitride as Bifunctional Electrocatalysts for Oxygen Reduction and Evolution Reactions. *Appl. Surf. Sci.* **2018**, *439*, 439−446.
(83) Riyajuddin, S.; Tarik Aziz, S.; Kumar, S.; Nessim, G. D.; Ghosh, K. 3D-Graphene Decorated with g-C_3N_4/Cu_3P Composite: A Noble Metal-Free Bifunctional Electrocatalyst for Overall Water Splitting. *ChemCatChem.* **2020**, *12* (5), 1394−1402.
(84) Xiao, J.; Xu, Y.; Xia, Y.; Xi, J.; Wang, S. Ultra-Small Fe_2N Nanocrystals Embedded into Mesoporous Nitrogen-Doped Graphitic Carbon Spheres as a Highly Active, Stable, and Methanol-Tolerant Electrocatalyst for the Oxygen Reduction Reaction. *Nano Energy* **2016**, *24* (C), 121−129.
(85) Wang, X.; Sun, M.; Guo, Y.; Hu, J.; Zhu, M. Three Dimensional Pt Island-on-Au Architectures Coupled with Graphite Carbon Nitride Nanosheets for Effective Photo-Accelerated Methanol Electro-Oxidation. *J. Colloid Interface Sci.* **2020**, *558*, 38−46.
(86) Konda, S.; Amiri, M.; Chen, A. Photo-Assisted Deposition of Palladium Nanoparticles on Carbon Nitride for Efficient Oxygen Reduction. *J. Phys. Chem. C* **2016**, *120* (27), 14467−14473.
(87) Sriram, B.; Baby, J. N.; Wang, S.-F.; M, R. R.; Govindasamy, M.; George, M. Eutectic Solvent-Mediated Synthesis of Nife-Ldh/Sulfur-Doped Carbon Nitride Arrays: Investigation of Electrocatalytic Activity for the Dimetridazole Sensor in Human Sustenance. *ACS Sustain. Chem. Eng.* **2020**, *8* (48), 17772−17782.
(88) Liu, B.; Yao, H.; Daniels, R. A.; Song, W.; Zheng, H.; Jin, L.; Suib, S. L.; He, J. A Facile Synthesis of F_3C@Mesoporous Carbon Nitride Nanospheres with Superior Electrocatalytic Activity. *Nanoscale* **2016**, *8* (10), 5441−5445.
(89) Niu, W.; Li, Z.; Marcus, K.; Zhou, L.; Li, Y.; Ye, R.; Liang, K.; Yang, Y. Surface-Modified Porous Carbon Nitride Composites as Highly Efficient Electrocatalyst for Zn-Air Batteries. *Adv. Energy Mater.* **2018**, *8* (1), 1701642.
(90) Yang, Z.; Zhang, Y.; Schnepp, Z. Soft and Hard Templating of Graphitic Carbon Nitride. *J. Mater. Chem. A* **2015**, *3* (27), 14081−14092.
(91) Kumar, S.; Gawande, M. B.; Kopp, J.; Kment, S.; Varma, R. S.; Zbořil, R. P-and F-Co-Doped Carbon Nitride Nanocatalysts for Photocatalytic CO_2 Reduction and Thermocatalytic Furanics Synthesis from Sugars. *ChemSusChem* **2020**, *13* (19), 5231−5238.
(92) Zhang, W.; Huang, H.; Li, F.; Deng, K.; Wang, X. Palladium Nanoparticles Supported on Graphitic Carbon Nitride-Modified Reduced Graphene Oxide as Highly Efficient Catalysts for Formic Acid and Methanol Electrooxidation. *J. Mater. Chem. A* **2014**, *2* (44), 19084−19094.
(93) Song, C.; Kim, S. Preparation and Electrochemical Characterization of Pt-Supported Flake-Like Graphitic Carbon Nitride on Reduced Graphene Oxide as Fuel Cell Catalysts. *J. Electrochem. Soc.* **2015**, *162*, F1181−F1190.
(94) Jindal, A.; Basu, S.; P, A. C. Electrospun Carbon Nitride Supported on Poly(Vinyl) Alcohol as an Electrocatalyst for Oxygen Reduction Reactions. *RSC Adv.* **2015**, *5* (85), 69378−69387.
(95) Idris, A. O.; Oseghe, E. O.; Msagati, T. A. M.; Kuvarega, A. T.; Feleni, U.; Mamba, B. Graphitic Carbon Nitride: A Highly Electroactive Nanomaterial for Environmental and Clinical Sensing. *Sensors* **2020**, *20* (20), 5743.
(96) Abdullahi, Y. Z.; Yoon, T. L.; Halim, M. M.; Hashim, M. R.; Lim, T. L. Mechanical and Electronic Properties of Graphitic Carbon Nitride Sheet: First-Principles Calculations. *Solid State Commun.* **2016**, *248*, 144−150.
(97) Tan, X.; Kou, L.; Tahini, H. A.; Smith, S. C. Conductive Graphitic Carbon Nitride as an Ideal Material for Electrocatalytically Switchable CO_2 Capture. *Sci. Rep.* **2015**, *5*, 17636.
(98) Liu, J.; Wang, H.; Antonietti, M. Graphitic Carbon Nitride "Reloaded": Emerging Applications Beyond (Photo)Catalysis. *Chem. Soc. Rev.* **2016**, *45* (8), 2308−2326.
(99) Zhang, X.; Wang, H.; Wang, H.; Zhang, Q.; Xie, J.; Tian, Y.; Wang, J.; Xie, Y. Single-Layered Graphitic-C_3N_4 Quantum Dots for Two-Photon Fluorescence Imaging of Cellular Nucleus. *Adv. Mater.* **2014**, *26* (26), 4438−4443.
(100) Gaddam, S. K.; Pothu, R.; Boddula, R. Graphitic Carbon Nitride (g-C_3N_4) Reinforced Polymer Nanocomposite Systems—a Review. *Polym. Compos.* **2020**, *41* (2), 430−442.
(101) Mortazavi, B.; Cuniberti, G.; Rabczuk, T. Mechanical Properties and Thermal Conductivity of Graphitic Carbon Nitride: A Molecular Dynamics Study. *Comput. Mater. Sci.* **2015**, *99*, 285−289.
(102) Kottappara, R.; Palantavida, S.; Vijayan, B. K. Enhancing Semiconductor Photocatalysis with Carbon Nanostructures for Water/Air Purification and Self-Cleaning Applications. In *Carbon Based Nanomaterials for Advanced Thermal and Electrochemical Energy Storage and Conversion*; Paul, R., Etacheri, V., Wang, Y., Lin, C.-T., Eds.; Elsevier, 2019; pp 139−172.
(103) Dong, G.; Zhang, Y.; Pan, Q.; Qiu, J. A Fantastic Graphitic Carbon Nitride (g-C_3N_4) Material: Electronic Structure, Photocatalytic and Photoelectronic Properties. *J. Photochem. Photobiol. C: Photochem. Rev.* **2014**, *20*, 33−50.
(104) Kroke, E.; Schwarz, M.; Horath-Bordon, E.; Kroll, P.; Noll, B.; Norman, A. D. Tri-s-Triazine Derivatives. Part I. From Trichloro-tri-s-triazine to Graphitic C_3N_4 Structures. *New J. Chem.* **2002**, *26*, 508−512.
(105) Dong, Q.; Mohamad Latiff, N.; Mazánek, V.; Rosli, N. F.; Chia, H. L.; Sofer, Z. k.; Pumera, M. Triazine-and Heptazine-Based Carbon Nitrides: Toxicity. *ACS Appl. Nano Mater.* **2018**, *1* (9), 4442−4449.
(106) Kumru, B.; Antonietti, M.; Schmidt, B. V. K. J. Enhanced Dispersibility of Graphitic Carbon Nitride Particles in Aqueous and Organic Media Via a One-Pot Grafting Approach. *Langmuir* **2017**, *33* (38), 9897−9906.
(107) Jaleh, B.; Nasrollahzadeh, M.; Nasri, A.; Eslamipanah, M.; Moradi, A.; Nezafat, Z. Biopolymer-Derived (Nano) Catalysts for

Hydrogen Evolution Via Hydrolysis of Hydrides and Electrochemical and Photocatalytic Techniques: A Review. *Int. J. Biol. Macromol.* **2021**, *182*, 1056−1090.
(108) Nasri, A.; Jaleh, B.; Khazalpour, S.; Nasrollahzadeh, M.; Shokouhimehr, M. Facile Synthesis of Graphitic Carbon Nitride/Chitosan/Au Nanocomposite: A Catalyst for Electrochemical Hydrogen Evolution. *Int. J. Biol. Macromol.* **2020**, *164*, 3012−3024.
(109) Wang, R.; Li, D.; Maurya, S.; Kim, Y. S.; Wu, Y.; Liu, Y.; Strmcnik, D.; Markovic, N. M.; Stamenkovic, V. R. Ultrafine Pt Cluster and RuO_2 Heterojunction Anode Catalysts Designed for Ultra-Low Pt-Loading Anion Exchange Membrane Fuel Cells. *Nanoscale Horiz.* **2020**, *5* (2), 316−324.
(110) Rono, N.; Kibet, J. K.; Martincigh, B. S.; Nyamori, V. O. A Review of the Current Status of Graphitic Carbon Nitride. *Crit. Rev. Solid State Mater. Sci.* **2021**, *46* (3), 189−217.
(111) Zhang, P.; Li, H.; Wang, Y. Post-Functionalization of Graphitic Carbon Nitrides by Grafting Organic Molecules: Toward C−H Bond Oxidation Using Atmospheric Oxygen. *Chem. Commun.* **2014**, *50* (48), 6312−6315.
(112) Sun, J.; Phatake, R.; Azoulay, A.; Peng, G.; Han, C.; Barrio, J.; Xu, J.; Wang, X.; Shalom, M. Covalent Functionalization of Carbon Nitride Frameworks through Cross-Coupling Reactions. *Chem. Eur. J.* **2018**, *24* (56), 14921−14927.
(113) Jia, J.; White, E. R.; Clancy, A. J.; Rubio, N.; Suter, T.; Miller, T. S.; McColl, K.; McMillan, P. F.; Brázdová, V.; Corà, F.; Howard, C. A.; Law, R. V.; Mattevi, C.; Shaffer, M. S. P. Fast Exfoliation and Functionalisation of Two-Dimensional Crystalline Carbon Nitride by Framework Charging. *Angew. Chem., Int. Ed* **2018**, *57* (39), 12656−12660.
(114) Windle, C. D.; Wieczorek, A.; Xiong, L.; Sachs, M.; Bozal-Ginesta, C.; Cha, H.; Cockcroft, J. K.; Durrant, J.; Tang, J. Covalent Grafting of Molecular Catalysts on $C_3N_xH_y$ as Robust, Efficient and Well-Defined Photocatalysts for Solar Fuel Synthesis. *Chem. Sci.* **2020**, *11* (32), 8425−8432.
(115) Wojtyła, S.; Śpiewak, K.; Baran, T. Doped Graphitic Carbon Nitride: Insights from Spectroscopy and Electrochemistry. *J. Inorg. Organomet. Polym. Mater.* **2020**, *30* (9), 3418−3428.
(116) Starukh, H.; Praus, P. Doping of Graphitic Carbon Nitride with Non-Metal Elements and Its Applications in Photocatalysis. *Catalysts* **2020**, *10* (10), 1119.
(117) Tan, S. M.; Pumera, M. Two-Dimensional Materials on the Rocks: Positive and Negative Role of Dopants and Impurities in Electrochemistry. *ACS Nano* **2019**, *13* (3), 2681−2728.
(118) Wang, L.; Sofer, Z.; Pumera, M. Catalytic Hydrogen Evolution Reaction on "Metal-Free" Graphene: Key Role of Metallic Impurities. *Nanoscale* **2019**, *11* (23), 11083−11085.
(119) Mazánek, V.; Luxa, J.; Matějková, S.; Kučera, J.; Sedmidubský, D.; Pumera, M.; Sofer, Z. Ultrapure Graphene Is a Poor Electrocatalyst: Definitive Proof of the Key Role of Metallic Impurities in Graphene-Based Electrocatalysis. *ACS Nano* **2019**, *13* (2), 1574−1582.
(120) Strmcnik, D.; Li, D.; Lopes, P. P.; Tripkovic, D.; Kodama, K.; Stamenkovic, V. R.; Markovic, N. M. When Small Is Big: The Role of Impurities in Electrocatalysis. *Top. Catal.* **2015**, *58* (18), 1174−1180.
(121) Spanos, I.; Masa, J.; Zeradjanin, A.; Schlögl, R. The Effect of Iron Impurities on Transition Metal Catalysts for the Oxygen Evolution Reaction in Alkaline Environment: Activity Mediators or Active Sites. *Catal. Lett.* **2021**, *151* (7), 1843−1856.
(122) Zhang, W.; Xu, D.; Wang, F.; Chen, M. Element-Doped Graphitic Carbon Nitride: Confirmation of Doped Elements and Applications. *Nanoscale Adv.* **2021**, *3*, 4370−4387.
(123) Liao, G.; Li, C.; Li, X.; Fang, B. Emerging Polymeric Carbon Nitride Z-Scheme Systems for Photocatalysis. *Cell Rep. Phys. Sci.* **2021**, *2* (3), 100355.
(124) Rathi, A. K.; Kmentová, H.; Naldoni, A.; Goswami, A.; Gawande, M. B.; Varma, R. S.; Kment, S.; Zbořil, R. Significant Enhancement of Photoactivity in Hybrid TiO_2/g-C_3N_4 Nanorod Catalysts Modified with Cu-Ni-Based Nanostructures. *ACS Appl. Nano Mater.* **2018**, *1* (6), 2526−2535.
(125) Pieta, I. S.; Rathi, A.; Pieta, P.; Nowakowski, R.; Hołdynski, M.; Pisarek, M.; Kaminska, A.; Gawande, M. B.; Zboril, R. Electrocatalytic Methanol Oxidation over Cu, Ni and Bimetallic Cu-Ni Nanoparticles Supported on Graphitic Carbon Nitride. *Appl. Catal., B* **2019**, *244*, 272−283.
(126) Mitchell, E.; Law, A.; Godin, R. Interfacial Charge Transfer in Carbon Nitride Heterojunctions Monitored by Optical Methods. *J. Photochem. Photobiol. C: Photochem. Rev.* **2021**, *49*, 100453.
(127) Huang, R.; Wu, J.; Zhang, M.; Liu, B.; Zheng, Z.; Luo, D. Strategies to Enhance Photocatalytic Activity of Graphite Carbon Nitride-Based Photocatalysts. *Mater. Des.* **2021**, *210*, 110040.
(128) Patnaik, S.; Martha, S.; Acharya, S.; Parida, K. M. An Overview of the Modification of g-C_3N_4 with High Carbon Containing Materials for Photocatalytic Applications. *Inorg. Chem. Front.* **2016**, *3* (3), 336−347.
(129) Ge, J.; Zhang, Y.; Park, S.-J. Recent Advances in Carbonaceous Photocatalysts with Enhanced Photocatalytic Performances: A Mini Review. *Materials* **2019**, *12* (12), 1916.
(130) Alaghmandfard, A.; Ghandi, K. A Comprehensive Review of Graphitic Carbon Nitride (g-C_3N_4)-Metal Oxide-Based Nanocomposites: Potential for Photocatalysis and Sensing. *Nanomaterials* **2022**, *12* (2), 294.
(131) Kumar, A.; Raizada, P.; Hosseini-Bandegharaei, A.; Thakur, V. K.; Nguyen, V.-H.; Singh, P. C-, N-Vacancy Defect Engineered Polymeric Carbon Nitride Towards Photocatalysis: Viewpoints and Challenges. *J. Mater. Chem. A* **2021**, *9* (1), 111−153.
(132) Guo, S.; Tang, Y.; Xie, Y.; Tian, C.; Feng, Q.; Zhou, W.; Jiang, B. P-Doped Tubular G- C_3N_4 with Surface Carbon Defects: Universal Synthesis and Enhanced Visible-Light Photocatalytic Hydrogen Production. *Appl. Catal., B* **2017**, *218*, 664−671.
(133) Liang, X.; Wang, G.; Dong, X.; Wang, G.; Ma, H.; Zhang, X. Graphitic Carbon Nitride with Carbon Vacancies for Photocatalytic Degradation of Bisphenol A. *ACS Appl. Nano Mater.* **2019**, *2* (1), 517−524.
(134) Liao, Y.; Wang, G.; Wang, J.; Wang, K.; Yan, S.; Su, Y. Nitrogen Vacancy Induced in Situ G-C_3N_4 P-N Homojunction for Boosting Visible Light-Driven Hydrogen Evolution. *J. Colloid Interface Sci.* **2021**, *587*, 110−120.
(135) Jiang, L.; Yang, J.; Yuan, X.; Guo, J.; Liang, J.; Tang, W.; Chen, Y.; Li, X.; Wang, H.; Chu, W. Defect Engineering in Polymeric Carbon Nitride Photocatalyst: Synthesis, Properties and Characterizations. *Adv. Colloid Interface Sci.* **2021**, *296*, 102523.
(136) Wu, Y. A.; McNulty, I.; Liu, C.; Lau, K. C.; Liu, Q.; Paulikas, A. P.; Sun, C.-J.; Cai, Z.; Guest, J. R.; Ren, Y.; et al. Facet-Dependent Active Sites of a Single Cu_2O Particle Photocatalyst for CO_2 Reduction to Methanol. *Nat. Energy* **2019**, *4* (11), 957−968.
(137) Bajracharya, S.; ElMekawy, A.; Srikanth, S.; Pant, D. Cathodes for Microbial Fuel Cells. In *Microbial Electrochemical and Fuel Cells*; Scott, K., Yu, E. H., Eds.; Woodhead Publishing: Cambridge, U.K., 2016; pp 179−213.
(138) Ma, R.; Lin, G.; Zhou, Y.; Liu, Q.; Zhang, T.; Shan, G.; Yang, M.; Wang, J. A review of oxygen reduction mechanisms for metal-free carbon-based electrocatalysts. *Npj Comput. Mater.* **2019**, *5*, 78.
(139) Woo, J.; Lim, J. S.; Kim, J. H.; Joo, S. H. Heteroatom-Doped Carbon-Based Oxygen Reduction Electrocatalysts with Tailored Four-Electron and Two-Electron Selectivity. *Chem. Commun.* **2021**, *57* (60), 7350−7361.
(140) Nguyen, V. N.; Blum, L. 5 - Reversible Fuel Cells. In *Hydrogen Energy Conversion*; Barbir, F., Basile, A., Veziroğlu, T. N., Eds.; Compendium of Hydrogen Energy, Vol. 3; Woodhead Publishing: Cambridge, U.K., 2016; pp 115−145.
(141) Seh, Z. W.; Kibsgaard, J.; Dickens, C. F.; Chorkendorff, I.; Nørskov, J. K.; Jaramillo, T. F. Combining Theory and Experiment in Electrocatalysis: Insights into Materials Design. *Science* **2017**, *355* (6321), No. eaad4998.
(142) Petrii, O. A. Chemistry, Electrochemistry, and Electrochemical Applications | Hydrogen. In *Encyclopedia of Electrochemical Power Sources*, Garche, J., Ed.; Elsevier, 2009; pp 751−761.

(143) Zhu, Y.; Zhang, D.; Gong, L.; Zhang, L.; Xia, Z. Catalytic Activity Origin and Design Principles of Graphitic Carbon Nitride Electrocatalysts for Hydrogen Evolution. *Front. Mater.* **2019**, *6*, 16.
(144) Lasia, A. Mechanism and Kinetics of the Hydrogen Evolution Reaction. *Int. J. Hydrog. Energy* **2019**, *44* (36), 19484−19518.
(145) Sahoo, P. K.; Bisoi, S. R.; Huang, Y.-J.; Tsai, D.-S.; Lee, C.-P. 2D-Layered Non-Precious Electrocatalysts for Hydrogen Evolution Reaction: Fundamentals to Applications. *Catalysts* **2021**, *11* (6), 689.
(146) Zoller, F.; Häringer, S.; Böhm, D.; Luxa, J.; Sofer, Z.; Fattakhova-Rohlfing, D. Carbonaceous Oxygen Evolution Reaction Catalysts: From Defect and Doping-Induced Activity over Hybrid Compounds to Ordered Framework Structures. *Small* **2021**, *17* (48), 2007484.
(147) Stelmachowski, P.; Duch, J.; Sebastián, D.; Lázaro, M. J.; Kotarba, A. Carbon-Based Composites as Electrocatalysts for Oxygen Evolution Reaction in Alkaline Media. *Materials* **2021**, *14* (17), 4984.
(148) Narayanan, H.; Viswanathan, B.; Krishnamurthy, K. R.; Nair, H. Hydrogen from Photo-Electrocatalytic Water Splitting. In *Solar Hydrogen Production*; Claise, F., D'Accadia, M. D., Santarelli, M., Lanzini, A., Ferrero, D., Eds.; Elsevier, 2019; pp 419−486.
(149) Ma, T. Y.; Dai, S.; Jaroniec, M.; Qiao, S. Z. Graphitic Carbon Nitride Nanosheet-Carbon Nanotube Three-Dimensional Porous Composites as High-Performance Oxygen Evolution Electrocatalysts. *Angew. Chem., Int. Ed* **2014**, *53* (28), 7281−7285.
(150) Wang, H.-F.; Tang, C.; Zhang, Q. A Review of Precious-Metal-Free Bifunctional Oxygen Electrocatalysts: Rational Design and Applications in Zn-Air Batteries. *Adv. Funct. Mater.* **2018**, *28* (46), 1803329.
(151) Rai, V.; Reddy, M. V.; Adams, S.; Blackwood, D. J. Comparative Oxygen Evolution Reaction Performance of Cobalt Oxide Electrocatalyst in Combination with Various Metal Ions MCo_2O_4 (M= Mn^{2+}, Cu^{2+}, Co^{2+}, Zn^{2+}, Fe^{2+}, Mg^{2+}). *IOP Conf. Ser.: Mater. Sci. Eng.* **2020**, *872*, No. 012182.
(152) Iwasita, T. Electrocatalysis of Methanol Oxidation. *Electrochim. Acta* **2002**, *47* (22−23), 3663−3674.
(153) Liu, H.; Song, C.; Zhang, L.; Zhang, J.; Wang, H.; Wilkinson, D. P. A Review of Anode Catalysis in the Direct Methanol Fuel Cell. *J. Power Sources* **2006**, *155* (2), 95−110.
(154) Wala, M.; Simka, W. Effect of Anode Material on Electrochemical Oxidation of Low Molecular Weight Alcohols—a Review. *Molecules* **2021**, *26* (8), 2144.
(155) Tian, H.; Yu, Y.; Wang, Q.; Li, J.; Rao, P.; Li, R.; Du, Y.; Jia, C.; Luo, J.; Deng, P.; et al. Recent Advances in Two-Dimensional Pt Based Electrocatalysts for Methanol Oxidation Reaction. *Int. J. Hydrog. Energy* **2021**, *46* (61), 31202−31215.
(156) Lu, S.; Li, H.; Sun, J.; Zhuang, Z. Promoting the Methanol Oxidation Catalytic Activity by Introducing Surface Nickel on Platinum Nanoparticles. *Nano Res.* **2018**, *11* (4), 2058−2068.
(157) Zeng, R.; Yang, Y.; Shen, T.; Wang, H.; Xiong, Y.; Zhu, J.; Wang, D.; Abruña, H. D. Methanol Oxidation Using Ternary Ordered Intermetallic Electrocatalysts: A Dems Study. *ACS Catal.* **2020**, *10* (1), 770−776.
(158) Yuda, A.; Ashok, A.; Kumar, A. A Comprehensive and Critical Review on Recent Progress in Anode Catalyst for Methanol Oxidation Reaction. *Catal. Rev.* **2022**, *64* (1), 126−228.
(159) Cheng, F.; Chen, J. metal−air Batteries: From Oxygen Reduction Electrochemistry to Cathode Catalysts. *Chem. Soc. Rev.* **2012**, *41* (6), 2172−2192.
(160) Li, X.; Zhao, L.; Yu, J.; Liu, X.; Zhang, X.; Liu, H.; Zhou, W. Water Splitting: From Electrode to Green Energy System. *Nano-Micro Lett.* **2020**, *12*, 131.
(161) Mansor, N.; Miller, T. S.; Dedigama, I.; Jorge, A. B.; Jia, J.; Brázdová, V.; Mattevi, C.; Gibbs, C.; Hodgson, D.; Shearing, P. R.; et al. Graphitic Carbon Nitride as a Catalyst Support in Fuel Cells and Electrolyzers. *Electrochim. Acta* **2016**, *222*, 44−57.
(162) Niu, W.; Marcus, K.; Zhou, L.; Li, Z.; Shi, L.; Liang, K.; Yang, Y. Enhancing Electron Transfer and Electrocatalytic Activity on Crystalline Carbon-Conjugated g-C_3N_4. *ACS Catal.* **2018**, *8* (3), 1926−1931.
(163) Chakraborty, I.; Ghosh, N.; Ghosh, D.; Dubey, B. K.; Pradhan, D.; Ghangrekar, M. M. Application of Synthesized Porous Graphitic Carbon Nitride and It's Composite as Excellent Electrocatalysts in Microbial Fuel Cell. *Int. J. Hydrog. Energy* **2020**, *45* (55), 31056−31069.
(164) Zhang, Q.; Liu, L. Cathodes of Membrane and Packed Manganese Dioxide/Titanium Dioxide/Graphitic Carbon Nitride/Granular Activated Carbon Promoted Treatment of Coking Wastewater in Microbial Fuel Cell. *Bioresour. Technol.* **2021**, *321*, 124442.
(165) Bhavani, K. S.; Anusha, T.; Brahman, P. K. Platinum Nanoparticles Decorated on Graphitic Carbon Nitride-ZIF-67 Composite Support: An Electrocatalyst for the Oxidation of Butanol in Fuel Cell Applications. *Int. J. Hydrog. Energy* **2021**, *46* (13), 9199−9214.
(166) Hussain, N.; Alawadhi, H.; Rahman, S. M. A.; Abdelkareem, M. A. Facile Synthesis of Novel Cu_2O-g-C_3N_4/Vulcan Carbon Composite as Anode Material with Enhanced Electrochemical Performances in Urea Fuel Cell. *Sustain. Energy Technol. Assess.* **2021**, *45*, 101107.
(167) Huang, H.; Yang, S.; Vajtai, R.; Wang, X.; Ajayan, P. M. Pt-Decorated 3D Architectures Built from Graphene and Graphitic Carbon Nitride Nanosheets as Efficient Methanol Oxidation Catalysts. *Adv. Mater.* **2014**, *26* (30), 5160−5165.
(168) Lee, I. H.; Cho, J.; Chae, K. H.; Cho, M. K.; Jung, J.; Cho, J.; Lee, H. J.; Ham, H. C.; Kim, J. Y. Polymeric Graphitic Carbon Nitride Nanosheet-Coated Amorphous Carbon Supports for Enhanced Fuel Cell Electrode Performance and Stability. *Appl. Catal., B* **2018**, *237*, 318−326.
(169) Chandrasekharan Meenu, P.; Datta, S. P.; Singh, S. A.; Dinda, S.; Chakraborty, C.; Roy, S. Polyaniline Supported G-C_3N_4 Quantum Dots Surpass Benchmark Pt/C: Development of Morphologically Engineered g-C_3N_4 Catalysts Towards "Metal-Free" Methanol Electro-Oxidation. *J. Power Sources* **2020**, *461*, 228150.
(170) Nazir, R.; Kumar, A.; Ali Saleh Saad, M.; Ali, S. Development of CuAg/Cu_2O Nanoparticles on Carbon Nitride Surface for Methanol Oxidation and Selective Conversion of Carbon Dioxide into Formate. *J. Colloid Interface Sci.* **2020**, *578*, 726−737.
(171) Hu, J.; Zhai, C.; Gao, H.; Zeng, L.; Du, Y.; Zhu, M. Enhanced Photo-Assisted Ethanol Electro-Oxidation Activity by Using Broadband Visible Light Absorption of a Graphitic C_3N_4/BiOI Carrier. *Sustain. Energy Fuels* **2019**, *3* (2), 439−449.
(172) Sarkar, S.; Sumukh, S. S.; Roy, K.; Kamboj, N.; Purkait, T.; Das, M.; Dey, R. S. Facile One Step Synthesis of Cu-g-C_3N_4 Electrocatalyst Realized Oxygen Reduction Reaction with Excellent Methanol Crossover Impact and Durability. *J. Colloid Interface Sci.* **2020**, *558*, 182−189.
(173) Dembinska, B.; Brzozowska, K.; Szwed, A.; Miecznikowski, K.; Negro, E.; Di Noto, V.; Kulesza, P. J. Electrocatalytic Oxygen Reduction in Alkaline Medium Atgraphene-Supported Silver-Iron Carbon Nitride Sitesgenerated Duringthermal Decomposition of Silver Hexacyanoferrate. *Electrocatalysis* **2019**, *10* (1), 112−124.
(174) Wassner, M.; Eckardt, M.; Gebauer, C.; Bourret, G. R.; Hüsing, N.; Behm, R. J. Synthesis and Electrocatalytic Performance of Spherical Core-Shell Tantalum (oxy)Nitride@Nitrided Carbon Composites in the Oxygen Reduction Reaction. *Electrochim. Acta* **2017**, *227*, 367−381.
(175) Kwon, K.; Sa, Y. J.; Cheon, J. Y.; Joo, S. H. Ordered Mesoporous Carbon Nitrides with Graphitic Frameworks as Metal-Free, Highly Durable, Methanol-Tolerant Oxygen Reduction Catalysts in an Acidic Medium. *Langmuir* **2012**, *28* (1), 991−996.
(176) Negro, E.; Vezzù, K.; Bertasi, F.; Schiavuta, P.; Toniolo, L.; Polizzi, S.; Di Noto, V. Interplay between Nitrogen Concentration, Structure, Morphology, and Electrochemical Performance of Pdconi "Core-Shell" Carbon Nitride Electrocatalysts for the Oxygen Reduction Reaction. *ChemElectroChem.* **2014**, *1* (8), 1359−1369.
(177) Ding, C.; Feng, C.; Mei, Y.; Liu, F.; Wang, H.; Dupuis, M.; Li, C. Carbon Nitride Embedded with Transition Metals for Selective Electrocatalytic CO_2 Reduction. *Appl. Catal., B* **2020**, *268*, 118391.

(178) Jo, W.-K.; Moru, S.; Lee, D.-E.; Tonda, S. Cobalt- and Iron-Coordinated Graphitic Carbon Nitride on Reduced Graphene Oxide: A Nonprecious Bimetallic M-N_x-C Analogue Electrocatalyst for Efficient Oxygen Reduction Reaction in Acidic Media. *Appl. Surf. Sci.* **2020**, *531*, 147367.
(179) Zorko, M.; Farinazzo Bergamo Dias Martins, P.; Connell, J. G.; Lopes, P. P.; Markovic, N. M.; Stamenkovic, V. R.; Strmcnik, D. Improved Rate for the Oxygen Reduction Reaction in a Sulfuric Acid Electrolyte Using a Pt (111) Surface Modified with Melamine. *ACS Appl. Mater. Interfaces* **2021**, *13* (2), 3369−3376.
(180) Sadhukhan, M.; Kundu, M. K.; Bhowmik, T.; Barman, S. Highly Dispersed Platinum Nanoparticles on Graphitic Carbon Nitride: A Highly Active and Durable Electrocatalyst for Oxidation of Methanol, Formic Acid and Formaldehyde. *Int. J. Hydrog. Energy* **2017**, *42* (15), 9371−9383.
(181) Jindal, A.; Gautam, D. K.; Basu, S. Electrocatalytic Activity of Electrospun Carbon Nitride-Polyacrylonitrile Nanofiber Towards Oxygen Reduction Reactions. *J. Electroanal. Chem.* **2016**, *775*, 198−204.
(182) Alawadhi, H.; Abdelkareem, M. A.; Hussain, N.; Wilberforce, T.; Sayed, E. T. A Composite of Graphitic Carbon Nitride and Vulcan Carbon as an Effective Catalyst Support for Ni in Direct Urea Fuel Cells. *J. Taiwan Inst. Chem. Eng.* **2020**, *116*, 160−168.
(183) Hussain, N.; Abdelkareem, M. A.; Alawadhi, H.; Alaswad, A.; Sayed, E. T. Two Dimensional Cu Based Nanocomposite Materials for Direct Urea Fuel Cell. *Int. J. Hydrog. Energy* **2021**, *46* (8), 6051−6060.
(184) Nubla, K.; Radhakrishnan, T.; Sandhyarani, N. A Graphitic Carbon Nitride−Titania Nanocomposite as a Promising Catalyst Support for Electro-Oxidation of Methanol. *New J. Chem.* **2019**, *43* (8), 3273−3279.
(185) Lopes, P. P.; Li, D.; Lv, H.; Wang, C.; Tripkovic, D.; Zhu, Y.; Schimmenti, R.; Daimon, H.; Kang, Y.; Snyder, J.; et al. Eliminating Dissolution of Platinum-Based Electrocatalysts at the Atomic Scale. *Nat. Mater.* **2020**, *19* (11), 1207−1214.
(186) Wang, M.; Park, J. H.; Kabir, S.; Neyerlin, K. C.; Kariuki, N. N.; Lv, H.; Stamenkovic, V. R.; Myers, D. J.; Ulsh, M.; Mauger, S. A. Impact of Catalyst Ink Dispersing Methodology on Fuel Cell Performance Using in-Situ X-Ray Scattering. *ACS Appl. Energy Mater.* **2019**, *2* (9), 6417−6427.
(187) Jung, S.-M.; Yun, S.-W.; Kim, J.-H.; You, S.-H.; Park, J.; Lee, S.; Chang, S. H.; Chae, S. C.; Joo, S. H.; Jung, Y.; Lee, J.; Son, J.; Snyder, J.; Stamenkovic, V.; Markovic, N. M.; Kim, Y.-T. Selective Electrocatalysis Imparted by Metal-Insulator Transition for Durability Enhancement of Automotive Fuel Cells. *Nat. Catal.* **2020**, *3* (8), 639−648.
(188) Zhang, W.; Yao, Q.; Wu, X.; Fu, Y.; Deng, K.; Wang, X. Intimately Coupled Hybrid of Graphitic Carbon Nitride Nanoflakelets with Reduced Graphene Oxide for Supporting Pd Nanoparticles: A Stable Nanocatalyst with High Catalytic Activity Towards Formic Acid and Methanol Electrooxidation. *Electrochim. Acta* **2016**, *200*, 131−141.
(189) Wang, Y.-J.; Fang, B.; Zhang, D.; Li, A.; Wilkinson, D. P.; Ignaszak, A.; Zhang, L.; Zhang, J. A Review of Carbon-Composited Materials as Air-Electrode Bifunctional Electrocatalysts for Metal-Air Batteries. *Electrochem. Energy Rev.* **2018**, *1* (1), 1−34.
(190) Tepavcevic, S.; Connell, J. G.; Lopes, P. P.; Bachhav, M.; Key, B.; Valero-Vidal, C.; Crumlin, E. J.; Stamenkovic, V. R.; Markovic, N. M. Role of Structural Hydroxyl Groups in Enhancing Performance of Electrochemically-Synthesized Bilayer V_2O_5. *Nano Energy* **2018**, *53*, 449−457.
(191) Yue, K.; Yan, Z.; Sun, Z.; Li, A.; Qian, L. Graphitic Carbon Nitride Modified with Pd Nanoparticles toward Efficient Cathode Catalyst for Li-O_2 Batteries. *Funct. Mater. Lett.* **2020**, *13* (07), 2051045.
(192) Tian, Y.; Xu, L.; Bao, J.; Qian, J.; Su, H.; Li, H.; Gu, H.; Yan, C.; Li, H. Hollow Cobalt Oxide Nanoparticles Embedded in Nitrogen-Doped Carbon Nanosheets as an Efficient Bifunctional Catalyst for Zn-Air Battery. *J. Energy Chem.* **2019**, *33*, 59−66.
(193) Ma, T. Y.; Cao, J. L.; Jaroniec, M.; Qiao, S. Z. Interacting Carbon Nitride and Titanium Carbide Nanosheets for High-Performance Oxygen Evolution. *Angew. Chem., Int. Ed* **2016**, *55* (3), 1138−1142.
(194) Ding, J.; Wu, D.; Huang, S.; Lu, C.; Chen, Y.; Zhang, J.; Zhang, L.; Li, J.; Ke, C.; Tranca, D.; et al. Topological Defect-Containing Fe/N Co-Doped Mesoporous Carbon Nanosheets as Novel Electrocatalysts for the Oxygen Reduction Reaction and Zn-Air Batteries. *Nanoscale* **2021**, *13* (31), 13249−13255.
(195) Li, X.; Zhao, Y.; Ding, L.; Wang, D.; Guo, Q.; Li, Z.; Luo, H.; Zhang, D.; Yu, Y. Enhancing the Capacity and Stability by $CoFe_2O_4$ Modified g-C_3N_4 Composite for Lithium-Oxygen Batteries. *Nanomaterials* **2021**, *11* (5), 1088.
(196) Guo, Q.; Zhang, C.; Zhang, C.; Xin, S.; Zhang, P.; Shi, Q.; Zhang, D.; You, Y. Co_3O_4 Modified Ag/g-C_3N_4 Composite as a Bifunctional Cathode for Lithium-Oxygen Battery. *J. Energy Chem.* **2020**, *41*, 185−193.
(197) Hang, Y.; Zhang, C.; Luo, X.; Xie, Y.; Xin, S.; Li, Y.; Zhang, D.; Goodenough, J. B. A-MnO_2 Nanorods Supported on Porous Graphitic Carbon Nitride as Efficient Electrocatalysts for Lithium-Air Batteries. *J. Power Sources* **2018**, *392*, 15−22.
(198) Li, D.; Liu, J.; Wang, W.; Li, S.; Yang, G.; Wang, P.; Zhu, K.; Li, Z. Synthesis of Porous N Deficient Graphitic Carbon Nitride and Utilization in Lithium-Sulfur Battery. *Appl. Surf. Sci.* **2021**, *569*, 151058.
(199) Huang, Y.; Chen, B.; Duan, J.; Yang, F.; Wang, T.; Wang, Z.; Yang, W.; Hu, C.; Luo, W.; Huang, Y. Graphitic Carbon Nitride (g-C_3N_4): An Interface Enabler for Solid-State Lithium Metal Batteries. *Angew. Chem., Int. Ed.* **2020**, *132* (9), 3728−3733.
(200) Jia, Y.; Ji, L.; Gao, H.; Liu, Y.; Yang, D.; Li, T.; Bai, J.; Hu, Q.; Wang, M.; Liu, J. Carbon Nitride Grafted Waste-Derived Carbon as Sustainable Materials for Lithium-Sulfur Batteries. *Nanotechnology* **2021**, *32* (31), 315403.
(201) Mehri, M.; Mousavi-Khoshdel, S.; Molaei, M. First-Principle Calculations Study of Pristine, S-, O-, and P-Doped g-C_3N_4 as ORR Catalysts for Li-O_2 Batteries. *Chem. Phys. Lett.* **2021**, *775*, 138614.
(202) Ren, J.-T.; Chen, L.; Weng, C.-C.; Yuan, G.-G.; Yuan, Z.-Y. Well-Defined Mo_2C Nanoparticles Embedded in Porous N-Doped Carbon Matrix for Highly Efficient Electrocatalytic Hydrogen Evolution. *ACS Appl. Mater. Interfaces* **2018**, *10* (39), 33276−33286.
(203) Yan, M.; Jiang, Q.; Yang, L.; He, H.; Huang, H. Three-Dimensional Ternary Hybrid Architectures Constructed from Graphene, MoS_2, and Graphitic Carbon Nitride Nanosheets as Efficient Electrocatalysts for Hydrogen Evolution. *ACS Appl. Energy Mater.* **2020**, *3* (7), 6880−6888.
(204) Wahab, M. A.; Joseph, J.; Atanda, L.; Sultana, U. K.; Beltramini, J. N.; Ostrikov, K.; Will, G.; O'Mullane, A. P.; Abdala, A. Nanoconfined Synthesis of Nitrogen-Rich Metal-Free Mesoporous Carbon Nitride Electrocatalyst for the Oxygen Evolution Reaction. *ACS Appl. Energy Mater.* **2020**, *3* (2), 1439−1447.
(205) Zulqarnain, M.; Shah, A.; Khan, M. A.; Jan Iftikhar, F.; Nisar, J. $FeCoSe_2$ Nanoparticles Embedded in g-C_3N_4: A Highly Active and Stable Bifunctional Electrocatalyst for Overall Water Splitting. *Sci. Rep.* **2020**, *10*, 6328.
(206) Durairaj, A.; Sakthivel, T.; Ramanathan, S.; Vasanthkumar, S. Quenching-Induced Structural Distortion of Graphitic Carbon Nitride Nanostructures: Enhanced Photocatalytic Activity and Electrochemical Hydrogen Production. *ACS Omega* **2019**, *4* (4), 6476−6485.
(207) Shakeel, M.; Zhang, X.; Yasin, G.; Arif, M.; Abbas, Z.; Zaman, U.; Li, B. Fabrication of Amorphous BiOCl/TiO_2-C_3N_4 Heterostructure for Efficient Water Oxidation. *ChemistrySelect* **2019**, *4* (28), 8277−8282.
(208) Gao, M.; Liu, D.; Yang, H.; Huang, H.; Luo, Q.; Huang, Y.; Yu, X.-F.; Chu, P. Modification of Layered Graphitic Carbon Nitride by Nitrogen Plasma for Improved Electrocatalytic Hydrogen Evolution. *Nanomaterials* **2019**, *9*, 568.
(209) Liao, C.; Yang, B.; Zhang, N.; Liu, M.; Chen, G.; Jiang, X.; Chen, G.; Yang, J.; Liu, X.; Chan, T.-S.; Lu, Y.-J.; Ma, R.; Zhou, W.

Constructing Conductive Interfaces between Nickel Oxide Nanocrystals and Polymer Carbon Nitride for Efficient Electrocatalytic Oxygen Evolution Reaction. *Adv. Funct. Mater.* **2019**, *29* (40), 1904020.

(210) Borthakur, P.; Boruah, P. K.; Das, M. R.; Ibrahim, M. M.; Altalhi, T.; El-Sheshtawy, H. S.; Szunerits, S.; Boukherroub, R.; Amin, M. A. CoS_2 Nanoparticles Supported on rGO, g-C_3N_4, BCN, MoS_2, and WS_2 Two-Dimensional Nanosheets with Excellent Electrocatalytic Performance for Overall Water Splitting: Electrochemical Studies and DFT Calculations. *ACS Appl. Energy Mater.* **2021**, *4* (2), 1269−1285.

(211) Wang, S.; He, P.; Jia, L.; He, M.; Zhang, T.; Dong, F.; Liu, M.; Liu, H.; Zhang, Y.; Li, C.; et al. Nanocoral-Like Composite of Nickel Selenide Nanoparticles Anchored on Two-Dimensional Multi-Layered Graphitic Carbon Nitride: A Highly Efficient Electrocatalyst for Oxygen Evolution Reaction. *Appl. Catal., B* **2019**, *243*, 463−469.

(212) Zhang, Z.; Lu, L.; Lv, Z.; Chen, Y.; Jin, H.; Hou, S.; Qiu, L.; Duan, L.; Liu, J.; Dai, K. Porous Carbon Nitride with Defect Mediated Interfacial Oxidation for Improving Visible Light Photocatalytic Hydrogen Evolution. *Appl. Catal., B* **2018**, *232*, 384−390.

(213) Zhang, Y.; Jiang, R.; Wang, Z.; Xue, Y.; Sun, J.; Guo, Y. (Fe, N-Codoped Carbon Nanotube)/(Fe-Based Nanoparticle) Nanohybrid Derived from Fe-Doped g-C_3N_4: A Superior Catalyst for Oxygen Reduction Reaction. *J. Colloid Interface Sci.* **2020**, *579*, 391−400.

(214) Pei, Z.; Zhao, J.; Huang, Y.; Huang, Y.; Zhu, M.; Wang, Z.; Chen, Z.; Zhi, C. Toward Enhanced Activity of a Graphitic Carbon Nitride-Based Electrocatalyst in Oxygen Reduction and Hydrogen Evolution Reactions Via Atomic Sulfur Doping. *J. Mater. Chem. A* **2016**, *4* (31), 12205−12211.

(215) Fu, X.; Hu, X.; Yan, Z.; Lei, K.; Li, F.; Cheng, F.; Chen, J. Template-Free Synthesis of Porous Graphitic Carbon Nitride/Carbon Composite Spheres for Electrocatalytic Oxygen Reduction Reaction. *Chem. Commun.* **2016**, *52* (8), 1725−1728.

(216) Zhu, A.; Qiao, L.; Tan, P.; Zeng, W.; Ma, Y.; Dong, R.; Pan, J. Boosted Electrocatalytic Activity of Nitrogen-Doped Porous Carbon Triggered by Oxygen Functional Groups. *J. Colloid Interface Sci.* **2019**, *541*, 133−142.

(217) Sun, T.; Zhang, P.; Chen, W.; Wang, K.; Fu, X.; Zheng, T.; Jiang, J. Single Iron Atoms Coordinated to g-C_3N_4 on Hierarchical Porous N-Doped Carbon Polyhedra as a High-Performance Electrocatalyst for the Oxygen Reduction Reaction. *Chem. Commun.* **2020**, *56* (5), 798−801.

(218) Nazir, R.; Kumar, A.; Ali, S.; Saad, M. A. S.; Al-Marri, M. J. Galvanic Exchange as a Novel Method for Carbon Nitride Supported Coag Catalyst Synthesis for Oxygen Reduction and Carbon Dioxide Conversion. *Catalysts* **2019**, *9* (10), 860.

(219) Liu, X.; Yang, W.; Chen, L.; Liu, Z.; Long, L.; Wang, S.; Liu, C.; Dong, S.; Jia, J. Graphitic Carbon Nitride (g-C_3N_4)-Derived Bamboo-Like Carbon Nanotubes/Co Nanoparticles Hybrids for Highly Efficient Electrocatalytic Oxygen Reduction. *ACS Appl. Mater. Interfaces* **2020**, *12* (4), 4463−4472.

(220) Feng, J.-J.; Chen, L.-X.; Song, P.; Wu, X.-l.; Wang, A.-J.; Yuan, J. Bimetallic AuPd Nanoclusters Supported on Graphitic Carbon Nitride: One-Pot Synthesis and Enhanced Electrocatalysis for Oxygen Reduction and Hydrogen Evolution. *Int. J. Hydrog. Energy* **2016**, *41* (21), 8839−8846.

(221) Kundu, M. K.; Bhowmik, T.; Barman, S. Gold Aerogel Supported on Graphitic Carbon Nitride: An Efficient Electrocatalyst for Oxygen Reduction Reaction and Hydrogen Evolution Reaction. *J. Mater. Chem. A* **2015**, *3* (46), 23120−23135.

(222) Yang, Y.; Gu, L.; Guo, S.; Shao, S.; Li, Z.; Sun, Y.; Hao, S. N-Doped Mesoporous Carbons: From Synthesis to Applications as Metal-Free Reduction Catalysts and Energy Storage Materials. *Front. Chem.* **2019**, *7*, 761.

(223) Sahu, R. S.; Doong, R.-A. Functionalized Fe/Ni@g-C_3N_4 Nanostructures for Enhanced Trichloroethylene Dechlorination and Successive Oxygen Reduction Reaction Activity. *Environ. Sci. Nano* **2020**, *7* (11), 3469−3481.

(224) Faraji, M.; Moradi Dehaghi, S. Pd-Doped g-C_3N_4 Decorated by Nitrogen-Doped Carbon Quantum Dot as a High Performance Electrocatalyst with Superior Durability and Methanol Tolerance for Oxygen Reduction Reaction. *Inorg. Chem. Commun.* **2021**, *123*, 108328.

(225) Yousaf, A. B.; Monnier, J. R.; Weidner, J. W.; Hassan, M. K.; Zaidi, S. J.; Kasak, P. A Precious-Metal-Free Fe-Intercalated Carbon Nitride Porous-Network with Enhanced Activity for the Oxygen Reduction Reaction and Methanol-Tolerant Oxygen Reduction Reaction. *Sustain. Energy Fuels* **2020**, *4* (10), 5050−5060.

(226) Jun, Y.-S.; Lee, E. Z.; Wang, X.; Hong, W. H.; Stucky, G. D.; Thomas, A. From Melamine-Cyanuric Acid Supramolecular Aggregates to Carbon Nitride Hollow Spheres. *Adv. Funct. Mater.* **2013**, *23* (29), 3661−3667.

(227) Shalom, M.; Inal, S.; Fettkenhauer, C.; Neher, D.; Antonietti, M. Improving Carbon Nitride Photocatalysis by Supramolecular Preorganization of Monomers. *J. Am. Chem. Soc.* **2013**, *135* (19), 7118−7121.

(228) Shalom, M.; Gimenez, S.; Schipper, F.; Herraiz-Cardona, I.; Bisquert, J.; Antonietti, M. Controlled Carbon Nitride Growth on Surfaces for Hydrogen Evolution Electrodes. *Angew. Chem., Int. Ed n* **2014**, *53* (14), 3654−3658.

(229) Paul, A. M.; Sajeev, A.; Nivetha, R.; Gothandapani, K.; Bhardwaj, P.; K, G.; Raghavan, V.; Jacob, G.; Sellapan, R.; Jeong, S. K.; Grace, A. N. Cuprous Oxide (Cu_2O)/Graphitic Carbon Nitride (g-C_3N_4) Nanocomposites for Electrocatalytic Hydrogen Evolution Reaction. *Diam. Relat. Mater.* **2020**, *107*, 107899.

(230) Zhao, X.; Xue, Z.; Tan, X.; Liu, Z.; Chen, W.; Zhang, B.; Yang, Y.; Mu, T. CO_2-Assisted Fabrication of Defect-Engineered Carbon Nitride for Enhanced Electrocatalytic Hydrogen Evolution. *Chem. Asian J.* **2020**, *15* (23), 4113−4117.

(231) Chebanenko, M. I.; Lobinsky, A. A.; Nevedomskiy, V. N.; Popkov, V. I. NiO-Decorated Graphitic Carbon Nitride toward Electrocatalytic Hydrogen Production from Ethanol. *Dalton Trans.* **2020**, *49* (34), 12088−12097.

(232) Zhao, Y.; Zhao, F.; Wang, X.; Xu, C.; Zhang, Z.; Shi, G.; Qu, L. Graphitic Carbon Nitride Nanoribbons: Graphene-Assisted Formation and Synergic Function for Highly Efficient Hydrogen Evolution. *Angew. Chem., Int. Ed.* **2014**, *53* (50), 13934−13939.

(233) Zheng, Y.; Jiao, Y.; Zhu, Y.; Li, L. H.; Han, Y.; Chen, Y.; Du, A.; Jaroniec, M.; Qiao, S. Z. Hydrogen Evolution by a Metal-Free Electrocatalyst. *Nat. Commun.* **2014**, *5*, 3783.

(234) Tian, J.; Ning, R.; Liu, Q.; Asiri, A. M.; Al-Youbi, A. O.; Sun, X. Three-Dimensional Porous Supramolecular Architecture from Ultrathin g-C_3N_4 Nanosheets and Reduced Graphene Oxide: Solution Self-Assembly Construction and Application as a Highly Efficient Metal-Free Electrocatalyst for Oxygen Reduction Reaction. *ACS Appl. Mater. Interfaces* **2014**, *6* (2), 1011−1017.

(235) Liang, J.; Zheng, Y.; Chen, J.; Liu, J.; Hulicova-Jurcakova, D.; Jaroniec, M.; Qiao, S. Z. Facile Oxygen Reduction on a Three-Dimensionally Ordered Macroporous Graphitic C_3N_4/Carbon Composite Electrocatalyst. *Angew. Chem., Int. Ed* **2012**, *51* (16), 3892−3896.

(236) Shinde, S. S.; Sami, A.; Lee, J.-H. Electrocatalytic Hydrogen Evolution Using Graphitic Carbon Nitride Coupled with Nanoporous Graphene Co-Doped by S and Se. *J. Mater. Chem. A* **2015**, *3* (24), 12810−12819.

(237) Lu, X.; Tan, T. H.; Ng, Y. H.; Amal, R. Highly Selective and Stable Reduction of CO_2 to CO by a Graphitic Carbon Nitride/Carbon Nanotube Composite Electrocatalyst. *Chem. Eur. J.* **2016**, *22* (34), 11991−11996.

(238) Fu, W.; He, H.; Zhang, Z.; Wu, C.; Wang, X.; Wang, H.; Zeng, Q.; Sun, L.; Wang, X.; Zhou, J.; Fu, Q.; Yu, P.; Shen, Z.; Jin, C.; Yakobson, B. I.; Liu, Z. Strong Interfacial Coupling of MoS_2/g-C_3N_4 Van De Waals Solids for Highly Active Water Reduction. *Nano Energy* **2016**, *27*, 44−50.

(239) Zheng, Y.; Jiao, Y.; Zhu, Y.; Cai, Q.; Vasileff, A.; Li, L. H.; Han, Y.; Chen, Y.; Qiao, S.-Z. Molecule-Level g-C_3N_4 Coordinated

Transition Metals as a New Class of Electrocatalysts for Oxygen Electrode Reactions. *J. Am. Chem. Soc.* **2017**, *139* (9), 3336−3339.
(240) Yan, Q.; Huang, G.; Li, D.-F.; Zhang, M.; Pan, A.-L.; Huang, W.-Q. Facile Synthesis and Superior Photocatalytic and Electrocatalytic Performances of Porous B-Doped g-C_3N_4 Nanosheets. *J. Mater. Sci. Technol.* **2018**, *34* (12), 2515−2520.
(241) Xu, C.; Han, Q.; Zhao, Y.; Wang, L.; Li, Y.; Qu, L. Sulfur-Doped Graphitic Carbon Nitride Decorated with Graphene Quantum Dots for an Efficient Metal-Free Electrocatalyst. *J. Mater. Chem. A* **2015**, *3* (5), 1841−1846.
(242) Lu, P.; Sun, Y.; Xiang, H.; Liang, X.; Yu, Y. 3D Amorphous Carbon with Controlled Porous and Disordered Structures as a High-Rate Anode Material for Sodium-Ion Batteries. *Adv. Energy Mater.* **2018**, *8* (8), 1702434.
(243) Qian, X.; Meng, X.; Sun, J.; Jiang, L.; Wang, Y.; Zhang, J.; Hu, X.; Shalom, M.; Zhu, J. Salt-Assisted Synthesis of 3D Porous g-C_3N_4 as a Bifunctional Photo- and Electrocatalyst. *ACS Appl. Mater. Interfaces* **2019**, *11* (30), 27226−27232.
(244) Woyessa, G. W.; dela Cruz, J.-a. B.; Rameez, M.; Hung, C.-H. Nanocomposite Catalyst of Graphitic Carbon Nitride and Cu/Fe Mixed Metal Oxide for Electrochemical CO_2 Reduction to CO. *Appl. Catal., B* **2021**, *291*, 120052.
(245) Li, T.-T.; Mei, Y.; Li, H.; Qian, J.; Wu, M.; Zheng, Y.-Q. Highly Selective and Active Electrochemical Reduction of CO_2 to CO on a Polymeric Co(II) Phthalocyanine@Graphitic Carbon Nitride Nanosheet-Carbon Nanotube Composite. *Inorg. Chem.* **2020**, *59* (19), 14184−14192.
(246) Feng, J.; Gao, H.; Zheng, L.; Chen, Z.; Zeng, S.; Jiang, C.; Dong, H.; Liu, L.; Zhang, S.; Zhang, X. A Mn-N_3 Single-Atom Catalyst Embedded in Graphitic Carbon Nitride for Efficient CO_2 Electroreduction. *Nat. Commun.* **2020**, *11*, 4341.
(247) Fu, S.; Liu, X.; Ran, J.; Jiao, Y.; Qiao, S.-Z. CO_2 Reduction by Single Copper Atom Supported on g-C_3N_4 with Asymmetrical Active Sites. *Appl. Sur. Sci.* **2021**, *540*, 148293.
(248) Tian, J.; Wang, M.; Shen, M.; Ma, X.; Hua, Z.; Zhang, L.; Shi, J. Highly Efficient and Selective CO_2 Electro-Reduction to HCOOH on Sn Particle-Decorated Polymeric Carbon Nitride. *ChemSusChem* **2020**, *13* (23), 6442−6448.
(249) Mulik, B. B.; Bankar, B. D.; Munde, A. V.; Chavan, P. P.; Biradar, A. V.; Sathe, B. R. Electrocatalytic and Catalytic CO_2 Hydrogenation on ZnO/g-C_3N_4 Hybrid Nanoelectrodes. *Appl. Surf. Sci.* **2021**, *538*, 148120.
(250) Fang, D.; Yang, L.; Yang, G.; Yi, G.; Feng, Y.; Shao, P.; Shi, H.; Yu, K.; You, D.; Luo, X. Electrodeposited Graphene Hybridized Graphitic Carbon Nitride Anchoring Ultrafine Palladium Nanoparticles for Remarkable Methanol Electrooxidation. *Int. J. Hydrog. Energy* **2020**, *45* (41), 21483−21492.
(251) Huang, B.; Wu, Y.; Chen, B.; Qian, Y.; Zhou, N.; Li, N. Transition-Metal-Atom-Pairs Deposited on g-CN Monolayer for Nitrogen Reduction Reaction: Density Functional Theory Calculations. *Chin. J. Catal.* **2021**, *42* (7), 1160−1167.
(252) Chang, B.; Li, L.; Shi, D.; Jiang, H.; Ai, Z.; Wang, S.; Shao, Y.; Shen, J.; Wu, Y.; Li, Y.; Hao, X. Metal-Free Boron Carbonitride with Tunable Boron Lewis Acid Sites for Enhanced Nitrogen Electroreduction to Ammonia. *Appl. Catal., B* **2021**, *283*, 119622.
(253) Askins, E. J.; Zoric, M. R.; Li, M.; Luo, Z.; Amine, K.; Glusac, K. D. Toward a Mechanistic Understanding of Electrocatalytic Nanocarbon. *Nat. Commun.* **2021**, *12*, 3288.
(254) Gan, C.; Yan, W.; Zhang, Y.; Jiang, Q.; Tang, J. Research Progress of Two-Dimensional Layered and Related Derived Materials for Nitrogen Reduction Reaction. *Sustain. Energy. Fuels* **2021**, *5* (13), 3260−3277.
(255) Ziegenbalg, D.; Zander, J.; Marschall, R. Photocatalytic Nitrogen Reduction: Challenging Materials with Reaction Engineering. *ChemPhotoChem.* **2021**, *5* (9), 792−807.
(256) Liu, J.; Ma, J.; Zhang, Z.; Qin, Y.; Wang, Y.-J.; Wang, Y.; Tan, R.; Duan, X.; Tian, T. Z.; Zhang, C. H.; et al. 2021 Roadmap: Electrocatalysts for Green Catalytic Processes. *J. Phys. Mater.* **2021**, *4*, 022004.
(257) Niu, L.; An, L.; Wang, X.; Sun, Z. Effect on Electrochemical Reduction of Nitrogen to Ammonia under Ambient Conditions: Challenges and Opportunities for Chemical Fuels. *J. Energy Chem.* **2021**, *61*, 304−318.
(258) Chen, J.; Wang, Z.; Lee, H.; Mao, J.; Grimes, C. A.; Liu, C.; Zhang, M.; Lu, Z.; Chen, Y.; Feng, S. P. Efficient Electroreduction of CO_2 to CO by Ag-Decorated S-Doped g-C_3N_4/CNT Nanocomposites at Industrial Scale Current Density. *Mater. Today Phys.* **2020**, *12*, 100176.
(259) Ouyang, C.; Wang, X.; Wang, S. Phosphorus-Doped CoS_2 Nanosheet Arrays as Ultra-Efficient Electrocatalysts for the Hydrogen Evolution Reaction. *Chem. Commun.* **2015**, *51* (75), 14160−14163.
(260) Su, J.; Zhou, J.; Wang, L.; Liu, C.; Chen, Y. Synthesis and Application of Transition Metal Phosphides as Electrocatalyst for Water Splitting. *Sci. Bull.* **2017**, *62* (9), 633−644.
(261) Sumi, V. S.; Sha, M. A.; Arunima, S. R.; Shibli, S. M. A. Development of a Novel Method of Nicop Alloy Coating for Electrocatalytic Hydrogen Evolution Reaction in Alkaline Media. *Electrochim. Acta* **2019**, *303*, 67−77.
(262) Popczun, E. J.; McKone, J. R.; Read, C. G.; Biacchi, A. J.; Wiltrout, A. M.; Lewis, N. S.; Schaak, R. E. Nanostructured Nickel Phosphide as an Electrocatalyst for the Hydrogen Evolution Reaction. *J. Am. Chem. Soc.* **2013**, *135* (25), 9267−9270.
(263) Ji, X.; Liu, B.; Ren, X.; Shi, X.; Asiri, A. M.; Sun, X. P-Doped Ag Nanoparticles Embedded in N-Doped Carbon Nanoflake: An Efficient Electrocatalyst for the Hydrogen Evolution Reaction. *ACS Sustain. Chem. Eng.* **2018**, *6* (4), 4499−4503.
(264) Jaiswal, A.; Pal, S.; Kumar, A.; Prakash, R. Metal Free Triad from Red Phosphorous, Reduced Graphene Oxide and Graphitic Carbon Nitride (red P-RGO-g-C_3N_4) as Robust Electro-Catalysts for Hydrogen Evolution Reaction. *Electrochim. Acta* **2020**, *338*, 135851.
(265) Woldetinsay, M.; Soreta, T. R.; Maiyalagan, T.; Femi, O. E. Effect of Support Material on the Electrocatalytic Activity of Palladium Nanoparticle toward Hydrogen Evolution Reaction. *Mater. Res. Express* **2021**, *8* (2), 025501.
(266) Sastre, F.; Muñoz-Batista, M. J.; Kubacka, A.; Fernández-García, M.; Smith, W. A.; Kapteijn, F.; Makkee, M.; Gascon, J. Efficient Electrochemical Production of Syngas from CO_2 and H_2O by Using a Nanostructured Ag/G-C_3N_4 Catalyst. *ChemElectroChem.* **2016**, *3* (9), 1497−1502.
(267) Lv, C.; Qian, Y.; Yan, C.; Ding, Y.; Liu, Y.; Chen, G.; Yu, G. Defect Engineering Metal-Free Polymeric Carbon Nitride Electrocatalyst for Effective Nitrogen Fixation under Ambient Conditions. *Angew. Chem., Int. Ed* **2018**, *57* (32), 10246−10250.
(268) Jin, H.; Liu, X.; Jiao, Y.; Vasileff, A.; Zheng, Y.; Qiao, S.-Z. Constructing Tunable Dual Active Sites on Two-Dimensional C_3N_4@MoN Hybrid for Electrocatalytic Hydrogen Evolution. *Nano Energy* **2018**, *53*, 690−697.
(269) Chebanenko, M.; Zakharova, N.; Lobinsky, A. A.; Popkov, V. Ultrasonic-Assisted Exfoliation of Graphitic Carbon Nitride and Its Electrocatalytic Performance in Process of Ethanol Reforming. *Semiconductors* **2019**, *53*, 2072.
(270) Kim, H.-E.; Lee, I. H.; Cho, J.; Shin, S.; Ham, H. C.; Kim, J. Y.; Lee, H. Palladium Single-Atom Catalysts Supported on C@C_3N_4 for Electrochemical Reactions. *ChemElectroChem.* **2019**, *6* (18), 4757−4764.
(271) Idris, M. B.; Devaraj, S. Mesoporous Graphitic Carbon Nitride Synthesized Using Biotemplate as a High-Performance Electrode Material for Supercapacitor and Electrocatalyst for Hydrogen Evolution Reaction in Acidic Medium. *J. Energy Storage* **2019**, *26*, 101032.
(272) Li, H.; Yang, L.; Wang, Z.; Jin, P.; Zhao, J.; Chen, Z. N-Heterocyclic Carbene as a Promising Metal-Free Electrocatalyst with High Efficiency for Nitrogen Reduction to Ammonia. *J. Energy Chem.* **2020**, *46*, 78−86.
(273) Nazir, R.; Kumar, A.; Saleh Saad, M. A.; Ashok, A. Synthesis of Hydroxide Nanoparticles of Co/Cu on Carbon Nitride Surface Via Galvanic Exchange Method for Electrocatalytic CO_2 Reduction into Formate. *Colloids Surf. A Physicochem. Eng. Asp.* **2020**, *598*, 124835.

(274) Peng, G.; Wu, J.; Wang, M.; Niklas, J.; Zhou, H.; Liu, C. Nitrogen-Defective Polymeric Carbon Nitride Nanolayer Enabled Efficient Electrocatalytic Nitrogen Reduction with High Faradaic Efficiency. *Nano Lett.* **2020**, *20* (4), 2879−2885.
(275) Li, X.; Zhang, K.; Zhou, M.; Yang, K.; Yang, S.; Ma, X.; Yu, C.; Xie, Y.; Huang, W.; Fan, Q. A Novel Approach to Synthesize Nitrogen-Deficient g-C_3N_4 for the Enhanced Photocatalytic Contaminant Degradation and Electrocatalytic Hydrogen Evolution. *Nano* **2020**, *15* (01), 2050006.
(276) Duraisamy, N.; S, P.; R, R.; Kandiah, K. Binder-Free Heterostructure (g-C_3N_4/PPy) Based Thin Film on Semi-Flexible Nickel Foam Via Hybrid Spray Technique for Energy Storage Application. *Prog. Nat. Sci.* **2020**, *30* (3), 298−307.
(277) Kumar, A.; Khanuja, M. Template-Free Graphitic Carbon Nitride Nanosheets Coated with Polyaniline Nanofibers as an Electrode Material for Supercapacitor Applications. *Renew. Energy* **2021**, *171*, 1246−1256.
(278) Sun, X.; Yang, H.; Zhu, H.; Wang, L.; Fu, Z.; Zhang, Q.; Zhu, H. Synthesis and Enhanced Supercapacitor Performance of Carbon Self-Doping Graphitic Carbon Nitride/Nis Electrode Material. *J. Am. Ceram. Soc.* **2021**, *104* (3), 1554−1567.
(279) Gonçalves, R.; Paiva, R. S.; Lima, T. M.; Paixão, M. W.; Pereira, E. C. Carbon Nitride/Polypyrrole Composite Supercapacitor: Boosting Performance and Stability. *Electrochim. Acta* **2021**, *368*, 137570.
(280) Zhu, J.; Kong, L.; Shen, X.; Zhu, G.; Ji, Z.; Xu, K.; Zhou, H.; Yue, X.; Li, B. Carbon Cloth Supported Graphitic Carbon Nitride Nanosheets as Advanced Binder-Free Electrodes for Supercapacitors. *J. Electroanal. Chem.* **2020**, *873*, 114390.
(281) Zhang, Y.; Chang, L.; Chang, X.; Chen, H.; Li, Y.; Fan, Y.; Wang, J.; Cui, D.; Xue, C. Combining in-Situ Sedimentation and Carbon-Assisted Synthesis of Co_3O_4/g-C_3N_4 Nanocomposites for Improved Supercapacitor Performance. *Diam. Relat. Mater.* **2021**, *111*, 108165.
(282) Nallapureddy, R. R.; Pallavolu, M. R.; Joo, S. W. Construction of Functionalized Carbon Nanofiber-g-C_3N_4 and TiO_2 Spheres as a Nanostructured Hybrid Electrode for High-Performance Supercapacitors. *Energy Fuels* **2021**, *35* (2), 1796−1809.
(283) Zhang, X.; Liao, H.; Liu, X.; Shang, R.; Zhou, Y.; Zhou, Y. Graphitic Carbon Nitride Nanosheets Made by Different Methods as Electrode Material for Supercapacitors. *Ionics* **2020**, *26* (7), 3599−3607.
(284) Song, Q.; Yang, C.; Yu, C.-M. The Green One-Step Electrodeposition of Oxygen-Functionalized Porous g-C_3N_4 Decorated with Fe_3O_4 Nanoparticles onto Ni-Foam as a Binder-Free Outstanding Material for Supercapacitors. *New J. Chem.* **2021**, *45* (2), 657−670.
(285) Murugan, C.; Subramani, K.; Subash, R.; Sathish, M.; Pandikumar, A. High-Performance High-Voltage Symmetric Supercapattery Based on a Graphitic Carbon Nitride/Bismuth Vanadate Nanocomposite. *Energy Fuels* **2020**, *34* (12), 16858−16869.
(286) Ranjithkumar, R.; Lakshmanan, P.; Devendran, P.; Nallamuthu, N.; Sudhahar, S.; Kumar, M. K. Investigations on Effect of Graphitic Carbon Nitride Loading on the Properties and Electrochemical Performance of g-C_3N_4/TiO_2 Nanocomposites for Energy Storage Device Applications. *Mater. Sci. Semicond. Process.* **2021**, *121*, 105328.
(287) Wu, S.; Xu, B.; Long, Y.; Luo, X.; Zhang, L. Oxygen-Functionalized g-C_3N_4 Layers Anchored with $Ni(OH)_2$ Nanoparticles Assembled onto Ni Foam as Binder-Free Outstanding Electrode for Supercapacitors. *Synth. Met.* **2020**, *270*, 116601.
(288) Vinoth, S.; Subramani, K.; Ong, W.-J.; Sathish, M.; Pandikumar, A. CoS_2 Engulfed Ultra-Thin S-Doped g-C_3N_4 and Its Enhanced Electrochemical Performance in Hybrid Asymmetric Supercapacitor. *J. Colloid Interface Sci.* **2021**, *584*, 204−215.
(289) Yang, Z.; Liu, Q.; Zhang, L.; Dai, J.; Shen, Z. Green One-Pot Synthesis of Binder-Free Porous Edge-Functionalized Graphitic Carbon Nitride/Iron Oxide Nanoparticles Nanocomposite as an Outstanding Electrode for Supercapacitors. *J. Energy Storage* **2020**, *32*, 101909.
(290) Bandyopadhyay, P.; Saeed, G.; Hoon Kim, N.; Mun Jeong, S.; Hee Lee, J. Fabrication of Hierarchical Zn-Ni-Co-S Nanowire Arrays and Graphitic Carbon Nitride/Graphene for Solid-State Asymmetric Supercapacitors. *Appl. Surf. Sci.* **2021**, *542*, 148564.
(291) Sharma, M.; Gaur, A. Designing of Carbon Nitride Supported $ZnCo_2O_4$ Hybrid Electrode for High-Performance Energy Storage Applications. *Sci. Rep.* **2020**, *10*, 2035.
(292) Wang, S.; Zhu, Y.; Jiang, M.; Cui, J.; Zhang, Y.; He, W. TiO_2 Nanotube/g-C_3N_4/Graphene Composite as High Performance Anode Material for Na-Ion Batteries. *Vacuum* **2021**, *184*, 109926.
(293) Wang, S.; Zhu, Y.; Jiang, M.; Cui, J.; Zhang, Y.; He, W. Interconnected $Na_2Ti_3O_7$ Nanotube/g-C_3N_4/Graphene Network as High Performance Anode Materials for Sodium Storage. *Int. J. Hydrog. Energy* **2020**, *45* (38), 19611−19619.
(294) Tang, Y.; Wang, X.; Chen, J.; Wang, X.; Wang, D.; Mao, Z. PVP-Assisted Synthesis of g-C_3N_4-Derived N-Doped Graphene with Tunable Interplanar Spacing as High-Performance Lithium/Sodium Ions Battery Anodes. *Carbon* **2021**, *174*, 98−109.
(295) Zhang, X.; Yang, S.; Chen, Y.; Li, S.; Tang, S.; Shen, D.; Dong, W.; Hao, D. Effect of Phosphorous-Doped Graphitic Carbon Nitride on Electrochemical Properties of Lithium-Sulfur Battery. *Ionics* **2020**, *26* (11), 5491−5501.
(296) Pathak, D. D.; Dutta, D. P.; Ravuri, B. R.; Ballal, A.; Joshi, A. C.; Tyagi, A. K. An Insight into the Effect of g-C_3N_4 Support on the Enhanced Performance of ZnS Nanoparticles as Anode Material for Lithium-Ion and Sodium-Ion Batteries. *Electrochim. Acta* **2021**, *370*, 137715.
(297) Wang, M.; Zhou, X.; Cai, X.; Wang, H.; Fang, Y.; Zhong, X. Hierarchically Porous, Ultrathin N-Doped Carbon Nanosheets Embedded with Highly Dispersed Cobalt Nanoparticles as Efficient Sulfur Host for Stable Lithium-Sulfur Batteries. *J. Energy Chem.* **2020**, *50*, 106−114.
(298) Bai, M.; Hong, B.; Zhang, K.; Yuan, K.; Xie, K.; Wei, W.; Lai, Y. Defect-Rich Carbon Nitride as Electrolyte Additive for in-Situ Electrode Interface Modification in Lithium Metal Battery. *Chem. Eng. J.* **2021**, *407*, 127123.
(299) Angamuthu, G.; Jayabal, E.; Rengarajan, V. Electrochemical Performance Evaluation of Carbon Nitride Synthesized at Different Temperatures as an Anode Material for Lithium-Ion Batteries. *Ionics* **2020**, *26* (8), 3863−3873.
(300) Wan, L.; Tang, Y.; Chen, L.; Wang, K.; Zhang, J.; Gao, Y.; Lee, J. Y.; Lu, T.; Xu, X.; Li, J.; Zheng, Y.; Pan, L. In-Situ Construction of G-C_3N_4/Mo_2CT_x Hybrid for Superior Lithium Storage with Significantly Improved Coulombic Efficiency and Cycling Stability. *Chem. Eng. J.* **2021**, *410*, 128349.
(301) Kesavan, T.; Partheeban, T.; Vivekanantha, M.; Prabu, N.; Kundu, M.; Selvarajan, P.; Umapathy, S.; Vinu, A.; Sasidharan, M. Design of P-Doped Mesoporous Carbon Nitrides as High-Performance Anode Materials for Li-Ion Battery. *ACS Appl. Mater. Interfaces* **2020**, *12* (21), 24007−24018.
(302) Nilkar, M.; Ghodsi, F.; Jafari, S.; Thiry, D.; Snyders, R. Effects of Nitrogen Incorporation on N-Doped DLC Thin Film Electrodes Fabricated by Dielectric Barrier Discharge Plasma: Structural Evolution and Electrochemical Performances. *J. Alloys Compd.* **2021**, *853*, 157298.
(303) Shiravani, F.; Tashkhourian, J.; Haghighi, B. One-Step Synthesis of Graphitic Carbon-Nitride Doped with Black-Red Phosphorus as a Novel, Efficient and Free-Metal Bifunctional Catalyst and its Application for Electrochemical Overall Water Splitting. *Sustain. Energy Fuels* **2021**, *5*, 3229−3239.
(304) Monsef, R.; Ghiyasiyan-Arani, M.; Salavati-Niasari, M. Design of Magnetically Recyclable Ternary Fe_2O_3/$EuVO_4$/g-C_3N_4 Nanocomposites for Photocatalytic and Electrochemical Hydrogen Storage. *ACS Appl. Energy Mater.* **2021**, *4* (1), 680−695.
(305) Yousefi, M.; Faraji, M.; Asgari, R.; Moshfegh, A. Z. Effect of Boron and Phosphorus Codoping on the Electronic and Optical

Properties of Graphitic Carbon Nitride Monolayers: First-Principle Simulations. *Phys. Rev. B* **2018**, *97*, 195428.
(306) Naseri, A.; Samadi, M.; Pourjavadi, A.; Moshfegh, A. Z.; Ramakrishna, S. Graphitic Carbon Nitride ($g\text{-}C_3N_4$)-Based Photocatalysts for Solar Hydrogen Generation: Recent Advances and Future Development Directions. *J. Mater. Chem. A* **2017**, *5*, 23406−23433.
(307) Tafreshi, S. S.; Moshfegh, A. Z.; de Leeuw, N. H. Mechanism of Photocatalytic Reduction of CO_2 by $Ag_3PO_4(111)/g\text{-}C_3N_4$ Nanocomposite: A First-Principles Study. *J. Phys. Chem. C* **2019**, *123*, 22191−22201.
(308) Rahimi, K.; Moshfegh, A. Z. Band Alignment Tuning of Heptazine-$g\text{-}C_3N_4$/g-ZnO vdW Heterostructure as a Promising Water-Splitting Photocatalyst. *Phys. Chem. Chem. Phys.* **2021**, *23*, 20675−20685.
(309) Yousefzadeh, S.; Fathi, B. Construction of Carbon Nanotube-$g\text{-}C_3N_4$Nanocomposite Photoanode for the Enhanced Photoelectrochemical Activity in Water Splitting. *J. Electroanal. Chem.* **2020**, *878*, 114580.
(310) Yousefzadeh, S.; Morovati, N. Modification of the Ultrasonication Derived-$g\text{-}C_3N_4$Nanosheets/Quantum Dots by MoS_2Nanostructures to Improve Electrocatalytic Hydrogen Evolution Reaction. *Int. J. Hydrog. Energy* **2020**, *45* (58), 33512−33520.
(311) Hassanzadeh-Tabrizi, S. A.; Nguyen, C.-C.; Do, T.-O. Synthesis of Fe_2O_3/Pt/Au Nanocomposite Immobilized on $g\text{-}C_3N_4$ for Localized Plasmon Photocatalytic Hydrogen Evolution. *Appl. Surf. Sci.* **2019**, *489*, 741−754.
(312) Orooji, Y.; Ghanbari, M.; Amiri, O.; Salavati-Niasari, M. Facile Fabrication of Silver Iodide/Graphitic Carbon Nitride Nanocomposites by Notable Photo-catalytic Performance through Sunlight and Antimicrobial Activity. *J. Hazard. Mater.* **2020**, *389*, 122079.
(313) Nasri, A.; Nezafat, Z.; Jaleh, B.; Orooji, Y.; Varma, R. S. Laser-Assisted Preparation of C_3N_4/Fe_2O_3/Au Nanocomposite: AMagnetic Reusable Catalyst for Pollutant Degradation. *Clean Technol. Environ. Policy* **2021**, *23* (6), 1797−1806.